National Library of Canada
Acquisitions and Bibliographic Services Branch
395 Wellington Street
Ottawa, Ontario
K1A 0N4

Bibliothèque nationale du Canada
Direction des acquisitions et des services bibliographiques
395, rue Wellington
Ottawa (Ontario)
K1A 0N4

Your file *Votre référence*

Our file *Notre référence*

NOTICE

The quality of this microform is heavily dependent upon the quality of the original thesis submitted for microfilming. Every effort has been made to ensure the highest quality of reproduction possible.

If pages are missing, contact the university which granted the degree.

Some pages may have indistinct print especially if the original pages were typed with a poor typewriter ribbon or if the university sent us an inferior photocopy.

Reproduction in full or in part of this microform is governed by the Canadian Copyright Act, R.S.C. 1970, c. C-30, and subsequent amendments.

AVIS

La qualité de cette microforme dépend grandement de la qualité de la thèse soumise au microfilmage. Nous avons tout fait pour assurer une qualité supérieure de reproduction.

S'il manque des pages, veuillez communiquer avec l'université qui a conféré le grade.

La qualité d'impression de certaines pages peut laisser à désirer, surtout si les pages originales ont été dactylographiées à l'aide d'un ruban usé ou si l'université nous a fait parvenir une photocopie de qualité inférieure.

La reproduction, même partielle, de cette microforme est soumise à la Loi canadienne sur le droit d'auteur, SRC 1970, c. C-30, et ses amendements subséquents.

Canada

UNIVERSITY OF ALBERTA

The Role of Tactile Sensing in Robot Manipulation

BY

Pavan Sikka ©

A thesis submitted to the Faculty of Graduate Studies and Research in partial fulfillment of the requirements for the degree of Doctor of Philosophy.

DEPARTMENT OF COMPUTING SCIENCE

Edmonton, Alberta
Fall 1994

National Library of Canada
Bibliothèque nationale du Canada

Acquisitions and Bibliographic Services Branch
Direction des acquisitions et des services bibliographiques

395 Wellington Street
Ottawa, Ontario
K1A 0N4

395, rue Wellington
Ottawa (Ontario)
K1A 0N4

Your file Votre référence

Our file Notre référence

The author has granted an irrevocable non-exclusive licence allowing the National Library of Canada to reproduce, loan, distribute or sell copies of his/her thesis by any means and in any form or format, making this thesis available to interested persons.

L'auteur a accordé une licence irrévocable et non exclusive permettant à la Bibliothèque nationale du Canada de reproduire, prêter, distribuer ou vendre des copies de sa thèse de quelque manière et sous quelque forme que ce soit pour mettre des exemplaires de cette thèse à la disposition des personnes intéressées.

The author retains ownership of the copyright in his/her thesis. Neither the thesis nor substantial extracts from it may be printed or otherwise reproduced without his/her permission.

L'auteur conserve la propriété du droit d'auteur qui protège sa thèse. Ni la thèse ni des extraits substantiels de celle-ci ne doivent être imprimés ou autrement reproduits sans son autorisation.

ISBN 0-315-95264-4

Canada

UNIVERSITY OF ALBERTA

RELEASE FORM

NAME OF AUTHOR: Pavan Sikka

TITLE OF THESIS: The Role of Tactile Sensing in Robot Manipulation

DEGREE: Doctor of Philosophy

YEAR THIS DEGREE GRANTED: 1994

Permission is hereby granted to the University of Alberta Library to reproduce single copies of this thesis and to lend or sell such copies for private, scholarly or scientific research purposes only.

The author reserves all other publication and other rights in association with the copyright in the thesis, and except as hereinbefore provided neither the thesis nor any substantial portion thereof may be printed or otherwise reproduced in any material form whatever without the author's prior written permission.

(Signed) . . . . . .

Pavan Sikka
8796, C–8
Vasant Kunj
New Delhi – 110 037
INDIA

Date: August 5, 1994

UNIVERSITY OF ALBERTA

FACULTY OF GRADUATE STUDIES AND RESEARCH

The undersigned certify that they have read, and recommend to the Faculty of Graduate Studies and Research for acceptance, a thesis entitled **The Role of Tactile Sensing in Robot Manipulation** submitted by Pavan Sikka in partial fulfillment of the requirements for the degree of Doctor of Philosophy.

. . . . . .

Dr. H. Zhang (Supervisor)

. . . . . .

Dr. A. Russell (External)

. . . . . .

Dr. A. Basu (Examiner)

. . . . . .

Dr. R. W. Toogood (Examiner)

. . . . . .

Dr. T. A. Marsland (Examiner)

. . . . . .

Dr. R. Rink (Examiner)

Dr. P. Rudnicki (Chair)

Date: August 5, 1994

To my parents,

Krishan Lal Sikka
and
Manorama Sikka

Abstract

Robots must sense their environment and be sensitive to the changes taking place if they are to move beyond performing a limited range of tasks in the structured surroundings of a factory, to performing a variety of tasks in an unstructured and unknown environment. This thesis addresses a key requirement for such robots, namely, the capability of manipulation based on touch sensing. Tactile array sensors provide information about the distribution of force and other parameters within the area of contact. To manipulate objects using information from these sensors, it is necessary (1) to understand these sensors, i.e., have a model of them, and then (2) to develop robot control strategies to do a given task.

The first contribution of this thesis is the development of models of contact between a tactile array sensor and objects of different shapes, specifically a knife edge, a rectangular bar, and a cylinder. Many assumptions are made in elasticity theory to obtain closed-form solutions for such problems. Some of these assumptions are not appropriate for studying tactile sensors. This is most notably true of the half space assumption in which the sensor is modeled as a semi-infinite elastic medium bounded by a plane. However, in the absence of this assumption, closed-form expressions cannot be obtained for many cases. The finite element method is presented as a general and convenient method to study such problems. Using this method, the sensor is modeled as a thin layer and sub-surface stress distributions are obtained for contact with different objects.

The second contribution of the thesis is the development of a new approach to robot motion control during manipulation. The approach presented here is called *tactile servo* and is based on information from a tactile array sensor. Analogous to image-based visual servo, tactile servo is based on the observation that the progress of a manipulation task can be characterized by the tactile images obtained from sensors mounted on the fingertips of a robot hand. The sub-surface stress distributions obtained using the finite element method are analyzed to identify various features that are predictive of the applied load given the shape of the contacting object. Amongst these features, the moments of the stress distributions are found to vary in a regular way with the applied load. Hence, the zeroth, first, and second order moments of the stress distributions are selected as the tactile features for use in tactile servo algorithms. A motion control algorithm based on tactile servo is developed for the task of rolling a pin on a planar surface using a planar robot finger equipped with a tactile sensor array. This algorithm is also implemented experimentally to show that

information from a tactile array sensor can be used in a simple, direct and effective way to control manipulation tasks.

Acknowledgements

I am greatly indebted to Dr. Hong Zhang, my supervisor. Without his support, this thesis could not have been completed.

Special thanks are due to Dr. Roger Toogood for introducing me to the finite element method, for building several "toys" that are now property of the Robotics Laboratory, and for the many discussions. Special thanks are also due to Steve Sutphen for getting all the hardware in the Laboratory up and running and for keeping it that way.

I am grateful to the members of my examining committee, Dr. Anup Basu, Dr. Tony Marsland, Dr. Ray Rink, and Dr. Andrew Russell, for their comments and suggestions.

I would also like to acknowledge financial support from the Foundation for Promotion of Advanced Automation Technology, Japan, and the Department of Computing Science, University of Alberta.

Contents

1 Introduction 1
- 1.1 Contributions . . . 3
- 1.2 Thesis outline . . . 4

2 Manipulation and tactile sensing — an overview 6
- 2.1 Manipulation . . . 6
  - 2.1.1 Force control/Compliance . . . 7
  - 2.1.2 Fine motion synthesis . . . 7
- 2.2 Touch sensing . . . 9
  - 2.2.1 The human sense of touch . . . 9
  - 2.2.2 Robot touch sensors . . . 10
  - 2.2.3 Tactile sensor technologies . . . 11
- 2.3 Models of tactile sensors . . . 11
- 2.4 Touch in robot exploration and recognition . . . 13
- 2.5 Tactile sensors and manipulation . . . 14
- 2.6 Discussion . . . 16

3 Finite element analysis of tactile sensors 18
- 3.1 Introduction . . . 19
- 3.2 Contact with a knife edge . . . 21
  - 3.2.1 Effect of the half space assumption . . . 22
  - 3.2.2 Effect of the plane strain assumption . . . 24
  - 3.2.3 Discussion . . . 25
- 3.3 Contact with a flat rectangular bar . . . 26
  - 3.3.1 Effect of the half space assumption . . . 27
- 3.4 Contact with a long cylinder . . . 30
- 3.5 Discussion . . . 30

4 Analyzing contact with tactile sensors 33
- 4.1 Introduction . . . 33
- 4.2 Line contact . . . 35
- 4.3 Contact with a rectangular bar . . . 39
  - 4.3.1 Relating stress to applied force . . . 44
  - 4.3.2 Recovering contact parameters from stress . . . 47

4.4 Contact with a long cylinder 50
4.5 Models of contact and superposition 53
4.6 Conclusion 56

5 Tactile sensing and manipulation **58**
5.1 Introduction 58
5.2 Tactile servo 59
5.3 Example task : Rolling a pin 63
5.3.1 Tactile images under varying loading conditions 63
5.3.2 Identifying tactile features 65
5.3.3 Obtaining the components of $\mathbf{J}_s$ 67
5.4 Summary 71

6 Tactile servo : An experiment **72**
6.1 Experimental setup 72
6.1.1 The hardware 72
6.1.2 The software 73
6.2 Tactile servo : Rolling a pin 77
6.3 Rolling a pin on a flat surface 84
6.3.1 Rolling a pin on a plane aligned with the base frame 84
6.3.2 Rolling a pin on an inclined plane 87
6.4 Rolling the pin on a moving table 93
6.4.1 Translation along z_0 93
6.4.2 Rotation about x_0 93
6.4.3 Rotation about z_0 95
6.4.4 Translation along x_0 96
6.5 Summary and discussion 98

7 Conclusion **99**
7.1 Summary 99
7.2 Contributions 100
7.3 Future work 101
7.3.1 Modeling contact 101
7.3.2 Tactile servo 102

Bibliography **104**

A Appendix **110**
A.1 Review of elasticity theory 110
A.1.1 Line contact 116
A.1.2 Contact with a flat indenter 121
A.1.3 Contact with a cylindrical indenter 124
A.2 Contact and the finite element method 126
A.2.1 General considerations 126

A.2.2 Contact with a flat indenter 128
A.3 References for appendix 130

List of Figures

2.1 *A tactile sensor. (a) A diagram of the Interlink tactile sensor and (b) an image obtained from the sensor.* 12

3.1 *A typical tactile sensor mounted on a robot finger.* 19
3.2 *A thin layer in contact with a knife edge.* 21
3.3 *A comparison of the stress distributions obtained using the half space assumption (equations 3.1 – 3.3) and a 25.4 mm thick layer. (a) σ_{xx}, the normal component of stress along x. (b) σ_{zz}, the normal component of stress along z.* 23
3.4 *A comparison of the stress distributions obtained using the half space assumption (equations 3.1 – 3.3) and a 0.8 mm thick layer. (a) σ_{xx}, the normal component of stress along x. (b) σ_{zz}, the normal component of stress along z.* 24
3.5 *A comparison of the stress distributions obtained with and without using the plane strain assumption for a thin 0.08 cm elastic layer. (a) σ_{xx}, the normal component of stress along x. (b) σ_{zz}, the normal component of stress along z.* 25
3.6 *A comparison of the stress distributions obtained with and without using the plane strain assumption for a thick 2.54 cm elastic layer. (a) σ_{xx}, the normal component of stress along x. (b) σ_{zz}, the normal component of stress along z.* 26
3.7 *The dimensions of the objects used in this study. All measurements are in mm.* 28
3.8 *The effect of varying the layer thickness. The normal stress distribution along z, σ_{zz}, on the surface of the sensor, is shown for layer thickness of 12.7 mm, 6.35 mm, and 0.8 mm.* 28
3.9 *The effect of varying the layer thickness. The normal stress distribution along z, σ_{zz}, within the medium at a depth of 0.8 cm, is shown for layer thickness of 12.7 mm, 6.35 mm, and 0.8 mm.* 29
3.10 *The effect of varying the layer thickness. The normal stress distribution along z, σ_{zz}, on the surface of the sensor, is shown for layer thickness of 0.8 mm, 3.2 mm, and 12.8 mm, and a half space.* 31
3.11 *The effect of varying the layer thickness. The normal stress distribution along z, σ_{zz}, within the medium at a depth of 0.8 mm, is shown for layer thickness of 0.8 mm, 3.2 mm, and 12.8 mm.* 31

4.1 *An approach to characterizing and using tactile sensors.* 34
4.2 *The variation in the sub-surface stress profile for increasing normal force with no tangential force.* 38
4.3 *The variation is stress distribution (a) with increasing normal force for a constant tangential force, and (b) with increasing tangential force with constant normal force.* 38
4.4 *The moments (a) M_0 (N/mm) and (b) M_1 (N) as a function of the relative displacements.* 39
4.5 *The stress distributions with and without the friction model. All forces are expressed in N/mm. (1) Q = 0.022 without friction. (2) Q = 0.022 with friction. (3) Q = 0.15 without friction. (4) Q = 0.15 with friction.* 41
4.6 *The normal component of the stress tensor σ_{zz} for different applied normal forces. The normal force is applied in the negative z direction and is expressed in N/mm. (1) 0.07 (2) 0.28 (3) 0.49 (4) 0.70.* 41
4.7 *The stress profiles for a force consisting of both a normal component and a tangential component. All forces are expressed in units of N/mm. (a) The variation in stress profile σ_{zz} for a tangential force applied in the positive x direction. (1) 0.0088 (2) 0.035 (3) 0.061 (4) 0.088. A fixed normal force of 0.18 is applied in the negative z direction. (b) The variation in stress profile σ_{zz} for a normal force applied in the negative z direction. (1) 0.18 (2) 0.35 (3) 0.53 (4) 0.70. A fixed tangential force of 0.044 is applied in the positive x direction.* 42
4.8 *An indenter is tilted as a result of the tangential force applied at the top.* 43
4.9 *The contact width as a function of normal and tangential force. The normal force is applied in the negative Z direction in units of N/mm. (1) P = 0.18 (2) P = 0.35 (3) P = 0.53 (4) P = 0.7. (a) Indenter width w_I = 7.9 mm. (b) Indenter width w_I = 15.1 mm.* 45
4.10 *The position of maximum stress, x_m, as a function of normal and tangential force. The normal force is applied in the negative z direction in units of N/mm. (1) P = 0.18 (2) P = 0.35 (3) P = 0.53 (4) P = 0.7. (a) Indenter width w_I = 7.9 mm. (b) Indenter width w_I = 15.1 mm.* 46
4.11 *The centroid of the stress distributions, x_c, as a function of the normal force, the tangential force, and the indenter width. The normal force is applied in the negative z direction in units of N/mm. (1) P = 0.18 (2) P = 0.35 (3) P = 0.53 (4) P = 0.7.* 46
4.12 *The first moment M_1 of the stress distributions as a function of the normal force, the tangential force, and the indenter width. The normal force is applied in the negative z direction in units of N/mm. (1) P = 0.18 (2) P = 0.35 (3) P = 0.53 (4) P = 0.7.* 47

4.13 *The second moment M_2 of the stress distributions as a function of the normal force, the tangential force, and the indenter width. The normal force is applied in the negative z direction in units of N/mm. (1) P = 0.18 (2) P = 0.35 (3) P = 0.53 (4) P = 0.7.* 48
4.14 *The third moment M_3 of the stress distributions as a function of the normal force, the tangential force, and the indenter width. The normal force is applied in the negative z direction in units of N/mm. (1) P = 0.18 (2) P = 0.35 (3) P = 0.53 (4) P = 0.7.* 48
4.15 *The algorithm used to study contact by specifying the surface displacements based on the indenter geometry.* 51
4.16 *The variation in the sub-surface stress profile for increasing normal force with no tangential force.* 52
4.17 *The variation in sub-surface stress distribution (a) with increasing values of the normal displacement for a constant tangential displacement of the indenter, and (b) with increasing values of the tangential displacement with constant normal displacement of the indenter.* 52
4.18 *The moments (a) M_0 (N/mm) and (b) M_1 (N) as a function of the relative displacements.* 53
4.19 *The stress distributions corresponding to a purely normal displacement and a purely tangential displacement.* 54
4.20 *The stress distributions obtained from the finite element method and using superposition. The normal force applied to the bar is 0.53 N/mm. (a) Tangential force of 0.09 N/mm. (b) Tangential force of 0.16 N/mm.* 55
4.21 *The stress distributions obtained from the finite element method and using superposition for a normal force of 0.18 N/mm and a tangential force 0f 0.14 N/mm.* 55

5.1 $\frac{\partial M_0}{\partial u_{z0}}$ *(N/mm²) for line contact, as a function of u_{z0} and u_{x0}.* 61
5.2 $\frac{\partial M_0}{\partial u_{x0}}$ *(N/mm²) for line contact, as a function of u_{z0} and u_{x0}.* 62
5.3 $\frac{\partial M_1}{\partial u_{z0}}$ *(N/mm) for line contact, as a function of u_{z0} and u_{x0}.* 62
5.4 $\frac{\partial M_1}{\partial u_{x0}}$ *(N/mm) for line contact, as a function of u_{z0} and u_{x0}.* 62
5.5 *Planar view of a robot arm equipped with a sensorized finger rolling a pin.* 63
5.6 *The two-dimensional stress distributions obtained experimentally from the tactile sensor in which the darkness represents the pressure intensity. The image on the right corresponds to a larger force applied along z compared to the image on the left. The z-axis is normal to the page.* 64
5.7 *The effect of a rotation about z, which is normal to the plane of this page.* 64
5.8 *The effect of a translation along x, which is along the vertical direction on this page.* 65

5.9 *The effect of a rotation about x. The image on the right results from an anti-clockwise rotation of the cylinder about x, which lies along the vertical direction in the plane of this page.* 66
5.10 $\frac{\partial M_0}{\partial z}$ *(N/mm^2) for contact with a cylinder, as a function of displacements along z and x.* 68
5.11 $\frac{\partial M_0}{\partial x}$ *(N/mm^2) for contact with a cylinder, as a function of displacements along z and x.* 69
5.12 $\frac{\partial M_1}{\partial z}$ *(N/mm) for contact with a cylinder, as a function of displacements along z and x.* 69
5.13 $\frac{\partial M_1}{\partial x}$ *(N/mm) for contact with a cylinder, as a function of displacements along z and x.* 69
5.14 *The variation of M_0 and M_x with applied force, obtained experimentally. (a) The relationship between M_0 and increasing normal force. (b) The variation of M_x with increasing tangential force.* 70

6.1 *The Experimental Setup.* 74
6.2 *The finite-state machine corresponding to the robot control program.* . . 75
6.3 *The organization of the robot control software.* 77
6.4 *The tactile servo algorithm.* 78
6.5 *A photograph of the robot, the pan-tilt table, and the rolling pin. The robot base frame, (y_0, z_0), and the sensor frame, (x_s, y_s), are both shown.* 80
6.6 *A photograph of the robot rolling the pin on the pan-tilt table.* 81
6.7 *Setting up the desired value of x_c.* 83
6.8 *The angles (a) θ_{z_s} and (b) θ_{x_s} used to demonstrate the effect of changing orientation of the pin on tactile servo.* 85
6.9 *The variation in (a) x_c and in (b) p_x while rolling the pin on a flat table aligned with the axes of the robot base frame.* 85
6.10 *The variation in (a) M_0 and in (b) p_z while rolling the pin on a flat table aligned with the axes of the robot base frame.* 86
6.11 *The variation in (a) M_x and in (b) θ_{z_s} while rolling the pin on a flat table aligned with the axes of the robot base frame.* 86
6.12 *The variation in (a) θ_p and in (b) θ_{z_s} while rolling the pin on a flat table aligned with the axes of the robot base frame.* 87
6.13 *The variation in (a) x_c, (b) p_x, (c) M_0, and (d) p_z, while rolling the pin on a flat table inclined about y_0.* 88
6.14 *The pan-tilt table shown with its axes aligned with the robot base frame.* 89
6.15 *The variation in (a) M_x and (b) θ_{z_s}, while rolling the pin on a flat table inclined about x_0.* 89
6.16 *The variation in (a) θ_p and (b) θ_{x_s}, while rolling the pin on a flat table rotated about z_0.* 90
6.17 *The variation in (a) x_c and (b) p_x while rolling the pin on a flat table inclined with respect to all three axes of the robot base frame.* 91
6.18 *The variation in (a) M_0 and (b) p_z while rolling the pin on a flat table inclined with respect to all three axes of the robot base frame.* 91

6.19 *The variation in (a) M_x and (b) θ_{z_s} while rolling the pin on a flat table inclined with respect to all three axes of the robot base frame.* 92
6.20 *The variation in (a) θ_p and (b) θ_{x_s} while rolling the pin on a flat table inclined with respect to all three axes of the robot base frame.* 92
6.21 *The variation in p_x, while rolling the pin on a flat table that is (1) stationary, (2) rotating about y_0, and (3) inclined about y_0.* 94
6.22 *The variation in (a) p_z as the pin is rolled on (1) a flat table aligned with the robot axes, (2) a flat table rotating about y_0, and (3) a flat table inclined about y_0-axis, and the variation in M_0 for (b) a flat table aligned with the robot axes, (c) a flat table rotating about y_0, and (d) a flat table inclined about the y_0.* 94
6.23 *The variation in (a) θ_{z_s} for the pin rolling on (1) a flat table aligned with the robot axes, (2) a flat table rotating about x_0, and (3) a flat table inclined about x_0, and the variation in M_y for (b) a flat table aligned with the robot axes, (c) a flat table rotating about x_0, and (d) a flat table inclined about x_0.* 95
6.24 *The variation in p_x while rolling the pin on a flat table that is (1) stationary, (2) rotating about z_0, and (3) inclined about z_0.* 96
6.25 *The variation in (a) θ_{x_s} for the pin rolling on (1) a flat table aligned with the robot axes, (2) a flat table rotating about z_0, and (3) a flat table inclined about z_0, and the variation in θ_p for (b) a flat table aligned with the robot axes, (c) a flat table rotating about z_0, and (d) a flat table inclined about z_0.* 97
6.26 *The variation in θ_{z_s} while rolling the pin on a flat table that is (1) stationary, (2) rotating about z_0, and (3) inclined about z_0.* 97
6.27 *The variation in (a) x_c and (b) p_x rolling the pin on a flat table, aligned with the axes of the robot base frame, and moved along x_0.* 98

A.1 *The different components of the stress tensor.* 111
A.2 *The contact between a smooth surface and a sharp edge.* 117
A.3 *The line contact problem in cylindrical coordinates.* 119
A.4 *The contact between a flat rectangular object and a semi-infinite elastic medium.* 123
A.5 *The contact between a cylinder and a semi-infinite elastic medium.* . . . 125
A.6 *A finite element mesh for modeling an elastic layer. The mesh density used in the analysis was larger than that shown in this figure.* 127
A.7 *A comparison between the sub-surface stress distributions in the case of edge contact for two different values of ν. The solid line corresponds to $\nu = 0.49$, while the dashed line corresponds to $\nu = 0.499999$.* 128
A.8 *The finite element model used for examining the relationship between the stress distribution and the applied normal force, tangential force, and the indenter width. In the analysis, a larger mesh density was used than that shown in this figure.* 129

List of Tables

A.1 *The material properties used in the thesis.* 127

Chapter 1

Introduction

Robots are now being used extensively in modern factories. They do tasks like painting, welding, and moving objects. In an industrial setting, these tasks are performed in a highly structured environment where the location and the orientation of the object being manipulated is known with a high degree of accuracy. The robots do these tasks by faithfully moving along predefined paths with good precision and accuracy. These robots are, therefore, sensitive to measurement errors and changing environments. Since these robots work by accurately controlling the position of the end-effector, they are poor at performing tasks that involve contact with the environment, in which even a small error in position can lead to large forces developing in the manipulator.

These limitations arise because modern industrial robots are impoverished in their ability to sense the environment. A key requirement for a robot to function in a changing and uncertain environment is the ability to sense and track the changes taking place in the environment. Consequently sensing is generally recognized as an important aspect of robots. The need for sensing varies depending on the task being carried out by the robot and the environment in which the task is being attempted. As mentioned before, in structured environments, such as a factory, the knowledge of the environment is complete, the tasks are well defined, and the sensory requirements are minimal. On the other hand, in an unstructured environment, knowledge of the environment is incomplete and the robot is required to learn about its environment to complete the required task. Here, sensory requirements are complex in that the robot needs to have several different sensory modalities and must combine the information from these different sources.

Many different sensory modalities have been studied extensively, both as independent research areas in their own right and in the context of robotics. There is an extensive body of literature on research in vision, speech perception, and other sensing modalities. In the context of robotics, the problems of integrating sensory information from several sensors forms an active research area. Many attempts to integrate different sensing modalities, for example vision and touch, can be found in the existing literature.

Touch sensing becomes important in tasks that involve contact with the environ-

ment or an object or both. For example, in an exploration task, touch could be used to obtain information about an object's shape, size, weight, hardness, texture, temperature and other features. Based on psychological experiments involving humans, Klatzky *et al.* [41] have proposed a set of exploratory primitives, i.e., stereotypical movements, that are used by humans to acquire such information about objects through touch. Similarly, in a manipulation task, touch can be used to obtain, and hence control, the forces acting in the contact area, and to monitor grasp stability and slip.

As illustrated by the human hand, the sense of touch is an indispensable sensing modality in tasks that require dextrous manipulation. Dextrous manipulation and multi-fingered hands, both human and robotic, have been studied from many different perspectives, for example, industrial assembly, prosthetic hand design, and human movement [62].

In prosthesis design, the goal is to restore lost functionality of the human hand and here a study of the human hand and of the neural mechanisms controlling the human hand becomes important. Many roboticists too have been inspired by *anthropomorphism* and this is reflected in the existence of several multi-fingered robot hands equipped with touch sensors [59].

In this context, it should be mentioned that the human sense of touch has been studied extensively. Several different types of touch sensors in the human skin have been identified and their characteristics studied in detail. However, the neural mechanisms responsible for using the information from these sensors to control the hand are not well understood. Hence, although the human haptic system provides an excellent example of a complex manipulation device, it cannot directly be used as a model for the design of artificial manipulation devices.

In contrast to prosthesis design, the main issue in industrial assembly tasks is the mechanical design of manipulators based on a study of the object to be manufactured and the manufacturing process. The goals of this research are clearly outlined in the well known paper by Whitney [67] about robots and jigs. The ability to handle contact is extremely important in assembly tasks and this is reflected in the design of devices and methods such as the Remote Centered Compliance (RCC) [66] and active force control [52]. This work also highlights the debate in the robotics community about the role of sensing in robotic systems. Human beings are a good existence proof of sensory-based manipulation. On the other hand, many industrial problems may not really need all the power of sensor-based manipulation — good industrial design may yield simple, elegant, and cheap solutions [67].

Thus, the sense of touch is a fundamental component of our ability to perceive and manipulate objects in our environment. In the context of robotics, tactile sensors consist of an array of sensors each of which usually measures a quantity that is related to the deformation in the area of contact or the normal component of the forces acting within the area of contact. It is only recently that robotics researchers have started to explore the domain of tactile sensing. Most of the research in tactile sensing for robots has concentrated in exploring the use of tactile sensors for object recognition and in

the design of tactile sensors. The use of tactile sensors in robotic fine manipulation, i.e., in tasks involving small motions and fine control over forces and velocities, is still a largely unexplored domain. This thesis studies parameter extraction from tactile sensory data to control robotic fine manipulation tasks that require physical contact between the object and the environment, where the forces acting at the interface need to be actively controlled.

1.1 Contributions

The contributions of this thesis are as follows :

- The use of finite element analysis as a tool for studying contact problems from the perspective of tactile sensing.

  A survey of the literature on contact problems in elasticity showed the many limitations, as simplifying assumptions, of the analytical techniques for obtaining the solution of such problems. The finite element method provides a general and convenient tool for studying contact problems for which analytical methods prove to be inadequate.

- A comprehensive study of several different types of contact.

  The finite element method was used to analyze the contact between several different objects and an elastic layer. The displacements and stresses within the elastic layer were obtained for contact with an edge, a cylindrical object, and a flat-based rigid indenter, for a range of different loading conditions.

- A new approach to robot control using touch — *tactile servo.*

  A new approach for controlling robot motion in real-time during a manipulation task using tactile sensors was proposed. This approach, called *tactile servo*, is motivated by the notion of *visual servo*, a method to control the movement of a robot based on visual information. The control is based on tracking several features, obtained from tactile sensory data, that characterize contact between the robot and an object or the environment. Tactile Servo was implemented for the task of rolling a cylindrical pin on a given surface whose orientation is not known *a priori* and changes over time. The implementation was tested experimentally using a PUMA 260 manipulator equipped with a tactile array sensor. The following steps made possible the realization of tactile servo.

  - Identification of *tactile features* that can be used in tactile servo control of different manipulation tasks. Moments have been used

extensively in image processing, both visual and tactile, for recognition purposes. However, here the moments are used as features in tactile servo control of manipulation tasks.

- Derivation of the feature sensitivity matrices for different types of contact. The analysis using the finite element method was used to study the variation of tactile features for small movements of the object with respect to the sensor.

1.2 Thesis outline

The thesis consists of three main parts. In the first part, existing literature on touch sensing and on manipulation is reviewed. This provides the motivation for the work reported in the next two parts. The second part presents a discussion on modeling contact and the third part presents some results on the use of touch sensing in manipulation tasks.

Broadly, there are three different types of touch sensors used in robot manipulators. The first is the six-axis force-torque sensor normally mounted on the wrist of the robot arm [63]. This sensor provides gross information about contact and cannot always be used to derive information about contact at the fingertip(s) of the robot. The second type of sensor is a miniature six-axis force-torque sensor that is mounted within the fingertip of the robot manipulator. This sensor is known as the *Intrinsic Tactile Sensor* [10] and can provide more robust information about fingertip contact. This sensor, too, is limited in that it cannot provide any information about contact shape and can provide contact location only for simple contact shapes known in advance. The third type of sensor is the tactile array sensor. This sensor consists of many closely spaced sensing sites, usually arranged as a rectangular array. Usually each sensing site provides information about only one component of force or displacement. These sensors provide information about the shape and location of contact, as well as the distribution of forces within the area of contact.

The second part of the thesis consists of an attempt to characterize theoretically the performance of a tactile array sensor with respect to different contact shapes and loading conditions. Three different types of contact are considered — edge, cylindrical, and flat. The stress response of the sensor is analyzed for several different combinations of displacements of the object with respect to the sensor. Many features of the stress distribution are considered, for example the center of the stress distribution, the area of the stress distribution, the skew of the stress distribution, and the various moments associated with the stress distribution. This is done with the objective of identifying features that could be useful in deriving control strategies for manipulation tasks to be performed with the help of tactile array sensors.

The models of contact studied in the second part of the thesis are constructed and solved using the finite element method. Analytical solutions for models of contact are difficult to derive except for the simplest of cases and require many simplifying assumptions to be made. The finite element method is a numerical method for solv-

ing boundary-value problems. The problem to be solved is specified geometrically, making the specification easy and intuitive. Since the solution is obtained numerically, complex boundary conditions can be specified and hence more realistic models of contact can be constructed.

The third part of the thesis identifies manipulation tasks that require the use of tactile array sensors. Using some of the features identified in the first part of the thesis, a method for real-time control of manipulation tasks using tactile sensors is presented. This approach is called *Tactile Servo* in analogy with visual servo. A complete experiment for rolling a cylindrical pin on a given surface, whose shape is not known in advance, is designed and implemented. The design is based on tactile servo and the experimental results obtained from the experiment are also presented.

The chapters in the thesis are organized as follows. The next chapter presents a detailed survey of the literature on tactile sensing and its applications. This survey is used to identify and motivate the research problems that are then explored in the thesis. The first problem is a study of the contact between a tactile sensor and an object. This problem is considered within the framework of elasticity theory and a brief review of elasticity as well as some existing results from the extensive literature on elasticity are included in the Appendix. Chapter 3 presents a comparison between the stress distributions obtained from the closed-form solutions and from the finite element method. Many of the assumptions made for obtaining the closed-form solutions are examined and shown to be inappropriate for modeling contact between a tactile sensor and a given object. The finite element method is found to be the best option for studying the problem of contact. Following this reasoning, the finite element method is used to model the contact between a tactile sensor and three given objects — a knife edge, a rectangular bar, and a cylinder. The sub-surface stress distributions are analyzed as a function of the load applied to the given object and several features are identified from these stress distributions. These results are presented in Chapter 4. The second problem considered in the thesis is the design of algorithms to control robot motion using tactile array sensors. Chapter 5 uses the results obtained so far and presents a new approach, called tactile servo, for controlling the motion of a robot during manipulation using tactile array sensors. The following chapter presents the experimental results obtained from an implementation of tactile servo for the task of rolling a cylindrical pin. Finally, a summary of the work done and the conclusions are presented in the last chapter. Some suggestions for future work are also presented.

Chapter 2

Manipulation and tactile sensing — an overview

The sense of touch plays an important role in exploration and manipulation. The latter includes operations such as grasping and moving objects in contact with the environment, as in pushing, sliding, rolling, and assembly tasks. The modality of touch provides information at various levels of processing, from low level perception of contact to high level perception of object properties.

Tactile sensing and manipulation have both been actively studied in psychology and robotics. In this chapter, the existing literature on manipulation and on tactile sensing is selectively reviewed to provide the background for the research reported in this thesis.

2.1 Manipulation

Manipulation refers to our ability to move objects, whether constrained or unconstrained, in a skillful manner. For example, assembly tasks as exemplified by the task of inserting a peg into a hole, and other tasks such as turning a crank, opening a door, and sliding along a surface involve manipulation. Manipulation involves two main capabilities. The first is the ability to plan the motion of an object, taking into account the constraints on the motion of the object, usually imposed by the environment or by the task requirements. In other words, from a general description of the task, the robot must devise the sequence of motions that will lead to the task being completed satisfactorily. This problem has been referred to as fine-motion synthesis [42]. The second capability is the ability to control the motion of an object during contact with another object or the environment. This problem is referred to as compliant motion or as force control and deals with the problem of controlling the force acting on the object or the environment [52]. It should be emphasized that fine-motion includes compliant motion and strategies for fine-motion synthesis usually assume that some mechanism for compliant motion is already available.

2.1.1 Force control/Compliance

Since manipulation is inextricably linked to compliant motion, any scheme for manipulation must build on some control scheme that allows both position and force control. Some of the schemes used for compliant motion are briefly outlined below.

An obvious method to do compliant motions is to specify the directions of motion that require force control. Motion along the remaining axes is then done under position control. For example, if the task is to insert a peg into a hole, then one could specify that position control be employed along the axis of the hole and that force control be employed along the two axes orthogonal to the axis of the hole. This approach has been referred to as hybrid control [52]. Mason [44] has developed a formal framework that allows the specification of how the degrees of freedom are to be controlled given the kinematics and geometry of the task. Khatib [37] provides a generalization of hybrid control that takes dynamics into account.

A more flexible method for combined position and force control is called stiffness control [55]. In this method, the manipulator is treated as a generalized spring. By specifying the stiffness along the different directions of freedom, one can vary the mode of control from position to force. Thus, if the stiffness along some direction is large then that direction of freedom will behave as if it is under position control since a high stiffness implies that even small displacements with respect to some specified position will lead to a large spring force. On the other hand, small values of stiffness will lead to force control. A generalized version of stiffness control is called impedance control [29].

2.1.2 Fine motion synthesis

Several attempts have been made to tackle the problem of fine manipulation in its entirety. Mason [44] describes a method by which one can derive the control strategies to be employed for a given task. This method relies on hybrid control to complete the task, which is formulated in terms of C-surfaces. A C-surface is defined as a task configuration in which freedom of motion occurs along the C-surface tangents and freedom of force occurs along the C-surface normals.

In this method, the manipulator trajectory that accomplishes the task is defined as a sequence of compliant motions joined together by guarded moves. A compliant motion is defined as the motion along a given C-surface. Thus, different task configurations are used to specify the different C-surfaces (which can be directly related to a particular control strategy). Guarded moves are used to accomplish the transition from one C-surface to another i.e., from one task configuration to another.

A major problem with the above approach is that it does not take into account the uncertainties and errors in the model of the task. The locations and the dimensions of objects may not be known accurately. Lozano-Perez *et al.* [42] describe a method that takes these uncertainties into account when planning the sequence of moves required to accomplish the task.

In this method, the objects are transformed into a configuration space in which

the object to be manipulated is a point. Then, for a given goal, the method involves the computation of a *pre-image* — the part of configuration space from which the goal can be reached by a single motion along a given direction. The algorithm starts by computing the pre-image of the goal and then continues by recursively computing pre-images until a pre-image including the current position in the configuration space is obtained. Finally, a sequence of velocity vectors and a sequence of corresponding termination predicates is computed from the sequence of pre-images.

The method takes uncertainty and errors into account by explicitly introducing them in the computation of the pre-image. Thus, the method computes a strong pre-image, i.e., a pre-image that takes uncertainties into account such that it does not intersect the pre-image of any surface where motion along the specified velocity vector may stick or not reach the goal. To determine that a motion has been executed satisfactorily, the method employs three basic termination conditions — motion corresponding to the current velocity vector can be ended when a predicate involving measurements of the position, the velocity, or the time elapsed is satisfied.

In this approach to planning fine manipulation strategies, the role of sensing is limited to the notion of termination conditions and it is assumed that these termination conditions can be reliably detected using sensors. During plan execution, the motion corresponding to each velocity vector is ended whenever the associated termination condition becomes true. The strategies developed by this approach are guaranteed to succeed but there is no provision for changing the strategy once it is being executed. This problem has been addressed in some recent work by Donald [22]. He has extended this method to develop error detection and recovery (EDR) strategies that, although not guaranteed to succeed, are guaranteed to end in some recognizable state. Desai [21] has developed a method to identify the configuration of the task after each guarded move using the notion of contact formations. This method relies primarily on a six-axis force/torque sensor.

In a recent paper, Donald [23] points out that the above approach emphasizes reachability as opposed to recognizability. The above approach concentrates attention on regions in configuration space that the robot can reach rather than regions in that space that the robot can identify using its sensors. A given sensor partitions the world into distinct regions that can be identified using that sensor. These partitions depend on the resolution and accuracy of the sensor and are called perceptual equivalence classes [23]. Based on this notion, Donald presents a framework for planning, sensing, and action that uses these perceptual equivalence classes, also called recognizable regions or configurations, as the basic building block.

This is a fundamental shift in how fine manipulation can be viewed. Instead of concentrating on motion, this view concentrates more attention on sensing. Thus, fine manipulation tasks can be solved by first finding out the distinct configurations that can be sensed and then planning motions and sensing strategies to find a path through this space of configurations from an initial configuration to the goal configuration.

There exists other work in the same vein. Desai [21] describes an approach based on different types of contact formations to derive constraints that can be used to

distinguish the different task configurations. His approach makes use of both position sensors and wrist-mounted six-axis force/torque sensors. Smith and Gini [57] also describe a system developed along the same lines. Their system uses finite-state automata as models of the assembly process. The system they describe distinguishes different states based on position sensors alone.

This emphasis on sensing and sensors highlights the need for tight coupling between the sensory data and the control process based on that sensory data. Visual servo [65] provides a good example of the importance of the coupling between sensation and action. In a system where the control is loosely coupled to the visual input, the performance is poor. On the other hand, when the visual input forms a part of the control algorithm at the lowest level, as in visual servo, the system performs well. Ideally, sensation and action need to be coupled at various levels of processing from fast acting low level control processes to slower but higher level perceptual processes.

2.2 Touch sensing

This section provides an overview of touch sensing in humans and robots. Both humans and robots have been equipped with several different types of touch sensors. These sensors have different characteristics and are used for different purposes in exploration and manipulation tasks. The following sections provide information about these different type of sensors and their applications in both man and machine.

2.2.1 The human sense of touch

The human ability to interact with the environment through the modality of touch is underscored by a variety of sensors located in the skin, the joints, and the muscles. All these sensors are tightly knit together by the nervous system at various levels leading to a high degree of sensory-motor integration.

The sensors present in the human skin are together referred to as the cutaneous receptors, and there are many different types of these sensors located at different depths within the skin. The sensors present in the joints and the muscles constitute a part of the kinesthetic system. These two types of sensors together are part of the haptic system [19].

There are four different types of cutaneous receptors present in the human skin [31]. These sensors have been extensively studied and characterized in the neurophysiological literature. The Meissner corpuscles and the Merkel disks are located just under the surface of the skin, and so provide a finer resolution of the stimuli acting on the skin. They have small receptive fields and are called type I sensors. The Meissner corpuscles respond better to rapidly changing stimuli and adapt quickly to slowly changing stimuli. Hence, they are called fast adapting type I sensors, or FA-I sensors. In contrast, the Merkel disks respond better to slowly changing stimuli and are called SA-I sensors. Buried deeper under the skin are the Pacinian corpuscles and the Ruffini endings. These sensors have larger receptive fields, i.e., they respond

to stimuli over a larger area on the surface of the skin, and they are called type II sensors. The Pacinian corpuscles respond well to rapidly changing stimuli and are called FA-II sensors while the Ruffini endings respond to slowly changing stimuli and are called SA-II sensors.

Owing to their different characteristics, each of these sensors is best suited to sense some particular parameter of the stimuli acting on the surface of the skin. Thus, FA-I sensors are useful for sensing skin stretch, whereas SA-I sensors are suited to sense curvature. Similarly, the FA-II sensors can sense vibration while the SA-II sensors can be useful for directional skin stretch.

In a recent paper, Johnson and Hsiao [36] have proposed that the SA-I sensors form the main spatial system and are responsible for tactual form and texture perception. The FA-II sensors are mainly responsible for sensing vibrations. However, if the skin is moving relative to the object and the surface variation is too small to be detected by the SA-I sensors, then the FA-I sensors become responsible for tactual form and texture perception.

Although the sensors themselves have been characterized extensively, the neural mechanisms responsible for human haptic perception and manipulation are currently not well understood. Hence, the human haptic system can only provide clues about the type of sensors that could be used in a robot manipulation system, and not about how to process and use the information derived from those sensors. Moreover, it is interesting to note that human tactile sensing involves the fusion of four different sensor types, while current robotic sensors typically use touch sensors of a single type.

2.2.2 Robot touch sensors

Many different types of touch sensors have been developed for robots. Broadly, contact sensors can be distinguished by whether they measure the distribution of some contact parameter over the area of contact or the average value of some parameter over the contact area [15]. Since stress, strain, and force are all tensor or vector quantities and have multiple components at any given point, these sensors can be further distinguished by the number of vector or tensor components sensed by them.

Force sensors [63] are usually mounted at the wrist of a robot manipulator and sense the three components of force and the three components of moment acting in a given frame. These sensors rely on several strain-gauges mounted within a mechanical structure. The force and torque components are related to the displacements sensed by the strain-gauges through a matrix that is obtained experimentally. These sensors find application in the many different force control schemes.

Smaller versions of these force sensors have been built and mounted within the fingertips of hands/grippers mounted at the wrist of a robot manipulator [11]. These sensors are close to the location of contact and thus provide more localized information about contact. These sensors are called Intrinsic Tactile Sensors.

In contrast, the third type of sensors measure the distribution of some parameter in the area of contact. These sensors are called tactile array sensors and they sense the distribution of stress (force) or strain (displacement) within the contact area. These

sensors have been studied extensively in the robotics literature and are discussed further in the remaining part of this chapter.

Some other sensors have also been reported in the robotics literature. The Skin Acceleration Sensor [33] is mounted just under the surface of the artificial finger to detect vibrations arising from contact, slip, and collisions. This sensor consists of an accelerometer and is similar to the FA-II sensors in the human skin. The Stress Rate Sensor [32] senses the changes in stress caused by the sliding motion between the fingertip and some object. This is similar to the FA-I type sensors in the human skin.

2.2.3 Tactile sensor technologies

Sensors employing many different transduction principles have been reported. For example, tactile sensors based on piezo-resistive materials, piezoelectric materials, capacitive materials, and optical principles, amongst others, have been built and characterized [54, 46, 47, 64, 31, 19]. The technology has matured enough that tactile array sensors are available commercially. For example, Interlink Electronics markets piezo-resistive tactile array sensors [34].

Most of these sensors provide a single component of stress (force) or strain (displacement). Recently, there have been attempts to build tactile array sensors that provide more than one component of stress or strain [40]. Detailed information about the different construction methods and transduction principles are provided in [64, 47, 46, 54, 31].

Figure 2.1 shows a diagram of the tactile sensor commercially available from Interlink Electronics in California. These sensors are piezo-resistive in nature. The substrate consists of a thin plastic sheet. Piezo resistive material is deposited on the sheet in a series of thin parallel lines, here sixteen. These are connected to thin metal wires or conductors that provide a connection for reading the sensor. The sensor itself is formed by overlaying two such sheets of plastic so that the lines of piezo-resistive material run across one another, thus forming a cross-point matrix. The resistance between a pair of conductors, one from each layer, is dependent on the applied force and decreases non-linearly but monotonically as the applied force is increased. Electronic interface circuitry is needed to select such a pair of wires, to prevent cross-currents, and to provide A/D conversion. The photograph on the right shows an image obtained from such a tactile sensor using 10-bit A/D conversion. The image, however, has only a few grey levels because of the limitations of the printer.

2.3 Models of tactile sensors

Most of the earlier work on tactile sensing ignored the issue of building mathematical models of tactile sensors. Techniques from the image processing literature were used to process tactile sensory data as an image. Fearing and Hollerbach [27] represents a first attempt at building a mathematical model of a tactile sensor to recover contact

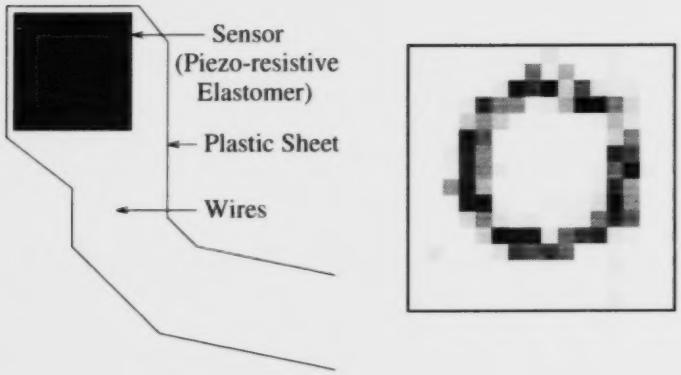

Figure 2.1: *A tactile sensor. (a) A diagram of the Interlink tactile sensor and (b) an image obtained from the sensor.*

parameters such as force and contact type from the stress distribution provided by a tactile sensor. This model was based on results taken from the mathematical theory of linear elasticity.

Since then, many other researchers have attempted to build and solve models of tactile sensors based on Elasticity theory. Fearing [27] reports the construction and verification of a tactile sensor based on model-theoretic consideration. Howe and Cutkosky [31] present a simple analysis of their stress rate sensor to show its effectiveness. De Rossi *et al.* [19] have used the technique of regularization to solve a model of the tactile sensor to recover the surface profile of an indenting object. Pati *et al.* [48, 49] present a neural network based approach to the same problem. The numerical solution of the model has also been explored by Speeter [60] and by Ricker and Ellis [53].

Within the framework of elasticity theory, there is a vast amount of literature on the problem of contact between two elastic bodies. In general, the problem is expressed as several simultaneous partial differential equations with the appropriate boundary conditions. Analytical closed-form solutions exist for only a few simple cases and are derived by making several simplifying assumptions. On the other hand, numerical techniques can be used to solve for more complex cases. This issue is considered in greater detail in the next chapter.

2.4 Touch in robot exploration and recognition

Several researchers have attempted to use tactile sensors mounted on robot end-effectors for a variety of tasks. The most common application domain has been object exploration and recognition.

An early application of tactile sensors was to explore unmodeled objects and characterize them. Based on experiments with humans, Lederman and Klatzky [41] proposed that humans explore unknown objects using touch by employing a set of stereotyped movements. These stereotyped movements are referred to as Exploratory Procedures, or EPs, and each EP provides information about some particular feature of the object, for example shape, texture, compliance etc.

Based on the work of Lederman and Klatzky, Bajcsy [7] describes some simple experiments using a tactile sensor mounted on a robot finger. In these experiments, the robot finger was actively used to acquire tactile sensory data, to be processed for features such as hardness, surface texture, and surface normals. These were the tactile primitives for which the robotic EPs were implemented. Based on this same general notion, Stansfield [61] designed a complex robotic system integrating touch and vision to characterize an object. The visual system was used to obtain the approximate location of the object to be explored and then the exploration was carried out using active touch. The system design was hierarchical with simple tactile primitives like elasticity, compliance, contact position, roughness, and contact type at the bottom of the hierarchy and more complex exploratory procedures higher up in the hierarchy and built on the simple primitive EPs. These complex EPs were responsible for determining object features such as surface shape, edges, corners, and semi-parts. Dario and Butazzo [18] also describe similar work. Allen [5] describes some more recent work based on EPs.

In contrast to the work reported above on exploration, the early work on object recognition using touch was based on the analogy between tactile sensory data from a tactile array sensor and a visual image. Hence, in these studies, the focus was on adapting image processing techniques to the processing of tactile images [47]. This approach focused on static tactile images and used various mathematical representations, for example, moment analysis, for classifying tactile images with the goal of object recognition. Hillis [28] describes a tactile sensing system consisting of a high resolution (16x16) tactile sensor mounted on a tendon-actuated finger and describes some simple experiments to recognize common objects such as nuts, bolts, and washers based on simple features such as shape, bumps, and stability of the object that can be acquired through the tactile sensor.

There has also been work in active recognition where the sensory data acquisition is an active process controlled by the current state of the process. Allen [6] describes work on object recognition based on vision and touch. The vision system is used to identify regions of interest on an object and touch is then used to explore each of these regions to build up a description of the object. The basic primitive for describing an object is the patch, a mathematical description of a surface patch on the object. The object description is then built up by specifying the relationships amongst the patches

constituting an object. Ellis [25] also describes a model-based recognition system. In this system, the next point to explore on a given object is determined from the model of the object built so far and the current tactile sensory data.

Other recent work on recognition focuses on recovering the shape of the surface that is in contact with the tactile sensor [26, 20]. This work is based on mathematical analysis of a model of the tactile sensor and uses various mathematical techniques to obtain the displacement profile on the surface of the sensor from the sensor output.

This work on robotic object exploration and recognition is important in that the notion of active touch is a central part of this approach. The perception of an object requires manipulation and touch in a synergistic manner. Berger and Khosla [8] describe an application of tactile sensors to edge tracking. In their system, the tactile sensory data is closely coupled to the control of the manipulator movement. The control scheme is hierarchical, with an inner control loop based on hybrid control and an outer control loop based on edge parameters derived from the tactile sensor. The tactile sensor also provides some force information for the inner control loop. Howe and Cutkosky [32] describe a system based on the Stress Rate Sensor that is used to detect fine surface features by sliding the sensor across the surface and relying on the stress rate information rather than the stress information. This work is based on an analysis of a model of the tactile sensor.

To summarize, two main points that can be derived from the above discussion are as follows. First, manipulation is often useful, and is sometimes required, in exploration and recognition tasks involving tactile sensing. Second, information from the tactile sensor can be used at many different levels in the hierarchical control system. For good system performance in a manipulation task, tactile sensory input must be tightly integrated into the innermost control loop.

2.5 Tactile sensors and manipulation

In contrast with the work done on using tactile sensors for object recognition, little work exists on using tactile sensors in manipulation. Dario [15] has classified manipulation into three broad categories according to the type of sensors that may be involved. These categories are gross motion, fine motion involving regular objects, and fine motion involving delicate objects. It is claimed that tactile sensors may have a role to play in the fine manipulation of delicate objects. Tactile array sensors provide information about the local, micro-level properties of contact, such as the distribution of force in the area of contact. In contrast, other touch sensors provide information about the macro-level properties of contact, such as the total force acting in a given frame.

An obvious application of tactile sensors is to recover information about the contact, such as the location and type of contact (point, line, or surface). Fearing and Hollerbach [27] present a detailed 2-d analysis of stress and strain for point, line and surface contacts. They assume a homogeneous elastic medium and they also assume that the tactile sensor readings are proportional to the strain. From this analysis,

they conclude that four sensors may be adequate for distinguishing between point and line contacts, and for determining the magnitude and direction of the contact force for the planar case.

Howe *et al.* [33] describe the use of a special type of tactile sensor — the Skin Acceleration Sensor (SAS). The SAS responds to vibrations and is able to detect vibrations generated by the making and breaking of contact and also the vibrations generated by slipping. This paper presents a simple experiment in manipulation that demonstrates that the SAS can be used to detect such phase changes during a manipulation task and this information can be used to select different force control schemes appropriate for the particular manipulation phase.

Bicchi *et al.* [12] describe the Intrinsic Tactile Sensor (ITS), a small six-axis force/torque sensor mounted in the interior part of the fingertip of a robot end-effector, and show its use in the control of grasping force. If the grasping force does not lie within certain bounds, the object being grasped will slip when the grasping force is less than the minimum required or be crushed when the grasping force is excessive. Bicchi *et al.* [12] outline a method to compute just the right amount of grasping force using an ITS. In a separate paper [11], Bicchi *et al.* show how contact location, contact force magnitude and direction can be obtained from an ITS when the shape of the contacting surfaces is known in advance.

Bicchi *et al.* [9] describe a system that integrates information from an ITS and a tactile array sensor to detect the onset of slip. This is an important application in that it shows that two different types of sensor can be integrated to obtain information that cannot be obtained from any one type of sensor alone.

Dario and Bergamasco [17] describe an integrated system (incorporating force and tactile sensors) that takes the pulse of a patient. In the ARTS laboratory at the University of Pisa in Italy, systems have been designed that can identify body structures by palpation [16]. These are based on models of the mechanical interaction between the robot end-effector and soft body tissue. The tactile sensors play an important role in detecting the pulse and hence, in the overall control of the entire process.

In contrast to the studies mentioned above, all of which involve the use of physical models, Houshangi and Koivo [30] present an approach to use tactile sensors for controlling a robotic manipulator. In experiments involving a rectangular block to be placed on a plane inclined surface, they use the tactile sensors to estimate the angle between the surface and the rectangular block. This estimate is then used as an input to the controller to command a rotation of the manipulator end-effector by the given angle to place the block vertically on the given surface. The relation between the tactile sensor output and the angle of inclination of the block with respect to the surface is obtained experimentally.

Recently, Maekawa *et al.* [43] describe a system that makes use of tactile sensors on a multi-fingered hand to manipulate an object. The task involves moving the object from one side to another while maintaining its vertical orientation. A kinematic analysis of rolling contact with multiple fingers is presented. This analysis is used

to derive a control algorithm for the task. The tactile sensors are used within this scheme to determine the contact location.

2.6 Discussion

This brief survey highlights several important aspects of manipulation and tactile sensing. First, the survey on manipulation suggests the need for tight coupling between sensing and action in the design of a manipulator system. Previous work has focused on planning the task while sensing has been relegated to the background. Second, in a similar vein, the work on force control has tended to assume that gross force in a given frame of reference needs to be controlled. Hence, the various force control schemes are difficult to apply to tasks where the local effects of distributed contact become important, and where the location of contact or the geometry of the object in contact is not known.

The survey on the human sense of touch shows that although this sensory modality has been characterized in detail, little is known about exactly how this modality functions in dextrous manipulation tasks. Thus, at best, we can take some pointers on the different type of sensors that may be required in building a robotic dextrous manipulation system.

The survey on robot exploration brings up some important issues as well. Robot exploration is an active process, and this implies that exploration and manipulation are not isolated procedures but interact with each other to obtain information about a given object or to accomplish a given task. Another issue is the organization of control processes. Tactile sensors provide information to a hierarchy of control processes, starting with basic contact information for low level processes to information about contact features for high level perceptual processes. So, the overall design of an intelligent manipulator system must be organized hierarchically with simple and fast control processes at the bottom and slower, perceptual processes at the top.

Finally, to derive useful information from the tactile sensor, there is a need to build models of the sensor that can predict the behavior of the sensor under different contact conditions. This knowledge can lead to the design of better tactile sensors and at the same time better control processes based on tactile sensory input.

This thesis focuses on two of the many aspects of tactile sensing mentioned above. First, the problem of analyzing contact is explored in great detail to better characterize the behavior of tactile sensors in contact with objects of different shapes under a variety of loading conditions, and in this sense, build a model for the tactile sensor. This is important for two reasons : (1) such models allow us to design better sensors, and (2) such models allow us to formulate model-based control strategies for contact tasks. In this thesis, the contact problem is surveyed in some detail and the finite element method is identified as a general and convenient method for studying contact problems. This method is then used to analyze different types of contact in great detail.

The second problem that is explored in this thesis is the design and implementation

of control processes that tightly couple tactile sensory input to manipulator motion. A new method to control manipulation tasks using tactile sensors is proposed. This method is called tactile servo and is based on the notion of visual servo. Tactile features, derived from tactile sensory data, are used directly to control the motion of a manipulator during a manipulation task involving contact.

Chapter 3

Finite element analysis of tactile sensors

Early work in the processing of tactile data using array tactile sensors was derived from image processing techniques, owing to the similarities in format between visual data and tactile data [45]. In both cases, sensory data consists of a two-dimensional array representing the spatial distribution of some physical quantity. However, the physical quantity represented in tactile images is radically different from the physical quantity in visual images and this has been considered in the more recent work [27, 26, 20], where an attempt is made to develop mathematical models of the tactile sensor to better characterize the information present in a tactile image.

Problems involving contact between deformable bodies have been extensively studied within the framework of the theory of elasticity [35]. The problem of contact between a rigid body representing an object and a deformable elastic medium representing a tactile sensor is considered in some detail in the Appendix. Several assumptions are made to obtain closed-form expressions for the stresses, strains, and displacements. An important and crucial assumption is that the elastic medium representing a tactile sensor is infinite. It is this assumption that allows the closed-form expressions to be obtained. It is also pointed out in the Appendix that if these assumptions are not made, then the problem becomes extremely complex and often closed-form expressions cannot be obtained.

The finite element method is used in this chapter to study the validity and applicability of these assumptions for the case of contact between a sensor and a knife edge, a rectangular bar, and a cylinder. It is shown that for tactile sensors these assumptions are not always valid and hence the closed-form expressions obtained by making these assumptions cannot be relied on in many cases. The finite element method is presented as a general and convenient method for theoretically characterizing the performance of tactile sensors.

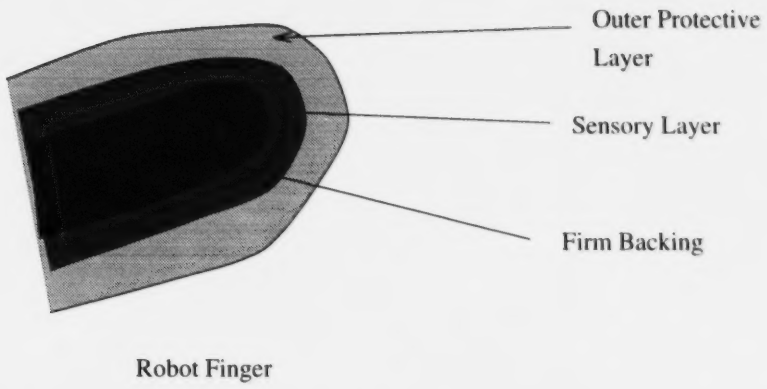

Figure 3.1: *A typical tactile sensor mounted on a robot finger.*

3.1 Introduction

Typically, tactile array sensors are mounted on the fingertip(s) of a robot manipulator. These sensors usually have several layers. The sensors (transducing elements) are located in the inner layers of the sensor while the outer layers are designed to provide protection for the sensor and some degree of compliance during contact. The design of the outer layer is governed by factors determined from the desired contact conditions and so the outer layer is normally constructed out of soft elastic material. The sensing elements are mounted on a hard innermost layer to provide for better sensing characteristics. This typical construction is shown in Figure 3.1.

When such a tactile sensor is in contact with an object or the environment, the outer layers of the sensor deform. This deformation is a function of the applied force, the geometrical shapes of the sensor and the object or the environment, and the elastic properties of the sensor and the object or the environment. This leads to the entire body of the sensor being deformed. A pressure distribution within the body of the sensor is also established. The transducers buried within the sensor detect some or all components of either the induced displacements or the induced pressure.

The problem of contact has been extensively studied within the framework of the theory of elasticity. Although the early work in tactile sensing did not consider models of tactile sensors and drew heavily from the literature in image processing, recently several authors have considered models of tactile sensors in the framework of elasticity theory. Fearing and Hollerbach [27] made an early attempt at using solid mechanics and basic contact theory to recover grasping information. They concentrated mainly on the problems of recovering information about line contact and distinguishing between line contact and plane contact. Speeter [60] considered the problem of contact between a rigid spherical object and an elastic medium. De Rossi *et al.* [19, 20] focused on the problem of recovering the contact profile caused by contact between an axi-symmetric indenter and an elastic medium from the stress information at a given depth.

In all the above studies, the elastic layer forming the outer protective layer (see Figure 3.1) in a tactile sensor is modeled as a semi-infinite elastic medium. Such a medium is also referred to as an elastic half space. The advantage of this assumption is that it simplifies the analysis of the model and often leads to closed-form solutions, as shown in the Appendix. This assumption is normally applicable when the contact is non-conforming [35]. Such contacts involve bodies with dissimilar profiles so that the area of contact between the two objects is small compared to the size of the objects. Therefore, the stresses do not critically depend on the shape of the bodies away from the contact area or the way in which the bodies are supported [35]. It is this property of contact that allows the treatment of the objects as semi-infinite elastic solids bounded by a plane surface. Such objects are also referred to as an elastic half space. The half space assumption simplifies the theoretical model and often makes it possible to obtain closed-form expressions for the stress distributions in the half space, as pointed out in the Appendix.

There are many cases in which it is not valid to apply the half space assumption to the contact between two objects. The two objects may have similar surface profiles and hence their area of contact may be comparable to their other dimensions. Alternatively, as in tactile sensors, one object may be a thin elastic layer. In that case, the thickness of the layer is comparable to even small areas of contact and the stress distributions in the area of contact become dependent on the thickness of the layer and on how the layer is supported.

When an object cannot be treated as an elastic half space, certain simplifying assumptions cannot be made in the model, as shown in the Appendix. As a result, it is not possible to obtain closed-form solutions to the model. Numerical methods must be used to solve the model in this case. This is well known and is treated in some detail by Alblas and Kuipers [2], Conway *et al.* [14] and Johnson [35], in the context of elasticity theory.

Several numerical methods can be used to solve contact problems once these have been properly specified. One method that stands out for its generality and its ease of use is the finite element method. In this method, the object under consideration is divided up geometrically into many small elements. The solution within each element is approximated by a function, usually a polynomial, in terms of the spatial distribution of the variable of interest. Each such function is specified in terms of several unknown constants depending on the differential equation governing the problem. These solutions are then substituted into the differential equation and lead to an expression that characterizes the total error in terms of these unknown quantities. This error is then minimized, leading to a system of algebraic equations that are a lot easier to solve than the differential equations. The system of equations is usually in terms of the values of the quantity of interest at certain points in each element. These points are called nodes. In elasticity problems, the displacements are taken as the unknown quantities to be determined. The system of algebraic equation can be solved using any standard method, such as Gauss elimination. The boundary conditions are defined in terms of the known quantities or their derivatives at the nodes. The finite

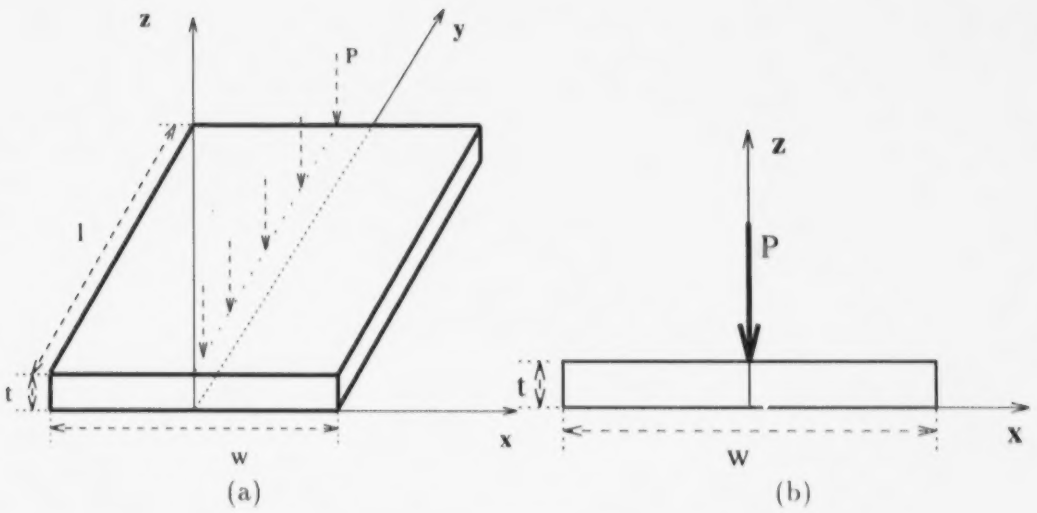

Figure 3.2: *A thin layer in contact with a knife edge.*

element method is a well established method in engineering and a discussion can be found in many standard texts, for example, Burnett [13].

The finite element method is a general method and can be used for solving a variety of problems. Elasticity problems involving nonlinear elastic materials, anisotropic materials, finite dimensions can all be solved using this method. Recently, Ricker and Ellis [53] have used this method to obtain the shear strain for reconstructing the contact geometry.

In this chapter, contact with a knife edge, a long cylinder, and a long rectangular bar, is examined using the finite element method and compared with the analytical results presented in the Appendix.

3.2 Contact with a knife edge

This is perhaps the simplest contact problem that can be considered. However, even for this problem, closed-form expressions cannot be obtained without making use of the half space assumption [58]. This problem is used here to illustrate the use of the finite element method in solving contact problems. Consider the simple case of a line load acting on a thin, rectangular piece of elastic material, as shown in Figure 3.2(a). The piece has thickness t, length l, and width w. The load P is uniformly distributed along the length of this piece. This corresponds to the contact between a tactile sensor and a long, sharp edge. The plane strain assumption can be used here and that simplifies the problem from three dimensions to two dimensions. With the plane strain assumption, analysis is focused on a cross-section of the bar. Figure 3.2(b) shows a two-dimensional view of the piece.

When a line load acts on an elastic half space, the plane strain assumption is used

to transform the elastic half space into an elastic half plane and reduce the number of stress components of interest from six to three. The closed-form expressions for the stress distributions within the half plane are presented in the Appendix (equations A.11 – A.13). These formulae were derived using the half space assumption and the plane strain assumption. The half space assumption implies that t, l, and w are all infinite. The plane strain assumption implies that l is infinite, which is consistent with the half space assumption. In these formulae, the x-axis of the coordinate frame lies along the surface of the half plane and the z-axis is perpendicular to the surface of the half plane. The load P is applied at the origin of the coordinate frame in the negative z direction and is uniform along the y-axis. No tangential load is applied to the half plane, i.e, $Q = 0$, and equations A.11 – A.13 reduce to:

$$\sigma_{xx} = -\frac{2P}{\pi}\frac{x^2 z}{(x^2+z^2)^2} \tag{3.1}$$

$$\sigma_{xz} = -\frac{2P}{\pi}\frac{xz^2}{(x^2+z^2)^2} \tag{3.2}$$

$$\sigma_{zz} = -\frac{2P}{\pi}\frac{z^3}{(x^2+z^2)^2} \tag{3.3}$$

where σ_{xx} is the normal stress component along x, σ_{zz} is the normal stress component along z, and σ_{yz} is the shear stress component in the $x-z$ plane. P is the line load per unit length acting on the half plane.

When one dimension becomes small compared to the other two, the half space assumption can no longer be used. For example, in a thin layer, $t \ll w$ and $t \ll l$. When the half space assumption is removed, it is not possible to obtain closed-form solutions for the stress distribution within the object and numerical methods must be used [2, 14, 35]. In the following, the finite element method is used to obtain the stress distributions for elastic layers of varying thickness and these distributions are compared with the closed-form expressions shown above to illustrate the use of the finite element method and to verify the validity of the various assumptions used to obtain the closed-form solutions, namely, the plane strain assumption and the half space assumption.

3.2.1 Effect of the half space assumption

This section presents a comparison between the stress distributions obtained numerically for a line load and the analytical expressions presented in the previous section (equations 3.1 – 3.3). The analytical solution was derived using the half space assumption. The stress distributions were obtained numerically for a thin elastic layer and for a thick elastic layer to study the effect of the half space assumption for line contact. The thick layer is closer to the half space assumption while the thin layer is a more accurate model of the outer layer used in tactile sensors. The plane strain assumption was used in both cases. The model used in finite element analysis of

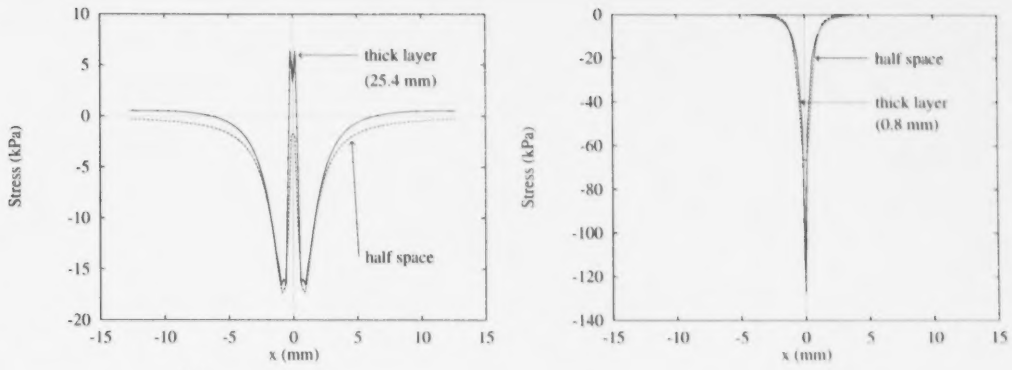

Figure 3.3: *A comparison of the stress distributions obtained using the half space assumption (equations 3.1 – 3.3) and a 25.4 mm thick layer. (a) σ_{xx}, the normal component of stress along x. (b) σ_{zz}, the normal component of stress along z.*

contact between a layer and a knife edge, corresponding to a line load, is shown in Figure 3.2(b). The stress distributions were obtained for elastic layers of thickness 25.4 mm and 0.8 mm. In this section, only the stress distributions at a depth of 0.8 mm within the medium were considered based on the premise that 0.8 mm is the depth at which the tactile sensors are located. The thickness of 0.8 mm corresponds to the thickness being used in our experimental system as well. The width of all elastic layers in this section was 250 mm.

Figure 3.3 shows the theoretical stress distributions at a depth of 0.8 mm for a half plane and for a 25.4 mm thick layer. Although the distributions are not identical, there is good agreement in the stress profiles obtained using equations 3.1 – 3.3 for a half plane and using the finite element method for a thick layer. The normal stress distributions along z, σ_{zz}, for a half plane and for a thick layer, agree closely (Figure 3.3(b)). The normal stress distributions along x, σ_{xx}, for a half plane and for thick layer, are also similar in their general shapes (Figure 3.3(a)). The distributions differ at the point of application where the finite element method yields higher values for the stress. The distributions also differ at the far ends away from the point of application of the force where the finite element method again yields higher values for the stress. However, the overall shapes are similar, indicating that the half space assumption can be used even for a layer of thickness 25.4 mm.

Figure 3.4 shows the stress distributions at a depth of 0.8 mm for the half plane and for a 0.8 mm thick layer. Here, the stress distributions are different. Figure 3.4(a) compares the normal component of stress along x, σ_{xx}, for a half plane and for a thin layer. According to the half space assumption, the stress is zero at the point of contact and has two symmetrical maxima at a distance of 0.8 mm away from the point of contact. In contrast, the distribution obtained from the finite element method has one maxima at the point of contact and decreases rapidly with distance from the contact point. The maximum values are also different. The maximum stress

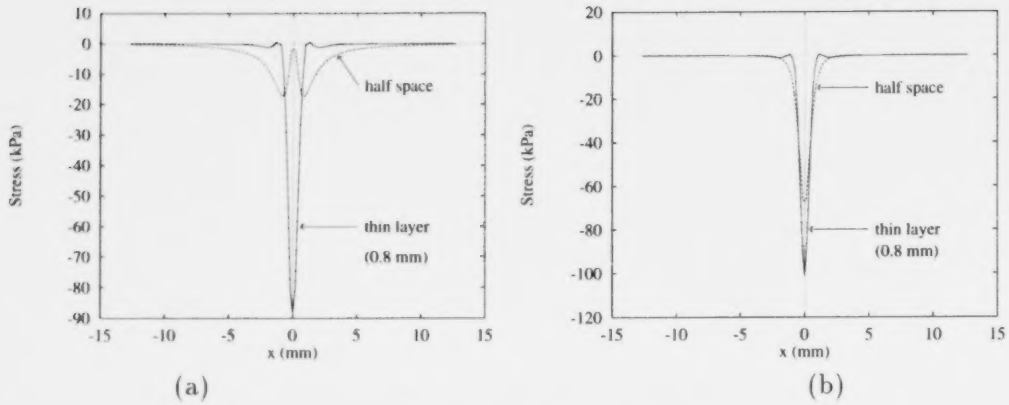

Figure 3.4: *A comparison of the stress distributions obtained using the half space assumption (equations 3.1 - 3.3) and a 0.8 mm thick layer. (a) σ_{xx}, the normal component of stress along x. (b) σ_{zz}, the normal component of stress along z.*

according to the half space assumption is about -18 kPa, while the maximum stress obtained from the finite element method is about -90 kPa. Figure 3.4(b) compares the normal component of stress along z, σ_{zz}, for a half plane and for a thin layer . The two stress distributions here are also different. The maximum stress obtained from the finite element method is about -100 kPa, while it is only about -65 kPa for the half plane. As the distance from the contact point increases, the stress for a half plane decreases rapidly and smoothly goes to 0. In contrast, the stress obtained using the finite element method decreases more rapidly and goes through an inversion. It becomes slightly positive, then becomes negative again before going to zero.

This shows that as the layer thickness is reduced, the validity of the half space assumption also decreases until, when the layer thickness becomes small compared to the layer width and the layer length, the half space assumption becomes invalid and the stress distributions obtained from the finite element method differ from the closed-form expressions. The difference in normal stress along the direction of the applied force is not significant, however, the difference in stress distributions along the direction tangential to the layer are significant.

3.2.2 Effect of the plane strain assumption

In this section, the effect of the plane strain assumption on the resulting stress distributions is studied. The stress distributions for two layers of varying thickness (25.4 mm and 0.8 mm) and fixed width (25.4 mm) are obtained using the finite element method and the plane strain assumption. The stress distributions are also obtained for the same two layers without the plane strain assumption. Here, the model becomes 3-dimensional and the layers are assumed to be 25.4 mm in length. The stress distributions now vary along the length of the layer as well. For comparison, consider a cross-section in the $x - z$ plane in the middle of the layer along x. This is the area

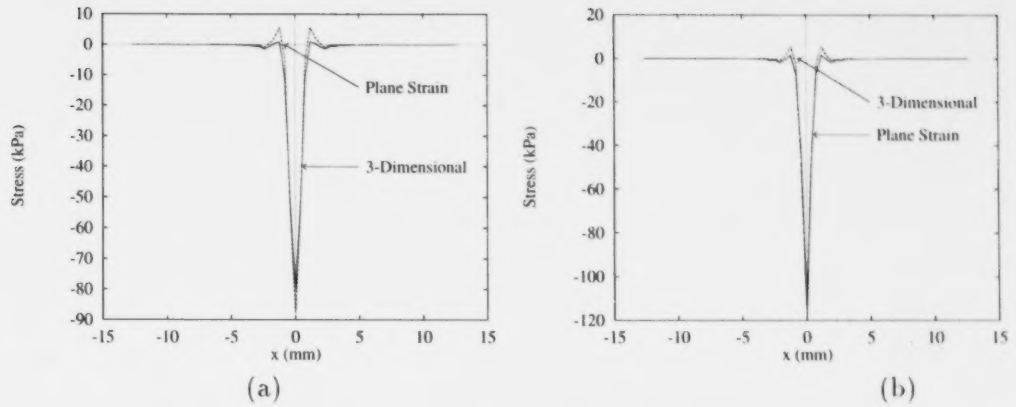

Figure 3.5: *A comparison of the stress distributions obtained with and without using the plane strain assumption for a thin 0.08 cm elastic layer. (a) σ_{xx}, the normal component of stress along x. (b) σ_{zz}, the normal component of stress along z.*

in the 3-dimensional model where the conditions of plane strain are most closely met.

Figure 3.5(a) shows the distributions corresponding to the normal components of stress along x, σ_{xx}, obtained using the finite element method with the 2-dimensional model assuming plane strain and the 3-dimensional model, both for a thin 0.8 mm elastic layer. Similarly, Figure 3.5(b) shows the stress distributions along z, σ_{zz}. Figures 3.6(a) and (b) show the corresponding stress distributions for a thick 25.4 mm elastic layer.

Although the distributions are not identical, Figures 3.5 and 3.6 show that for the dimensions involved, the plane strain assumption has minimal effect on the stress distributions at the center of the sensor. For simplicity and clarity of the presentation, the plane strain assumption is retained. Illustrations showing the stress distributions can be better appreciated with the plane strain assumption than without it since the plane strain assumption focuses attention on a plane. Furthermore, the plane strain assumption does not qualitatively change the major conclusions to be made in the rest of the thesis. Since the plane strain assumption requires the object being modeled to be infinitely long along the direction normal to the plane, all forces are expressed in terms of units of force per unit length, for example N/mm.

3.2.3 Discussion

In this section, the use of the finite element method in solving contact problems was shown. For thick layers, it was found that the solutions were close to the closed-form expressions obtained using the half space assumption. The finite element method allowed the layer thickness to be varied with ease and hence, the effect of layer thickness on the stress distributions could be studied. It was found that the behavior of a thin layer is different from that of a thick layer and therefore, the half space assumption is not valid for modeling thin layers. Since closed-form solutions do not exist for

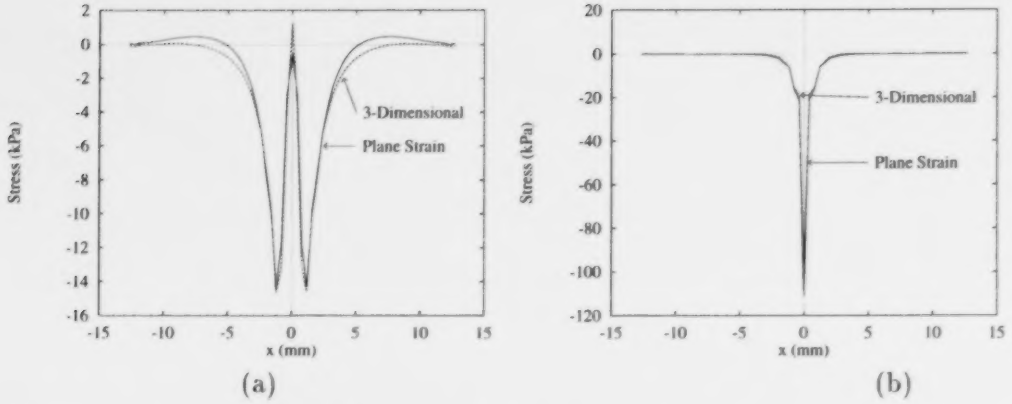

Figure 3.6: *A comparison of the stress distributions obtained with and without using the plane strain assumption for a thick 2.54 cm elastic layer. (a) σ_{xx}, the normal component of stress along x. (b) σ_{zz}, the normal component of stress along z.*

thin layers, the finite element method provides an easy and general way to study the behavior of thin layers.

The closed-form expressions for a half plane show a singularity at the origin where the load is applied. Since the finite element method is providing a numerical solution of the same boundary-value problem, it is instructive to consider its behavior near singularities. When there is a singularity in the problem definition, the solution obtained by the finite element method near the singularity is not accurate and special techniques are required to model singularities using this method [13]. This is so because the finite element method uses polynomials to approximate the displacements within each element and polynomials cannot properly be used to model singularities. However, a singularity is usually because of a mathematical idealization. In practice, if the mesh is small enough, the knife edge can be modeled as some smooth shape with a small radius. In this sense, the approximate behavior of the finite element method could actually be an advantage.

3.3 Contact with a flat rectangular bar

This section compares the stress distributions resulting from contact with a flat rectangular bar obtained using the finite element method with the stress distributions obtained using the half space assumption in the Appendix (equations A.16 – A.17). This type of contact is more complicated than the contact with a knife edge studied in the previous section and the effect of the layer thickness on the stress distributions is more pronounced. It will be shown that for contact with a flat rectangular bar, the half space assumption leads to radically different stress distributions compared to those obtained by the finite element method for a thin layer.

3.3.1 Effect of the half space assumption

The finite element method was used to obtain the stress distributions for layers of varying thickness to study the effect of using the half space assumption. These distributions were then compared with the closed-form expressions based on the half space assumption and presented in the Appendix. Figure 3.7 illustrates the model used in this case. The applied load was maintained at a fixed value of about 1.96 N/mm directed along the negative z direction, while the layer thickness was varied from 12.7 mm to 0.8 mm. The stress distributions at the surface and at a depth of 0.8 mm were compared.

Figure 3.8 shows the normal stress distributions on the surface of the layer in the direction of the applied load. The difference between the closed-form solution and the finite element method is small for the thick layer. At the edges of the area of contact, the stress is infinite according to the closed-form solution and the stress distribution obtained from the finite element method follows it closely. However, as the thickness of the layer is reduced, the difference between the two distributions becomes large. For a thin layer, the distributions are radically different. For example, using the half space assumption, the stress is minimum towards the center and increases to infinity at the edges of the contact. It is zero outside the area of contact. In contrast, using the finite element method, the stress distribution for a thin layer is maximum at the center and reduces continuously to zero outside the area of contact, with a discontinuity near the edges of the indenter.

Figure 3.9 illustrates the effect of varying the layer thickness on the sub-surface stress distribution at a depth of 0.08 cm within the elastic medium. Again, there is a large difference between the stress distribution obtained for a thin layer using the finite element method and for a half space. According to the closed-form solution for a half space, the stress is small in the center and increases as the edges of contact are approached. There is a discontinuity near the edges and then the stress reduces slowly as the distance from the edge of the contact increases. This discontinuity arises from the discontinuity in the stress distribution on the surface, as the sub-surface stress distribution is obtained by summing up the effects of the surface stress distribution. In contrast, according to the finite element solution for a thick layer, although the stress profile is similar to that of the half space, the stress is generally higher within the area of contact and falls rapidly to zero as the distance from the edges of the contact is increased. Furthermore, as the layer thickness is decreased, the stress profile changes radically. The stress is maximum in the center and reduces gradually towards the edges of contact, falling rapidly to zero beyond the edges of the indenter.

This clearly shows that the half space assumption is inappropriate for the analysis of contact between a thin layer and a flat rectangular bar. The half space assumption is valid when the size of the contact area is small compared to the size of the bodies in contact. As an example, for contact between an elastic layer and a flat rigid indenter, the validity of the half space assumption depends on the ratio of the thickness of the layer to the width of the indenter. As long as this ratio is large, the half space

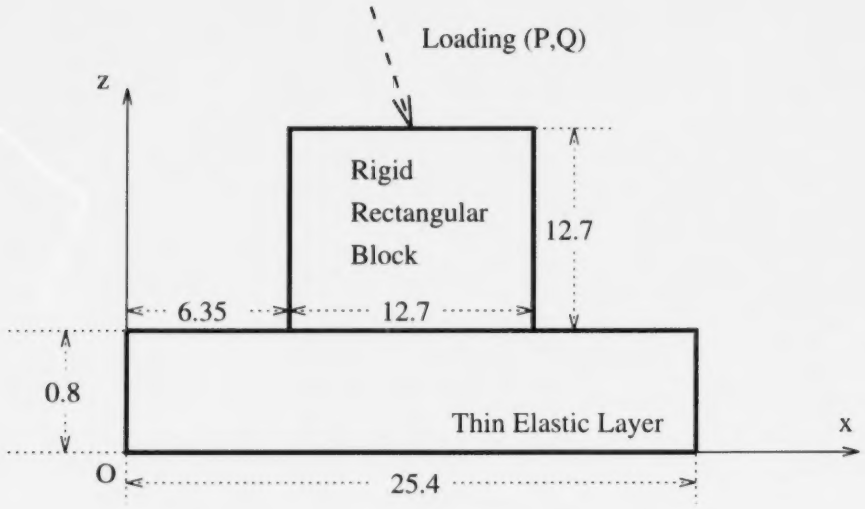

Figure 3.7: *The dimensions of the objects used in this study. All measurements are in mm.*

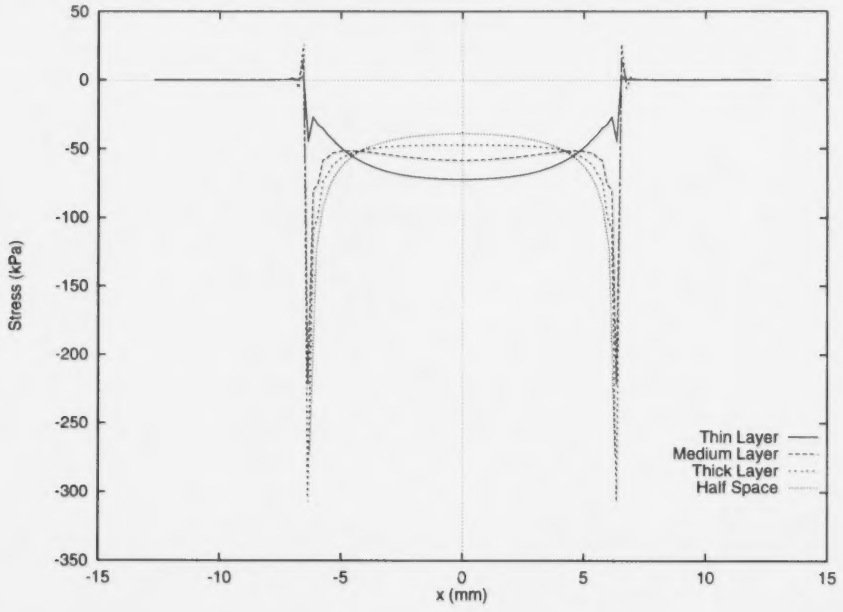

Figure 3.8: *The effect of varying the layer thickness. The normal stress distribution along z, σ_{zz}, on the surface of the sensor, is shown for layer thickness of 12.7 mm, 6.35 mm, and 0.8 mm.*

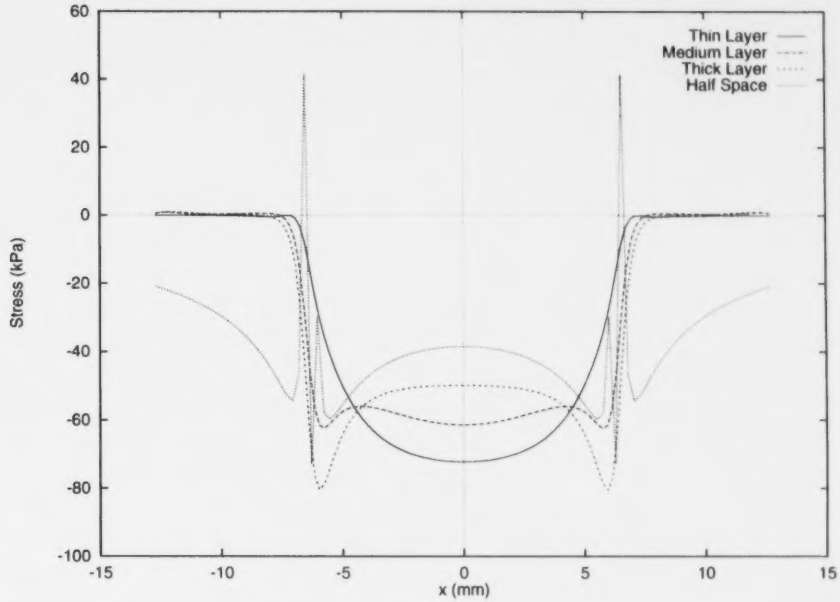

Figure 3.9: *The effect of varying the layer thickness. The normal stress distribution along z, σ_{zz}, within the medium at a depth of 0.8 cm, is shown for layer thickness of 12.7 mm, 6.35 mm, and 0.8 mm.*

assumption remains valid. As this ratio becomes smaller, the results using the half space assumption can no longer be used. This is shown by comparing the stress distributions obtained analytically using the half space assumption and by using the finite element method for a thick layer and for a thin layer.

Figure 3.8 compares the stress distribution on the surface. The stress distributions are similar for the half space and for the thick layer. However, for the thin layer, the stress distribution is radically different from the half space. The same effect can be observed for sub-surface stresses, as shown in Figure 3.9. The sub-surface stress distribution, obtained from the closed-form expression shown in Equation A.17 in the Appendix, exhibits a strange behavior. There is a sharp peak around the edges of the contact, and the stress becomes positive. When the plot is restricted to just this region, it is found that the stress distribution around the contact edge oscillates several times between positive and negative values. This is an artifact that is introduced into the solution because the pressure distribution at the surface becomes infinite at the corners of the flat rectangular bar.

The radical difference in the forms of the sub-surface stress distributions obtained using the closed-form expression and the finite element method, has important implications for the modeling of tactile sensors, especially when the surface deformation profile is to be obtained from sub-surface stress or strain [20]. If the tactile sensor is accurately modeled as a thin layer, then the analysis based on the half space assumption will be inaccurate.

This effect also points out a major advantage of using the finite element method. The finite element method is more generally applicable and provides accurate results for problems that do not have any closed-form solutions that can be analytically obtained. For example, closed-form solutions for the contact between a thin layer and a flat rigid indenter cannot be obtained [58]. For this case, solutions have been obtained numerically [14] and by analytical approximations [2].

3.4 Contact with a long cylinder

Edge contact and contact with a flat rectangular bar represent two extremes amongst the many different contact shapes possible. Contact with a long cylindrical object is analyzed in this section as a third type of contact that lies somewhere between the two extremes mentioned above.

The closed-form expressions for the surface pressure and the sub-surface stress distribution are presented in the Appendix. The finite element method was used, as in the previous section, to analyze the stress distributions resulting from contact with a thick layer and with a thin layer. The finite element model was similar to that for the flat rectangular bar. The only difference was that the indenter shape was circular rather than a straight line. The cylinder had a radius of 25.4 mm and three layers of thickness 0.8 mm, 3.2 mm, and 12.8 mm were considered. The elastic properties were identical to those used for the contact with a flat bar.

The stress distributions are compared in Figures 3.10 and 3.11. Here, the difference between the distributions obtained using the half space assumption and the distributions obtained from the finite element method is not as drastic as that for the contact with the flat bar. There is almost no difference in the distributions obtained for the layers of thickness 3.2 mm and 12.8 mm. The peak value of stress is higher for the thick and medium layers compared to the half space and even higher for the thin layer. Thus, the peak stress is a function of the layer thickness and this effect cannot be modeled by the half space.

3.5 Discussion

The half space assumption is an extremely important step in the solution of elasticity problems since it makes it possible to obtain closed-form solutions for these problems. Simply stated, the assumption specifies that all stresses and strains within the elastic medium vanish at large distances from the area of contact. The parameters of the problem being considered determine the distance beyond which the stresses and the strains are negligible. Mathematically, this assumption is stated by specifying that the elastic medium is infinitely large, and that the stresses at infinity are zero. Such a medium is called a half space or a semi-infinite elastic medium. The assumption greatly simplifies the boundary conditions and it is this simplification that allows closed-form solutions to be obtained for several contact conditions. When this as-

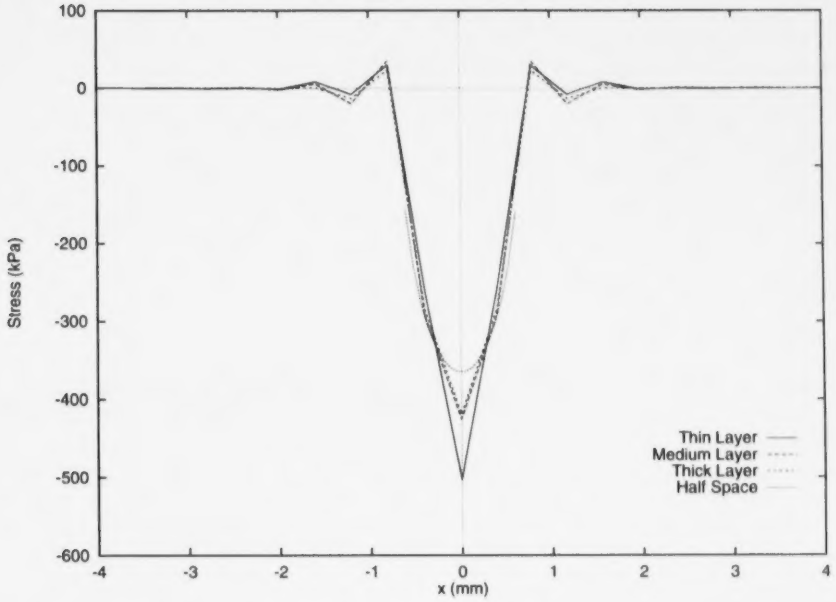

Figure 3.10: *The effect of varying the layer thickness. The normal stress distribution along z, σ_{zz}, on the surface of the sensor, is shown for layer thickness of 0.8 mm, 3.2 mm, and 12.8 mm, and a half space.*

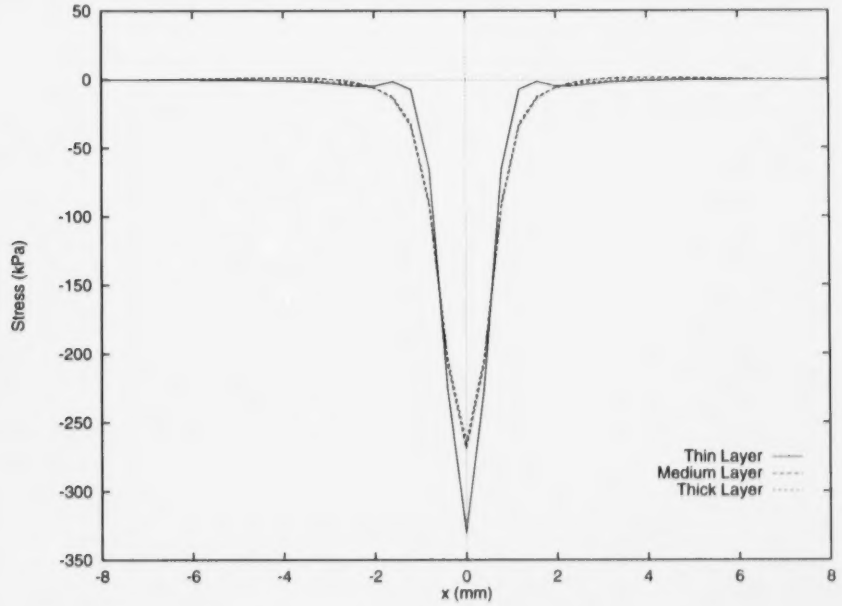

Figure 3.11: *The effect of varying the layer thickness. The normal stress distribution along z, σ_{zz}, within the medium at a depth of 0.8 mm, is shown for layer thickness of 0.8 mm, 3.2 mm, and 12.8 mm.*

sumption cannot be made, it is usually difficult to obtain closed-form solutions [58]. For example, Sneddon [58] states that closed-form solutions for a thin strip cannot usually be obtained. Some approximate solutions for a thin strip are presented in the work by Alblas and Kuipers [2].

This chapter considered the contact between a tactile sensor modeled as an elastic layer and an object modeled as a rigid indenter with a simple profile. The plane strain assumption was used to simplify the problem to two dimensions. The finite element method was used to obtain the stress distributions for a sharp indenter, a circular indenter, and a flat indenter. A thin layer and a thick layer were used to study the effect of layer thickness on the stress distributions. The results were compared with the closed-form expressions based on the half space assumption and presented in the Appendix. It was found that the stress distributions for the thin layer were different from those obtained for a thick layer and for a half space, thus indicating that the half space assumption is not valid for modeling tactile sensors covered by a thin elastic layer.

The analysis in this chapter shows that the finite element method provides a good basis for studying contact problems, since it provides solutions for the thin layer for which closed-form expressions cannot be obtained. Furthermore, this method can also be used for 3-dimensional analysis where many mathematical techniques, for example complex analysis [58], that apply to the two-dimensional problems cannot be generalized.

Chapter 4

Analyzing contact with tactile sensors

4.1 Introduction

In the previous chapter, it was shown that the half space assumption leads to an incorrect characterization of contact with a tactile sensor. This chapter uses the finite element method to analyze the contact between a tactile sensor modeled as a thin elastic layer and different objects modeled as rigid indenters of simple profiles. A rigid indenter with a sharp edge, a circular profile, and a flat rectangular profile are considered. The stress distributions are obtained for a variety of forces applied to the indenter. The purpose of this analysis is to study the variation of the stress profiles corresponding to different indenter shapes and applied loads and to infer properties of these stress distributions that could be predictive of the applied force and indenter shapes.

Several features are identified and the moments associated with the normal stress distribution are found to vary monotonically but non-linearly with the applied loads. These are found to be useful in developing a new approach to tactile sensor-based manipulation. Several finite element models are considered to study the contact with objects of different shapes and a general technique is presented that can be used for analyzing contact with objects of any given shape in three dimensions.

Such an analysis is important for the following reason. Typically, tactile sensors are mounted on the fingertips on a dextrous hand. In a manipulation task, the object is gripped by the robot and the tactile sensors are used to sense the contact between the gripper and the object. The response of a tactile sensor is dependent on the external forces acting on the object because of contact with the environment. In an exploration task such as following an edge using a tactile sensor [8], the response of the tactile sensor depends on both the contact geometry and the contact forces. It is important to characterize the relationship between the applied forces, the contact geometry, and the resulting stress distribution to control these tasks and to obtain useful information from exploration.

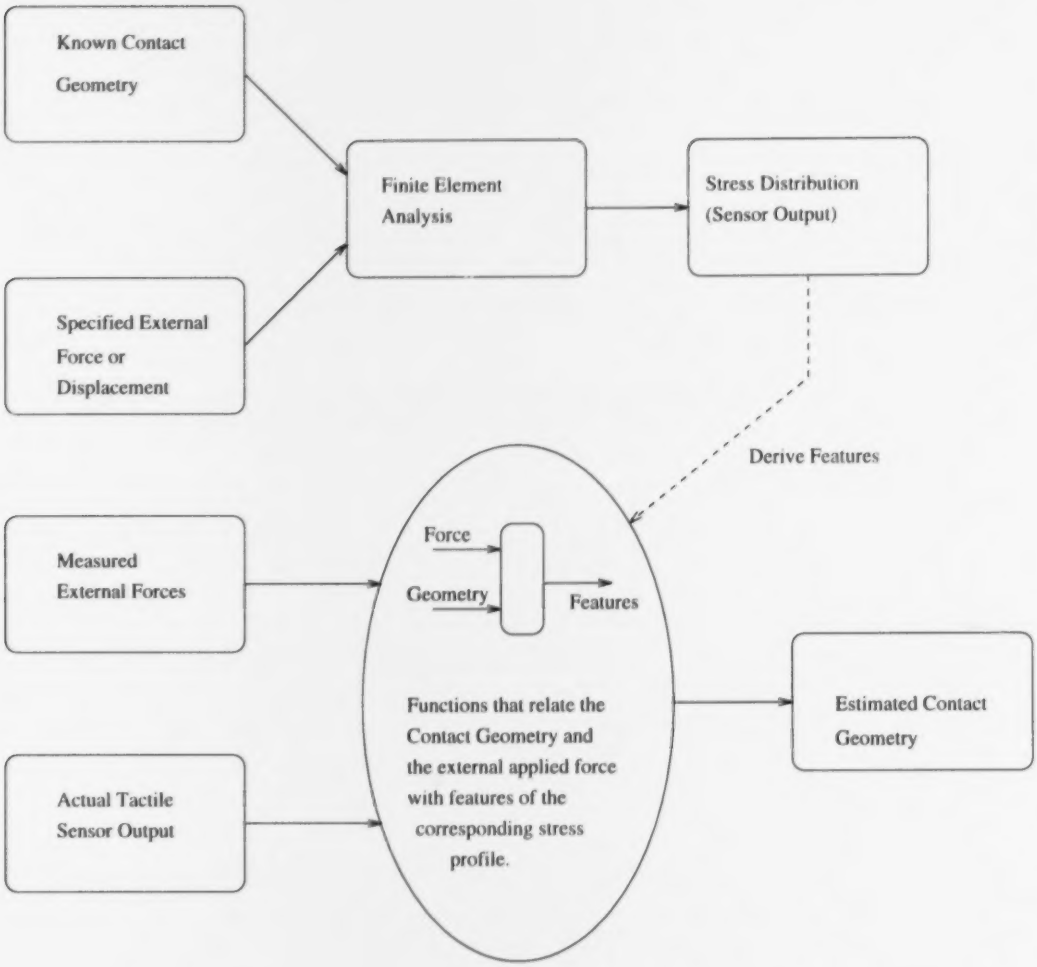
Known Contact Geometry
Finite Element Analysis
Stress Distribution (Sensor Output)
Specified External Force or Displacement
Derive Features
Force
Geometry
Features
Measured External Forces
Functions that relate the Contact Geometry and the external applied force with features of the corresponding stress profile.
Estimated Contact Geometry
Actual Tactile Sensor Output

Figure 4.1: *An approach to characterizing and using tactile sensors.*

Figure 4.1 shows the general approach used in this thesis for analyzing the contact between a tactile sensor and a given object, and for using this information to control a particular task involving contact between the tactile sensor and the given object.

This chapter presents an analysis of contact between a thin elastic layer and three different rigid indenters — a sharp edge, a cylinder, and a flat bar. Section 2 presents an analysis of line contact. Using the expressions presented in the Appendix and derived from the half space assumption, a relation is derived between the moments of the stress distribution and the relative displacement of the edge with respect to the sensor. The presentation is used to point out weaknesses of the method. A relation between the moments and the displacements is then derived numerically from the stress distributions obtained by solving the finite element models. Section 3 presents an analysis of contact with a flat rectangular bar. A finite element model

is presented along with an analysis of the stress distributions obtained from it. This is used to derive relationships between the force acting on the indenter and several features of the resulting stress distribution. An analysis of contact with a cylinder is presented in Section 4. A more general model of contact and also a method to derive relations between displacements and resulting sub-surface stress distributions is presented. Section 5 presents a discussion on the applicability of the superposition principle. Finally, the chapter concludes with a summary and a discussion.

4.2 Line contact

In this section, contact between a tactile sensor and a straight, sharp edge is studied in detail to characterize the response of a tactile sensor for different applied loads. This is the simplest type of contact that can be studied. The exploration task of following an edge [8] is an example that provides a motivation for studying this type of contact. The task of following an edge requires the computation of the position and the orientation of the edge with respect to the end-effector so that it can maintain a desired position and orientation and also maintain a desired force with respect to the edge.

The expressions for normal stress distribution for the case of two-dimensional line contact are presented in the Appendix. Since most tactile sensors measure only the component of stress that acts normal to the sensor surface, σ_{zz} is the only component of stress considered in this chapter. The closed-form expression based on the half space assumption is reproduced below (equation A.12):

$$\sigma_{zz} = -\frac{2P}{\pi}\frac{z^3}{(x^2+z^2)^2} - \frac{2Q}{\pi}\frac{xz^2}{(x^2+z^2)^2}$$

Here, the stress distribution is a function of the applied normal force P, the applied tangential force Q, the position of the sensor specified by its depth z and the x coordinate, and the specified geometry of the indenter — a sharp edge. Since x and z are determined by the sensor construction, the problem can be specified as finding P and Q from the stress distribution provided by the sensor.

Normally, a tactile array sensor consists of several individual sensing sites called tactels distributed over a small area. Each tactel provides a sample of the stress distribution at its location. Since only two parameters are required, any two tactels can be used to obtain two equations from the expression shown above. These equations can then be solved to obtain P and Q, and this is similar to the method followed in [27]. This indicates that a tactile sensor with only two tactels should be sufficient for the purpose of obtaining P and Q. However, the objective of this thesis is to explore the use of tactile array sensors. Since an array sensor consists of a number of tactels, one possible method to obtain P and Q would be to solve for P and Q using all pairs of tactels in the tactile array sensor. For a sensor with n tactels, $n(n-1)/2$ values for P and Q would be obtained. An estimate of P and Q can be obtained from these values using techniques from sensor fusion [1]. A major limitation of this approach

is that it becomes difficult to apply as the number of parameters to be obtained increases. As Fearing and Hollerbach show in [27], if the location of contact is also required, three sensors need to be used and the equations become non-linear.

An alternative method is to derive features from the stress distribution that vary in a well-defined manner. Consider, for example, the moments of the stress distribution, as defined below:

$$M_n = \int x^n \sigma_{zz}(x) dx.$$

Here, M_n refers to the n-th order moment of the function σ_{zz} and x is the independent variable.

Using this definition and the expression for the stress distribution σ_{zz} shown above, and assuming that the contact is centered around the origin, the following expressions for the zeroth order moment, M_0, and the first order moment, M_1, can be obtained:

$$\begin{aligned} M_0 &= \int \sigma_{zz}(x) dx = -P \\ M_1 &= \int x \sigma_{zz}(x) dx = -Qz \end{aligned}$$

Thus, the applied force can be easily recovered from the stress distribution by choosing the first two moments of the stress distribution as the features. Other features can also be considered. For example, consider the value of x for which the stress σ_{zz} is maximum. This point, called x_m, varies as a function of the applied load. The function can be obtained by minimizing the stress using equation A.12. Solving,

$$\frac{d\sigma_{zz}}{dx} = 0,$$

the following expression can be obtained from the resulting quadratic equation:

$$x_m = \frac{z\sqrt{4P^2 + 3Q^2} - 2Pz}{3Q}.$$

When Q is zero, an indeterminate form results which can be evaluated in the limit to yield zero, which is consistent with the symmetry of the stress distribution in the absence of a tangential force.

However, unlike the moments, x_m is related non-linearly to both P and Q. From the expressions above, the two moments provide a simple way to recover the applied force from a stress distribution in the case of edge contact with a half space, and so they are good features in this way. If the location of contact is also not known, then the three features have to be used together. In this case, the equations become non-linear. However, compared to the eight-order polynomial equation that Fearing and Hollerbach [27] need to solve to obtain the contact location, using these three features, M_0, M_1, and x_m, requires the solution of a quadratic equation.

Often, it is desirable to study the relative displacements of the indenter with respect to the tactile sensor. This is especially so when the manipulator is being controlled using position rather than force. Here, a relationship between the relative movement and the changes in the resulting sub-surface stress distribution can be used to control the movement of the manipulator using the output of the tactile sensor.

The expressions relating the displacements to the applied force are shown in the Appendix, Equations A.14 – A.15. If the elastic layer is made of rubber, i.e., $\nu = 0.5$, and if the displacements are measured at a given depth h and directly under the point of application $x_1 = 0$, and the first two moments of the stress distribution are used instead of the applied force, then the following simplified expressions can be obtained:

$$u_{z0} = -\left(\frac{2(1-\nu^2)}{\pi E}\ln\frac{d}{h} + \frac{(1+\nu)}{\pi E}\right) M_0 \tag{4.1}$$

$$u_{z1} = -\left(\frac{2(1-\nu^2)}{\pi E}\frac{1}{h}\ln\frac{d}{h}\right) M_1 \tag{4.2}$$

Here, d is arbitrary and is assumed to be large with respect to the dimensions of the object being considered.

The expressions presented here are based on a number of simplifying assumptions. First, they are all based on the half space assumption. It was shown in the previous chapter that the half space assumption is not valid in general, and the disparity between the stress distributions obtained using this assumption and those obtained using the finite element method for thin layer increases as the layer thickness is reduced. Second, it is assumed that the tactile sensors can measure tensile as well as compressive stress. However, many tactile sensors can only measure compressive stress. These assumptions limit the applicability of the expressions presented above. Another limitation of the approach presented above is that it requires the existence of closed-form expressions for sub-surface stress. Such expressions exist only for the simplest type of contacts and are derived using the half space assumption.

The finite element method provides an alternative way to analyze contact without making any of the simplifying assumptions mentioned above. The model described in the previous chapter was used to study the stress distributions corresponding to different applied forces. Figure 4.2 shows the stress distributions obtained when only a normal force is applied to the knife edge. The stress distributions are symmetric about the line of application of the load. The peak stress increases with increasing normal force.

Figure 4.3(a) shows the effect of varying the normal force P when the tangential force Q is maintained at a constant value, while Figure 4.3(b) shows the variation in stress distribution when the normal force P remains constant and the tangential force Q is varied. Once again, the peak value of the stress depends on the applied normal force and does not vary with the applied tangential force. However, the tangential force leads to a stress distribution that is asymmetric about the line of applied load. The degree of asymmetry, measured by the distance between the line of applied load

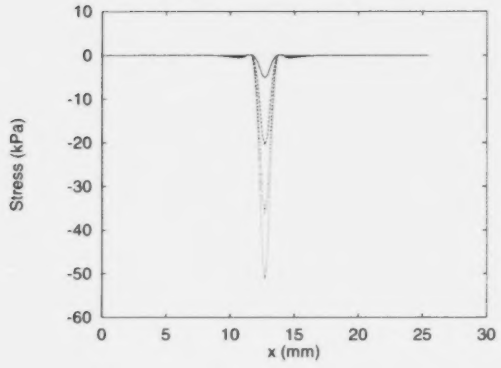

Figure 4.2: *The variation in the sub-surface stress profile for increasing normal force with no tangential force.*

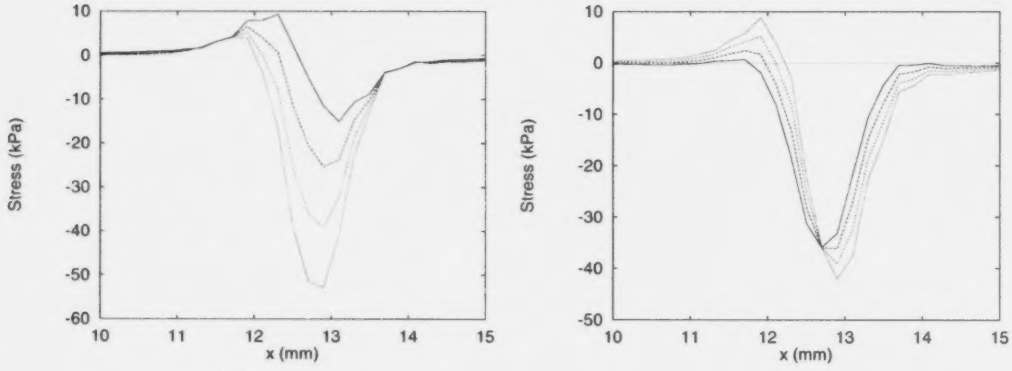

Figure 4.3: *The variation is stress distribution (a) with increasing normal force for a constant tangential force, and (b) with increasing tangential force with constant normal force.*

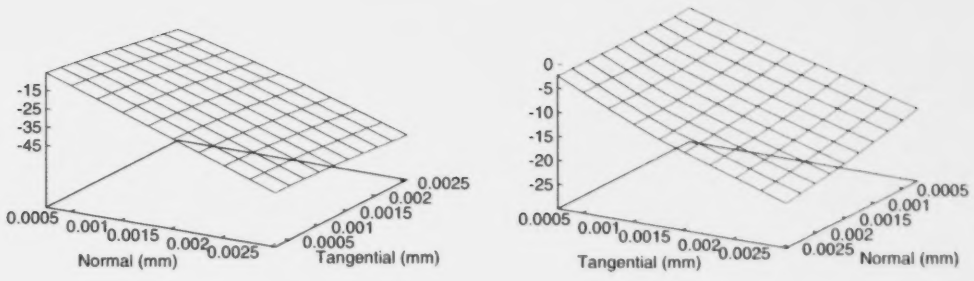

(a) (b)

Figure 4.4: *The moments (a) M_0 (N/mm) and (b) M_1 (N) as a function of the relative displacements.*

and the position of the peak stress or the first moment of the stress distribution about the line of applied load, depends on both the normal force and the tangential force.

The stress distributions obtained for different loads were used to compute the zeroth and the first moment of the stress about the line of applied load. In computing these moments, only the negative values of stress, i.e. compressive stress, were used to satisfy the constraint that the tactile sensor cannot measure tensile stress. This is a limitation of the finite element model considered here. The behavior of a real tactile sensor depends on the construction of the sensor and on how the different layers are bonded together. For example, in the piezo-resistive sensors used in this work, the two layers forming the sensor are not bonded together and so they can slide or delaminate, depending on the direction of the tensile stress. Figure 4.4 shows the relation between the moments of the stress distribution and the relative movement of the manipulator and the sensor. As the figure shows, the zeroth moment varies almost linearly with the normal force and is independent of the tangential force while the first moment varies with both the normal force and the tangential force.

4.3 Contact with a rectangular bar

This section considers the contact between a tactile sensor and a flat object, as shown in Figure 3.7. As mentioned before, contact with a flat rectangular bar represents the other extreme in the space of different contact types. The geometry of the object in the area of contact is an important determinant of the stress distribution. For example, the stress distribution obtained for contact with a flat object is different from the stress distribution obtained for contact with a cylindrical object, all other factors remaining constant. The method presented here can easily be used to analyze any other contact geometry that may be of interest. The protective layer on the sensor is modeled as a thin elastic layer and no closed-form solutions have yet been

identified. The finite element method is used to analyze the model under different conditions.

To analyze the effect of tangential forces on contact, a model of friction is required, and a simple local model of friction is used [38]. Also, it is assumed that in the area of contact, the force due to friction at any point within the area of contact is proportional to the normal force at that point. This is not strictly true since it is the maximum tangential force before slip occurs that is proportional to the normal force with the coefficient of friction as the constant of proportionality. Hence this is a limitation of the model. Another limitation of the model is that it is assumed that no slip occurs within the area of contact. The largest ratio of Q/P in this study is 1 and so the coefficient of friction must be larger than 1. The coefficient of friction for rubber is typically greater than 1. Since the system is in static equilibrium, the total force because of friction must equal the applied tangential force. The final solution is obtained iteratively until the normal and tangential forces within the area of contact become stable. Figure 4.5 shows the difference between the stress distributions obtained by using the simple model of friction described above and by rigidly constraining motion in the tangential direction (the rigid constraint provides the tangential reaction force needed for static equilibrium). The elastic constants associated with the boundary elements that are used to constrain rigid body motion are very small. So, after the iterative process ends, the forces in the boundary elements are negligible.

It must be pointed out here that the force is applied to the center of the indenter at the top. The length of the indenter is 6.35 mm. Hence, the tangential force leads to an additional moment in the area of contact. Therefore, in this study, when the applied tangential force is varied, there is a variation in the tangential force and the moment in the area of contact. Since the length of the indenter remains constant, the increases in the tangential force and the moment are proportional. In the remaining discussion, a tangential force refers to the force applied on the top of the indenter and implies tangential force as well as a moment in the area of contact.

Figure 4.6 shows the normal component of the stress tensor σ_{zz} for different normal forces applied to the object. When only normal force is applied to the object, the normal stress profile is symmetrical. It is near zero outside the area of contact, increases rapidly near the boundaries of the area of contact, and peaks in the middle of the area of contact. The peak value increases monotonically with applied normal force. Figure 4.7 shows the normal component of stress σ_{zz} when both normal and tangential forces are applied to the object. Figure 4.7(a) shows the change in stress with the changing tangential force for a fixed normal force. Figure 4.7(b) shows the change in stress for a changing normal force when the tangential force remains constant. As these figures show, when the applied force consists of both a normal component and a tangential component, the resulting stress profile changes significantly. The tangential force changes the profile of the stress distribution from relatively flat in the area of contact to skewed. It is no longer symmetrical. The peak stress is greater and the spread of the stress distribution is smaller.

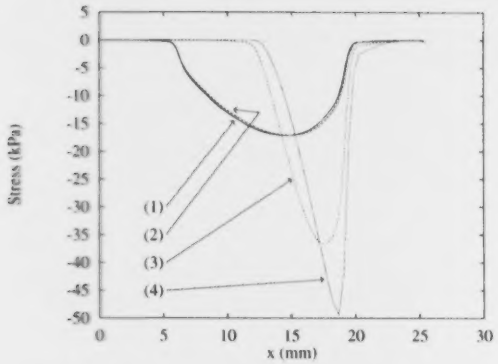

Figure 4.5: *The stress distributions with and without the friction model. All forces are expressed in N/mm. (1) Q = 0.022 without friction. (2) Q = 0.022 with friction. (3) Q = 0.15 without friction. (4) Q = 0.15 with friction.*

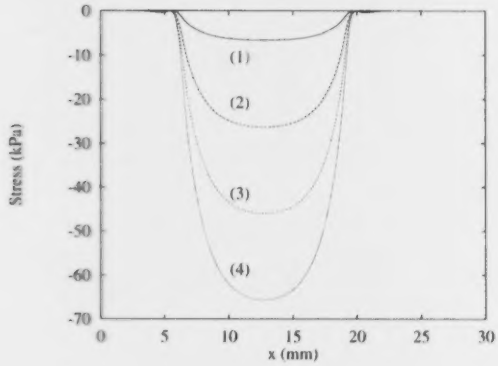

Figure 4.6: *The normal component of the stress tensor σ_{zz} for different applied normal forces. The normal force is applied in the negative z direction and is expressed in N/mm. (1) 0.07 (2) 0.28 (3) 0.49 (4) 0.70.*

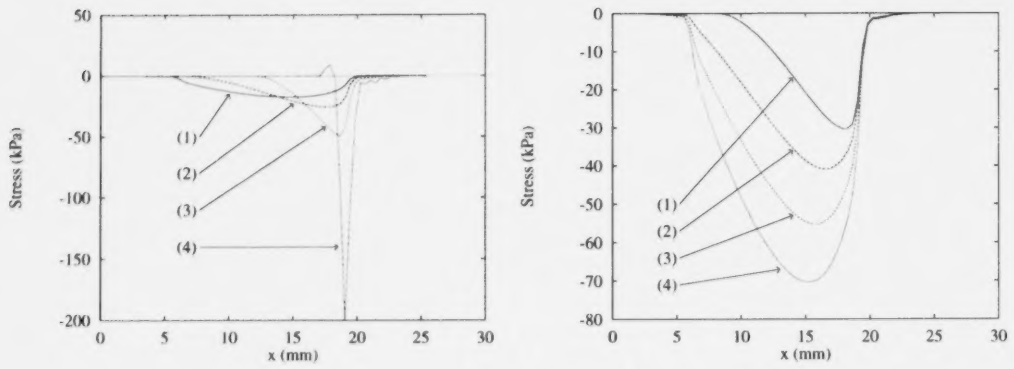

Figure 4.7: *The stress profiles for a force consisting of both a normal component and a tangential component. All forces are expressed in units of N/mm. (a) The variation in stress profile σ_{zz} for a tangential force applied in the positive x direction. (1) 0.0088 (2) 0.035 (3) 0.061 (4) 0.088. A fixed normal force of 0.18 is applied in the negative z direction. (b) The variation in stress profile σ_{zz} for a normal force applied in the negative z direction. (1) 0.18 (2) 0.35 (3) 0.53 (4) 0.70. A fixed tangential force of 0.044 is applied in the positive x direction.*

As a result of the tangential force applied to the top of the indenter, the object indents the layer at a small angle from the vertical. This is illustrated in Figure 4.8. The tilt reduces the width of the contact area between the indenting object and the sensor, denoted by w_c in the figure. Since the tactile sensor responds to compressive normal stress σ_{zz}, the contact width obtained from the sensor, denoted by w_s in the figure, is smaller than the width of the indenting object, denoted by w_I in the figure. The reduction in contact width is a function of the normal force P, the tangential force Q, and the width of the indenting object w_I. Hence, when tangential forces are present, and especially when the ratio of the tangential force to the normal force is large, the contact width w_s obtained from the tactile sensor image becomes a poor estimate of the width of the indenting object, w_I, and the contact width, w_c. Under these conditions, the contact width w_s obtained from the sensor cannot be used directly to estimate the width of the indenting object, w_I, or the contact width, w_c.

For example, consider the contact presented in Figure 3.7. The width of the indenting object is 12.7 mm and the contact between the object and the sensor extends from 6.35 mm to 19.05 mm along x. Figure 4.7 shows the stress profiles corresponding to different applied forces. For a normal force of 0.175 N/mm [1] and a tangential force of 0.0613 N/mm, the contact width w_s reduces to about 7 mm extending from about

[1]The force is expressed in terms of force per unit length because the plane strain assumption assumes that the force is applied uniformly along the direction normal to the plane and that the object is infinitely long in this direction.

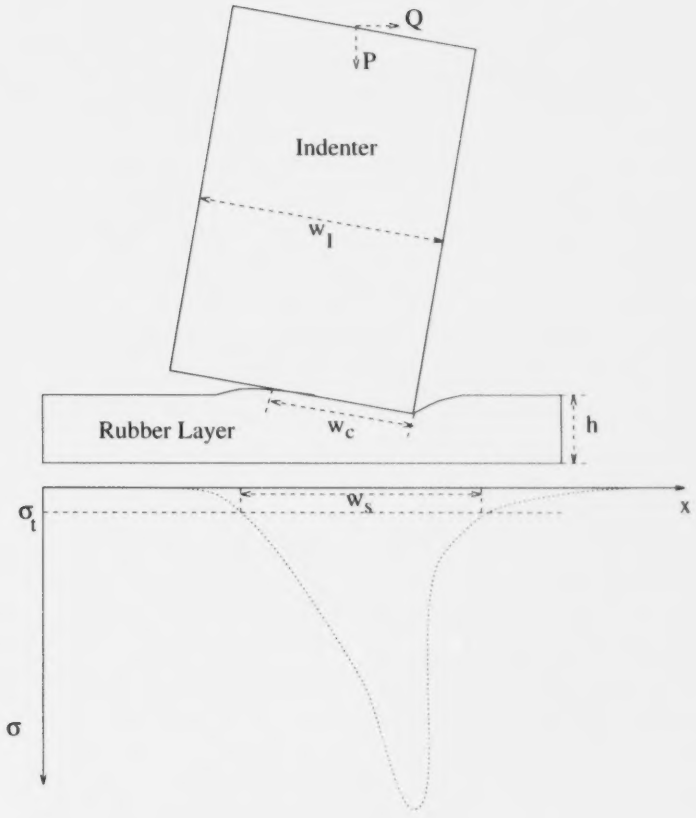

Figure 4.8: *An indenter is tilted as a result of the tangential force applied at the top.*

12 mm to about 20 mm. Figure 4.7(a) shows that the contact width w_s is a function of both the applied normal force and the applied tangential force. It must be pointed out that since the normal stress never becomes exactly zero, it is necessary to have a stress threshold σ_t to determine contact width w_s from the stress profiles. The contact width w_s then becomes dependent on the selected threshold σ_t. This introduces an additional parameter σ_t into the relation between the applied force, the indenter width, and the contact width w_s as obtained from the tactile sensor. For this reason, the feature w_s is not very useful in recovering contact parameters.

4.3.1 Relating stress to applied force

It is important to know the location of contact in many robot manipulation and exploration tasks. For example, to maintain a stable grasp, it is important to detect slip since it can alter the grasp. Rolling an object, or following the contours of an object, are examples of some other manipulation and exploration tasks that require the location of the contact. In this section, the contact between a rectangular bar and a tactile sensor is analyzed in detail. This analysis is used to derive relationships between parameters of the stress distribution, the applied force, and the area of contact.

The model of contact between a flat rectangular bar and a planar tactile sensor is shown in Figure 3.7. Many cases were analyzed using the finite element method. Four different indenter widths, w_I, were considered. For each of these widths, normal stress distributions σ_{zz} were obtained for applied normal forces varying from 0.175 N/mm to 0.7 N/mm in increments of 0.175 N/mm and applied tangential forces varying from 0.00876 N/mm to 0.0876 N/mm in increments of 0.00876 N/mm.

To better understand the relationship between the applied force and the resulting stress distribution as obtained from the tactile sensor, several features of the stress distributions, obtained using the finite element method, were considered. The first feature considered was the contact width as obtained from the stress distribution, denoted by w_s in Figure 4.8. Several values of the stress threshold σ_t were considered. A threshold proportional to the maximum stress within a distribution was also considered. As expected, higher values of the threshold led to smaller values for the corresponding contact widths w_s. For small thresholds, the contact widths w_S became erratic for larger indenter widths w_I. Figure 4.9 shows the contact width w_s as a function of indenter width w_I, normal force P, and the tangential force Q. The contact width w_s decreases with increasing tangential force until it bottoms out for small normal force and small indenter width. This is because as the tangential force is increased, the indenter tilts slightly and indents the sensor at a small angle, as shown in Figure 4.8. When the tangential force is increased further, the tilt is large enough that the flat indenter begins to act as a wedge indenter. As the normal force is increased, the sensitivity of the contact width w_s to the tangential force decreases. The general nature of the function does not vary with the indenter width w_I. As the indenter width w_I increases, the contact widths w_s increase correspondingly. Note that it is possible to have the same contact width w_s for more than one combinations

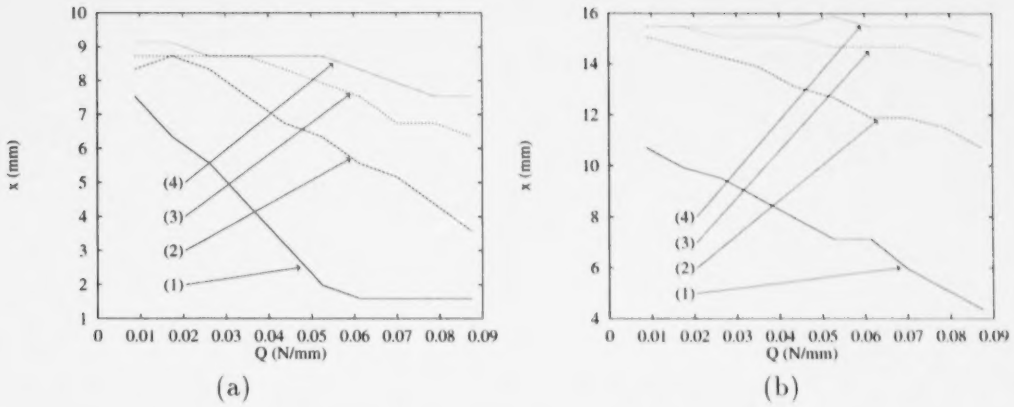

Figure 4.9: *The contact width as a function of normal and tangential force. The normal force is applied in the negative Z direction in units of N/mm. (1) P = 0.18 (2) P = 0.35 (3) P = 0.53 (4) P = 0.7. (a) Indenter width w_I = 7.9 mm. (b) Indenter width w_I = 15.1 mm.*

of normal force, tangential force, and indenter width w_I.

The second feature considered was the position of the peak stress value, denoted by x_m. Figure 4.10 shows the variation in the position of the maximum stress as a function of normal force, tangential force, and indenter width. The position of the peak stress shifts as the tangential force is increased. There is a limiting effect with increasing tangential force as the contact changes from flat contact to wedge contact. The shift is moderated by increasing normal force. Unlike the contact width w_s, x_m varies only slightly with indenter width w_I.

The third feature considered was the centroid of the stress distribution. This is given by the formula shown below:

$$x_c = \frac{\int x\sigma_{zz}(x)dx}{\int \sigma_{zz}(x)dx} = \frac{M_1}{M_0},$$

where x_c refers to the centroid. Figure 4.11 shows the variation of the centroid value x_c with the normal force P, the tangential force Q, and the indenter width w_I. x_c increases linearly with increasing tangential force, increases monotonically but non-linearly with increasing normal force, and is independent of the indenter width w_I. As before, there are non-linearities as the tangential force is increased and the indenter width is decreased. As the contact changes in nature from flat to wedge, the change in x_c with increasing tangential force decreases and finally levels off. The point at which this non-linear behavior starts depends on the indenter width w_I and the material properties of the elastic layer. Smaller indenter widths lead to a similar change in behavior for smaller tangential forces.

The first-, second-, and third-order moments of the stress distribution, M_1, M_2, and M_3, were considered next. Figure 4.12 shows the variation of the first moment M_1 with the applied force and the indenter width w_I. Similar to the centroid x_c,

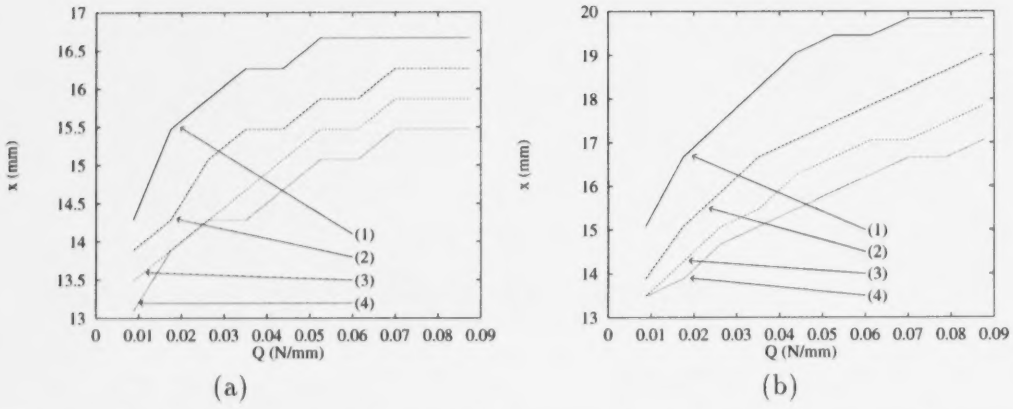

Figure 4.10: *The position of maximum stress, x_m, as a function of normal and tangential force. The normal force is applied in the negative z direction in units of N/mm. (1) P = 0.18 (2) P = 0.35 (3) P = 0.53 (4) P = 0.7. (a) Indenter width w_I = 7.9 mm. (b) Indenter width w_I = 15.1 mm.*

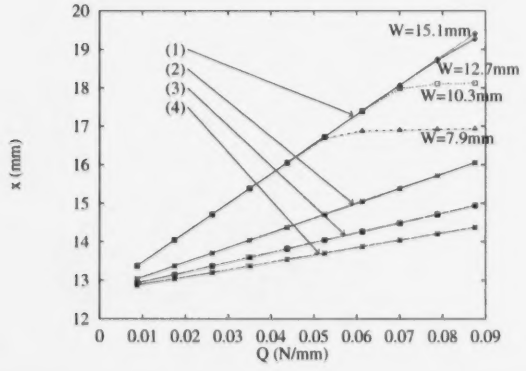

Figure 4.11: *The centroid of the stress distributions, x_c, as a function of the normal force, the tangential force, and the indenter width. The normal force is applied in the negative z direction in units of N/mm. (1) P = 0.18 (2) P = 0.35 (3) P = 0.53 (4) P = 0.7.*

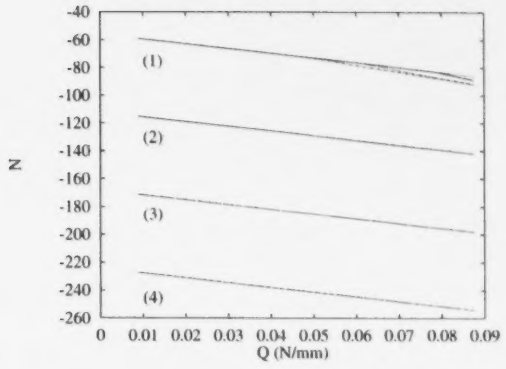

Figure 4.12: *The first moment M_1 of the stress distributions as a function of the normal force, the tangential force, and the indenter width. The normal force is applied in the negative z direction in units of N/mm. (1) $P = 0.18$ (2) $P = 0.35$ (3) $P = 0.53$ (4) $P = 0.7$.*

the first moment is independent of the indenter width w_I, varies linearly with the tangential force Q and shows slightly non-linear behavior for small indenter widths and large tangential forces because of the contact changing from flat to wedge. Unlike the centroid, however, the first moment varies linearly with the applied normal force as well.

Figure 4.13 shows the second moment of the stress distribution, M_2, as a function of the applied force and the indenter width w_I. The variation is similar to the first moment with the exception that the second moment is not independent of the indenter width w_I. Figure 4.14 shows the third moment M_3 as a function of the applied force and the indenter width w_I. Here, the behavior is similar to the second moment except that the variation with indenter width is larger.

4.3.2 Recovering contact parameters from stress

In the previous section, the relationships between applied force, indenter width, and several features derived from the stress distributions were obtained. Figures 4.9 to 4.14 specify these relationships. The relationships between the applied force, the indenter width, and the contact width and the peak stress locations are nonlinear. It is not clear if inverse relationships could be derived for these features. Although the relationship between the centroid and the tangential force is linear, the dependence of the centroid on the normal force is nonlinear.

The relationships between the various moments and the applied force and indenter width are nearly linear. The first moment M_1 varies almost linearly with the normal force P and the tangential force Q and is independent of the indenter width W. With M_1 as the dependent variable and P and Q as the independent variables, multiple linear regression was used on the data in Figure 4.12 for $W = 15.1$ mm to obtain the following equation relating M_1 to P and Q. For this equation, the *coefficient*

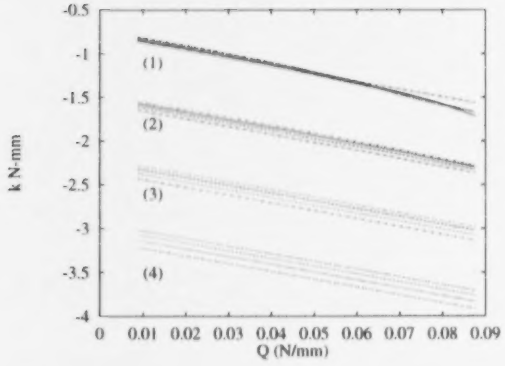

Figure 4.13: *The second moment M_2 of the stress distributions as a function of the normal force, the tangential force, and the indenter width. The normal force is applied in the negative z direction in units of N/mm. (1) P = 0.18 (2) P = 0.35 (3) P = 0.53 (4) P = 0.7.*

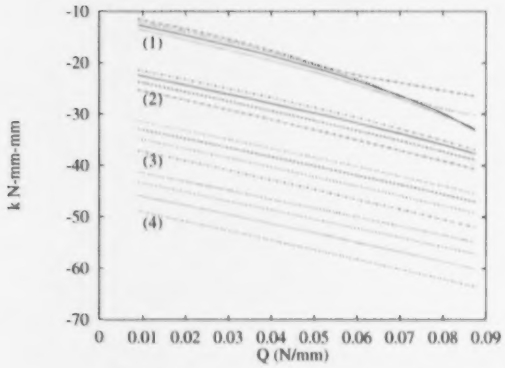

Figure 4.14: *The third moment M_3 of the stress distributions as a function of the normal force, the tangential force, and the indenter width. The normal force is applied in the negative z direction in units of N/mm. (1) P = 0.18 (2) P = 0.35 (3) P = 0.53 (4) P = 0.7.*

of multiple determination, also called the *multiple correlation coefficient* [24], R^2 was 0.99999, indicating a good linear fit.

$$M_1[\sigma_{zz}(y)] = 319.9P - 339.3Q - 0.016. \tag{4.3}$$

An indication that the actual relation is not linear is that this relation predicts a small but finite value for the first moment even when both P and Q are zero. This value is - 0.016 N, corresponding to 1.6 gm-force. This is a small value when compared to the minimum value of the first moment in Figure 4.12, about -60 N. Thus, this relation could be used as a good approximation to the actual function relating the first moment to the applied force.

Figure 4.13 shows that while the relationship between the second moment M_2 and Q is linear, the variation of M_2 with P and W is not obviously linear. The variation in M_2 with P is a function of W. This suggests that the relationship should include the product of P and W as a first approximation. Several different combinations of variables were tried and the equation that provided the best fit is given below. This equation was obtained with M_2 as the dependent variable and P, Q and WP as the independent variables using multiple linear regression on the data in Figure 4.13. For this equation, the coefficient of multiple determination R^2 was 0.99936, again indicating a good linear relationship.

$$M_2[\sigma_{zz}(y)] = 3786P - 9324Q + 40.5WP - 19. \tag{4.4}$$

Here, too, the relation predicts a relatively small but finite value for the second moment when the applied force is zero. Again, this value of -19 N-mm is small compared to the smallest value of the second moment in Figure 4.13, -750 N-mm. Hence, this relation, too, can be used as a good approximation to the actual function relating the second moment to the applied force and the indenter width.

In any given task, depending on the sensors available and the information that is known *a priori*, we can use the two equations to obtain information about the contact. We consider four different cases below. In each of these cases, it is assumed that the contact is between a planar tactile sensor and a flat rectangular object whose width is less than that of the tactile sensor.

Case I. Consider the case where the indenter width W is known while the applied force $\mathbf{F}$ is not known. This can happen when a known object is being manipulated by a robot and the applied force cannot be measured. The first moment and the second moment of the stress distribution can be obtained from the tactile sensor output. Substituting the known value of W and the two moments obtained from the tactile sensor into the equations above, we obtain two linear equations in two unknowns and $\mathbf{F}$ can be obtained by solving these two equations.

Case II. Consider the case where the applied force can be measured using a force/torque sensor. The robot is performing an exploration task and hence, the indenter width W is not known. Here, the indenter width W can be obtained by

using the equation relating the second moment with the applied force and indenter width.

Case III. Consider the case where a known object is being manipulated by a robot where the applied force can be measured by a force/torque sensor. Here, both $\mathbf{F}$ and W_{act} are known, and we have many redundant sources of information that can all be used to control task execution.

Case IV. Consider an exploratory task being performed by a robot where the applied force cannot be measured by a force/torque sensor. Here, both W and $\mathbf{F}$ are not known. There are two equations in three unknowns and the system of equations is underdetermined. Hence, at best we can obtain an equation that provides a constraint on the possible values for force and indenter width.

4.4 Contact with a long cylinder

The finite element model used for analyzing contact between a flat rectangular bar and a tactile sensor, as presented in the previous section, can be adapted for the analysis of contact with a long cylinder. It is only required to modify the shape of the indenter. In this model, the contact is modeled by using gap elements. These are special type of elements provided by the finite element software for constructing models [3, 4]. These elements do not allow the gap between the connected nodes to become less than the specified gap. Thus, if the specified gap is zero, then the elements remain inactive as long as the distance between the nodes is greater than zero. As soon as the distance becomes less than zero, the gap is forced to zero by applying a force on the nodes. This force is calculated using the distance required to bring the gap back to zero and a specified stiffness for the gap element. A problem with this method of modeling contact is that the gap elements are directional, i.e., the gap between the two nodes is measured as the projection of the distance between the two nodes on the vector defined by the original orientation of the two nodes. Thus, the gap elements do not allow the control of tangential displacements.

A more accurate model can be built by modeling the elastic layer explicitly and by specifying the normal and tangential displacements of the top surface of the elastic layer directly. For example, for contact with a cylinder, initial contact consists of just the initial point of contact. As a small displacement is applied, the nodes displace vertically as well as tangentially. Using small displacements, and checking for nodes that displace into the cylinder at each step, the behavior of the sensor can be studied incrementally. For each small step, the nodes on the elastic layer that displace into the volume of the cylinder are constrained to lie on the cylinder surface. This algorithm is shown in Figure 4.15.

Using this method for analyzing contact, the stress distributions were obtained for a range of normal and tangential displacements of the cylinder with respect to the sensor. The cylinder had a radius of 22.9 mm. The variation in the stress distributions with normal displacement and no tangential displacement is shown in Figure 4.16. The stress distribution is symmetric about the center of contact and the peak stress

let
Surface : set of nodes on the surface
In : set of surface nodes currently in contact
CurPos : current position/orientation of the indenter
Delta : small translation/rotation applied to the indenter
compute NewPos = CurPos . Delta
let
NewIn : set of surface nodes within the volume of the displaced indenter
NewOut : set of surface nodes outside the volume of the displaced indenter
while (NewIn is not empty)
apply the small displacement Delta to each node in NewIn
compute surface deformation using the finite element method
let NewIn = nodes that are within the volume of the displaced indenter

Figure 4.15: *The algorithm used to study contact by specifying the surface displacements based on the indenter geometry.*

increases with increasing normal load. This behavior is qualitatively similar to that for the other contact types studied so far — contact between the sensor and an edge and a flat rectangular bar.

Figure 4.17(a) shows the effect of varying the normal displacement when the tangential displacement is maintained at a constant value, while Figure 4.17(b) shows the variation in stress distribution when the normal displacement remains constant and the tangential displacement is varied. Once again, the peak value of the stress depends on the applied normal displacement and does not vary with the applied tangential displacement. However, the tangential displacement leads to a stress distribution that is asymmetric about the line of applied load. The degree of asymmetry, measured by the distance between the line of applied load and the position of the peak stress or the first moment of the stress distribution about the line of applied load, depends on both the normal displacement and the tangential displacement.

The stress distributions obtained above were used to compute the zeroth and the first moment of stress about the center of contact. The relationship between the moments of the stress distribution and the normal and tangential displacement of the cylinder is shown in Figure 4.18. Here, the zeroth moment varies only with the normal displacement. The variation is monotonic but non-linear. The first moment varies with both the normal displacement and the tangential displacement.

The advantage of this method is that it can easily be extended to a three-dimensional analysis of contact. Another advantage is that it is computationally

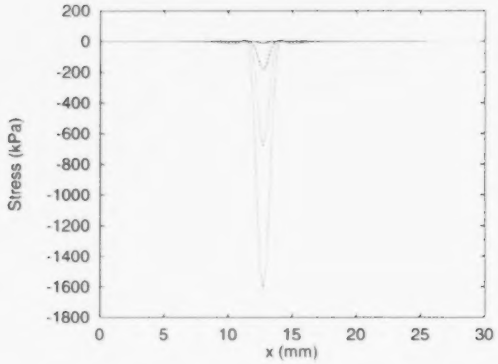

Figure 4.16: *The variation in the sub-surface stress profile for increasing normal force with no tangential force.*

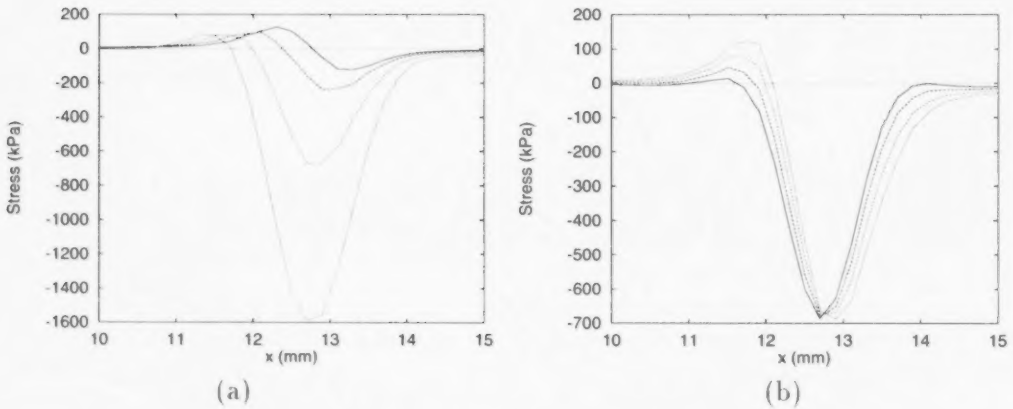

(a) (b)

Figure 4.17: *The variation in sub-surface stress distribution (a) with increasing values of the normal displacement for a constant tangential displacement of the indenter, and (b) with increasing values of the tangential displacement with constant normal displacement of the indenter.*

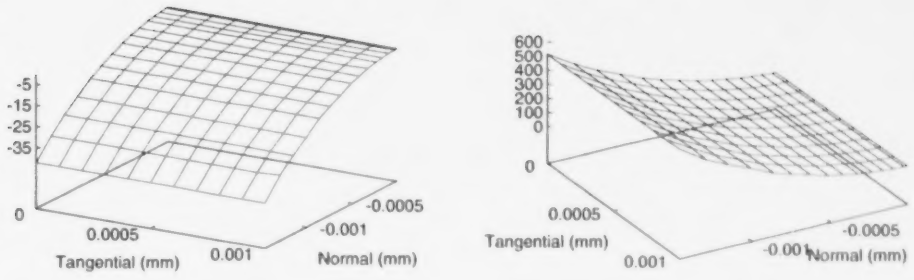

(a) (b)

Figure 4.18: *The moments (a) M_0 (N/mm) and (b) M_1 (N) as a function of the relative displacements.*

inexpensive compared to the models built using the gap elements.

4.5 Models of contact and superposition

The finite element models considered in this chapter have all been based on linear elasticity. This implies that the principle of superposition can be used to obtain stress distributions for different combinations of force or displacement. If the applied force can be expressed as a linear combination of other applied forces for which the stress distributions are known, then the stress distribution for the applied force can be obtained as a linear combination of the corresponding stress distributions.

This is valid for the case of edge contact and has been verified using the distributions obtained from the finite element method. A force applied to the knife leads to a line force acting on the sensor surface. This causes the surface to deform and leads to a small displacement of the knife. The stress distributions for a normal force and a tangential force can be obtained using the finite element method. The stress distribution corresponding to some other applied force or displacement can then be obtained using superposition.

However, this method is not applicable to the case of contact with a flat rectangular bar under any combination of forces or displacements applied to the indenter. As mentioned before, a tangential force applied at the top of the bar is equivalent to a tangential force and a moment applied to the sensor surface and causes the bar to tilt. If the normal force is not large, then the tilt can lead to a reduction in the area of contact, w_c, as shown in Figure 4.8. This reduction in the contact width w_c introduces a non-linearity into the relation between the force or displacement applied to the rectangular bar and the resulting stress distribution. For this reason, the stress distribution cannot always be obtained using superposition based on the applied force or displacement.

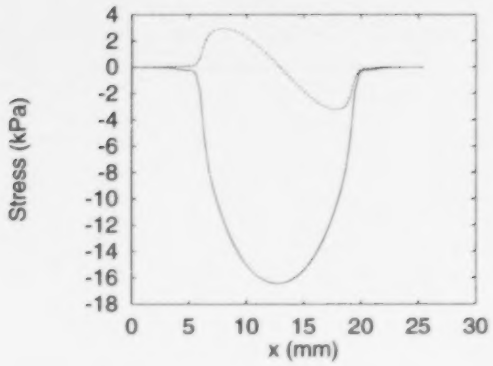

Figure 4.19: *The stress distributions corresponding to a purely normal displacement and a purely tangential displacement.*

Using the finite element method, the sub-surface stress distributions were obtained for several values of force applied to the indenter. The normal force varied from 0.175 N/mm to 0.7 N/mm in increments of 0.175 N/mm, while the tangential force varied from 0.00876 N/mm to 0.0876 N/mm in increments of 0.00876 N/mm. Let the sub-surface stress distributions be denoted by $\sigma_{zz}^{i,j}$, where i refers to a value of the applied normal force and j refers to a value of the applied tangential force. So, for example, the stress distribution corresponding to a normal force of 0.35 N/mm and a tangential force of 0.0438 N/mm will be denoted by $\sigma_{zz}^{2,5}$. Since the model was not used to obtain stress distributions corresponding to purely normal or purely tangential forces, these have to be obtained indirectly from the stress distributions that are available. If it is assumed that superposition applies, then the stress distribution corresponding to a purely normal force can be obtained as $\sigma_{zz}^{i+1,j} - \sigma_{zz}^{i,j}$, while the stress distribution corresponding to a purely tangential force can be obtained as $\sigma_{zz}^{i,j+1} - \sigma_{zz}^{i,j}$. For example, the stress distributions shown in Figure 4.19 correspond to a purely normal force and a purely tangential force and were obtained as $\sigma_{zz}^{2,1} - \sigma_{zz}^{1,1}$ and $\sigma_{zz}^{3,2} - \sigma_{zz}^{3,1}$, respectively.

Figure 4.20 shows the stress distributions obtained using superposition and using the finite element method. The stress distributions in Figure 4.20(a) correspond to a normal force of 0.53 N/mm and a small tangential force of 0.09 N/mm. The difference in the stress distribution obtained using the two methods is small, indicating that superposition is applicable in this case. In contrast, Figure 4.20(b) shows the stress distributions corresponding to a normal force of 0.53 N/mm and a tangential force of 0.16 N/mm. Here, there is some disagreement between the stress distribution obtained from superposition and the stress distribution obtained from the finite element method. Finally, Figure 4.21 shows the stress distributions corresponding to a normal force of 0.18 N/mm and a tangential force of 0.14 N/mm. Here, the disagreement between the stress distributions obtained form the two methods is large, indicating that superposition is not applicable.

The contact between a sensor and a cylinder has been studied by specifying the motion of the cylinder with respect to the sensor. Since the area of contact changes

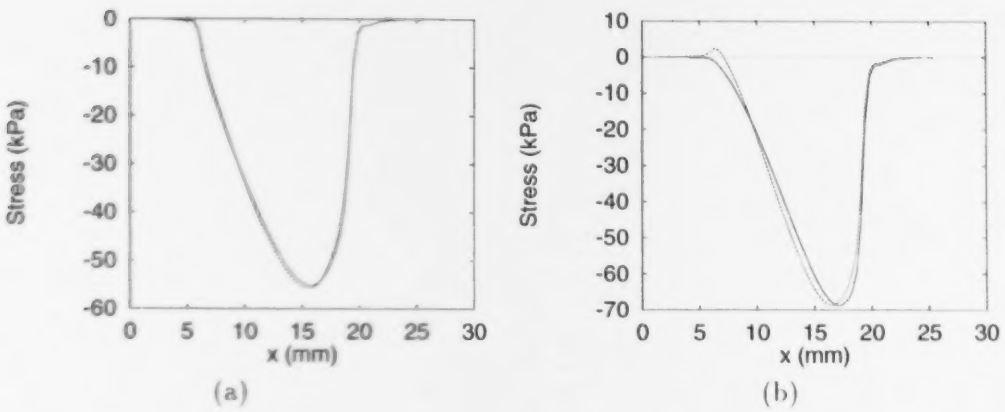

Figure 4.20: *The stress distributions obtained from the finite element method and using superposition. The normal force applied to the bar is 0.53 N/mm. (a) Tangential force of 0.09 N/mm. (b) Tangential force of 0.16 N/mm.*

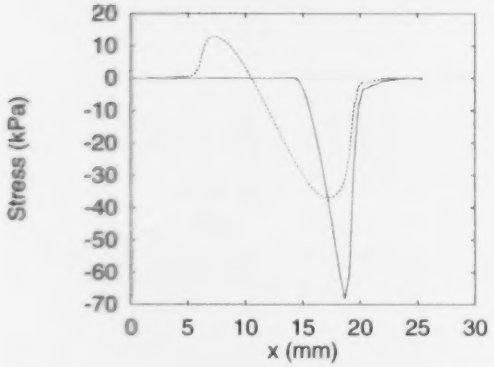

Figure 4.21: *The stress distributions obtained from the finite element method and using superposition for a normal force of 0.18 N/mm and a tangential force 0f 0.14 N/mm.*

as the cylinder moves with respect to the sensor, superposition is not applicable in terms of the relative displacements of the cylinder. However, assuming that there is no slip in the area of contact, the relative displacement of the cylinder is used to determine the displacement within the area of contact on the top surface of the sensor, and then superposition can be applied. This displacement on the top surface can be expressed as a sum of scaled and shifted displacements, each of which corresponds to the displacement because of an edge contact. The stress distribution can then be obtained by summing the corresponding scaled and shifted stress distributions.

Superposition can only be used when the system being studied is linear. The procedures used in this chapter to study contact are quite general and can be used when the system is non-linear. For example, if the non-linearity in the material properties is explicitly modeled and a model of friction is also incorporated, the procedures used in this chapter will be applicable.

4.6 Conclusion

The discussion in this chapter shows that even though tactile sensors provide information about only one component of the stress tensor, it is possible to obtain contact information such as the applied force, the relative displacement, and the indenter width using features derived from the tactile sensor output.

The most common surfaces encountered in robot manipulation are flat, cylindrical, and spherical. In this study, the problem of contact between a planar tactile sensor and an edge, a flat rectangular bar, and a cylinder, was examined. The protective layer of the tactile sensor was modeled as a thin elastic layer of finite thickness. Contact between the sensor and a knife edge was analyzed first, using both closed-form expressions based on the half space assumption and using the finite element method. The analysis was used to demonstrate the advantages of using the finite element method and also of using features of the sub-surface stress distribution to recover contact parameters.

Next, contact between the sensor and a flat rectangular bar was studied. A finite element model using gap-cable elements was constructed, and an attempt was made to consider the effects of friction. The finite element method was used to obtain the sub-surface stress distributions corresponding to several combinations of normal and tangential force applied to the top of the indenter. Several different indenter widths were considered. The results showed that obtaining contact parameters from tactile sensors is non-trivial. The response of the tactile sensor is greatly modified because of the tangential forces acting on the object. The tangential displacements, and the extent of contact as obtained from the tactile sensor, are a function of the normal force, the tangential force, and the indenter width. Several features obtained from the sub-surface stress distributions, for example centroids, moments, and contact widths, were studied as a function of the applied forces and the indenter width. The stress distributions were used to derive functions between the applied forces, the indenter width and the zeroth- and first-order moments of the sub-surface stress. Several

examples were given to illustrate how these relationships can be used in recovering contact information in manipulation and exploration tasks.

Finally, contact between the sensor and a cylinder was considered. A different model was used to study this type of contact, and the relation between normal and tangential displacements of the cylinder and the zeroth- and first-order moments of the resulting sub-surface stress was established. A general method was presented for analyzing contact with objects of any given shape in 2 or 3 dimensions using the finite element method. The discussion presented in this chapter demonstrates that the finite element method is well suited for analyzing contact problems.

The analysis presented in this chapter focused on the determination of contact forces and contact geometry using only the normal component of the stress tensor. It is difficult to establish a direct relationship between these parameters and the stress distribution. However, certain features derived from the stress distributions lead to monotonic, and sometimes also linear, relationships between the derived features and the input parameters. An alternative approach to establish such relationships is to consider more than one component of the stress tensor simultaneously, for example, the normal stress and the shear stress. Recently, tactile sensors that measure more than one component of the stress tensor have been reported [40] and hence this alternative approach is not just of theoretical interest but could lead to practical methods of using tactile sensors.

Finally, it must be pointed out that the analysis in this chapter is theoretical and only qualitative conclusions can be drawn from it. Most tactile sensors are noisy and do not transduce stress in a linear manner. Hence, a more accurate model is required for experimental calibration. Another important aspect that needs to be modeled is the discrete nature of real sensors. The spatial sampling frequency of a real sensor must also be built into an accurate model of a tactile sensor.

Chapter 5

Tactile sensing and manipulation

In the previous chapters, stress distributions arising from contact between rigid indenters of different shapes were analyzed for a variety of loading conditions. Several features that were predictive of the loading conditions, given the indenter shape, were identified. Based on these features, this chapter presents a new approach, called tactile servo, to control robot motion based on tactile sensory feedback. In this method, features of a stress distribution, as obtained from a tactile sensor, are used to control the motion of a robot manipulator. A task is specified in terms of the desired values, or sequence of values, of a set of tactile features. The predictive relationship between the motion of a manipulator relative to the sensor and the corresponding change in the values of the selected tactile features is used to estimate the desired motion of the robot manipulator. This approach presents a general way to perform tasks based on touch and in that way satisfies the objective of the thesis.

5.1 Introduction

The possibility of controlling the motion of a robot manipulator using tactile feedback has been explored recently by several researchers. Houshangi and Koivo [30] conducted a simple empirical study in which the robot determined the angle between a cylindrical peg and a planar surface using the tactile sensor output from the robot hand. No attempt was made however to model the tactile sensing process or generalize the experiment to other types of contact.

Berger and Khosla [8] formulated an algorithm to track an edge using tactile feedback. The approach was novel in that tactile information was used actively to control the motion of the robot. A hierarchical control architecture was used for the task with an inner control loop consisting of a hybrid controller driving the manipulator and an outer control loop using the information from the tactile sensor to derive the next position command for the inner hybrid controller. An empirical study of the behavior of tactile sensors was presented and this knowledge was used in developing the algorithms for the processing of tactile data. However, a model of tactile sensors was not constructed, and tactile sensory data was processed using techniques adapted

from image processing to determine the edge parameters of a stationary object. Furthermore, there was no manipulation of objects. In a manipulation operation such as rolling a cylindrical object between the fingers of a dextrous hand, the identity as well as the geometric description of the object being manipulated is known, and the objective of the task is to cause purposeful motion of the object. This is different from robot motion control using tactile feedback such as the edge following task described above [8] in that the object being manipulated is in motion whereas the edge that is being tracked remains stationary.

Most recently, Maekawa *et al.* [43] have presented a task based on rolling contact. They presented a kinematic model of rolling contact based on the assumption that the location of contact is known. This model was used to develop a control algorithm for tasks involving rolling contact using tactile sensors to estimate the location of contact. They showed that manipulation is significantly improved when tactile sensors are used to provide feedback about the location of contact between the finger and the object being manipulated.

The understanding of active object manipulation using tactile sensing is important since it often provides the most direct, intuitive, and sometimes the only observation of the progress of a task. This chapter presents a new approach to tactile-based object manipulation. It is referred to as *tactile servo* by analogy with image-based visual servo [65]. The approach makes use of the simple observation that the progress of a manipulation task can be characterized by the tactile images obtained from tactile sensors mounted in the robot hand used to actively manipulate objects. Tactile servo has been applied successfully to the manipulation task of pushing a rolling pin on a planar surface using a planar robot finger equipped with a tactile sensor array. The work is being extended to other tasks involving a dextrous multi-fingered robot hand.

5.2 Tactile servo

A manipulation task can be described in terms of a sequence of stages or states. The number of such states for a given task depends on the type of sensors available [23]. The progress of the task can be represented as an ordered sequence of these states. For a robot contact task such as manipulation, if the contact can be monitored by tactile sensors, each state in the task sequence can be characterized by the tactile image acquired from the tactile sensors. To make the required transitions between states, therefore, it is only necessary for the robot control system to control the motion of the robot so that the desired goal image is obtained. Instead of using a complete tactile image to characterize task states, it is often more useful to characterize task states in terms of a finite set of tactile signatures or features that are derived from a tactile image. This notion can be expressed in the following form:

$$\vec{F} = \vec{f}(\vec{X})$$

where $\vec{X}$ is a vector that defines the state of a task in terms of parameters related to the manipulator and the object, and $\vec{F}$ is a vector consisting of several features derived

from a tactile image that characterizes the given state of the task. The dimension and representation of $\vec{F}$ and $\vec{X}$ vary from task to task. For example, in the operation of pushing a cylindrical object with a planar end-effector equipped with a tactile sensor, as in rolling a cylinder over the table top (see Figure 5.5), $\vec{F}$ can be represented by the position and the area of the rectangle whose boundaries represent the area of contact.

It is possible that for some tasks, the mapping shown in Equation 5.1 is not one-to-one. This may occur when the sensors being used in the task are unable to fully and unambiguously characterize the various states of the task. The problem may be overcome by adding other types of sensors which could provide additional features.

As the task progresses, a small change in the state of the task, as characterized by a small change in $\vec{X}$, will lead to a corresponding change in the feature vector $\vec{F}$. If this relationship between the feature vector and the task state vector can be accurately identified, then the changes in the feature vector can be used to estimate the changes in the task state vector and this knowledge can then be used to control a robot to track a given sequence of task state vectors that specify a given task. This relationship between differential changes in task state vectors and feature vectors can be expressed as a Jacobian matrix, $\mathbf{J}_s$, as described in [65] :

$$\mathbf{J}_s = \frac{d\vec{F}}{d\vec{X}}. \tag{5.1}$$

This matrix is called the *feature sensitivity matrix* or the *feature Jacobian matrix.*

Let $\mathbf{J}_\theta$ represent the manipulator Jacobian that relates a differential change in the joint angles of the robot to a differential change in the position of the robot in Cartesian coordinates. This is expressed in the following form :

$$\mathbf{J}_\theta = \frac{d\vec{X}}{d\vec{\theta}} \tag{5.2}$$

where $\vec{\theta}$ is the vector consisting of the joint angles of the robot arm. Using these equations, the following relationship between a differential change in the joint angles and a differential change in the tactile features can be derived :

$$d\vec{\theta} = \mathbf{J}_\theta^{-1} d\vec{X} = \mathbf{J}_\theta^{-1}\mathbf{J}_s^{-1} d\vec{F}. \tag{5.3}$$

This relationship can be used to control the motion of a robot in a manipulation task specified in terms of a sequence of desired values of the tactile features $\vec{F}_d$. At any given instant, the differential change in the feature vector is taken to be the difference between the feature vector obtained from the tactile sensor, $\vec{F}_a$, and the desired feature vector $\vec{F}_d$, and is specified as :

$$d\vec{F} = \vec{F}_d - \vec{F}_a. \tag{5.4}$$

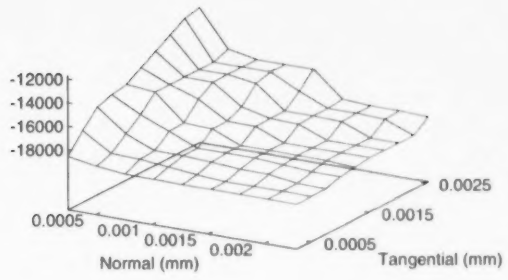

Figure 5.1: $\frac{\partial M_0}{\partial u_{z0}}$ (N/mm^2) *for line contact, as a function of* u_{z0} *and* u_{x0}.

Equation 5.3 is then used to obtain the corresponding differential change in the joint angles of the robot, $d\vec{\theta}$. This is then added to the current robot configuration in joint space, $\vec{\theta}$, to arrive at the desired values for the robot joint angles used to drive the position servo controlling the arm.

As a simple illustration of this approach, consider the case of line contact, as discussed in the previous chapters. Let the feature vector $\vec{F}$ consist of the zeroth moment and the first moment of the stress distribution obtained from a tactile sensor. Equations 4.3 and 4.4 specify the relationship between these moments in terms of the displacements of the layer and were obtained by using the half space assumption. The displacements correspond to the movements of the knife edge relative to the layer. As these equations show, the Jacobian matrix relating the given features to the displacements is diagonal. A problem associated with the analytical approach is that the displacements are infinite at the surface of the layer where the contact is being made. This is because of the stress singularity at that point. Furthermore, these equations contain the arbitrary factor d which is used to provide a reference point and cannot be determined from the problem specification.

The relationships between the moments and the displacements were presented in Chapter 4 and were obtained from contact models using the finite element method. Four components of the feature Jacobian matrix, $\frac{\partial M_0}{\partial u_{z0}}$, $\frac{\partial M_0}{\partial u_{x0}}$, $\frac{\partial M_1}{\partial u_{z0}}$, and $\frac{\partial M_1}{\partial u_{x0}}$, can be obtained from the above relations using numerical differentiation, and are presented in Figures 5.1, 5.2, 5.3, and 5.4. As these figures show, the Jacobian matrix is no longer diagonal. However, the diagonal elements are large compared to the off-diagonal elements and so the matrix is dominated by the diagonal elements.

The information provided in these figures can be used to control contact tasks involving edge contact. A simple example of such a task is to track an edge. Another example is to grasp an object along its edges.

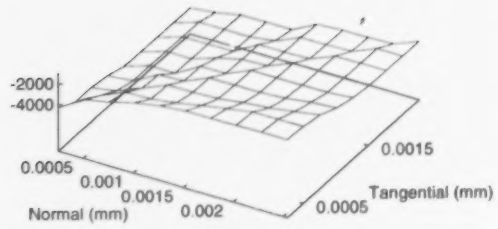

Figure 5.2: $\frac{\partial M_0}{\partial u_{x0}}$ *(N/mm²) for line contact, as a function of* u_{z0} *and* u_{x0}.

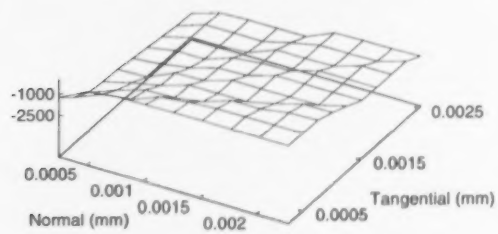

Figure 5.3: $\frac{\partial M_1}{\partial u_{z0}}$ *(N/mm) for line contact, as a function of* u_{z0} *and* u_{x0}.

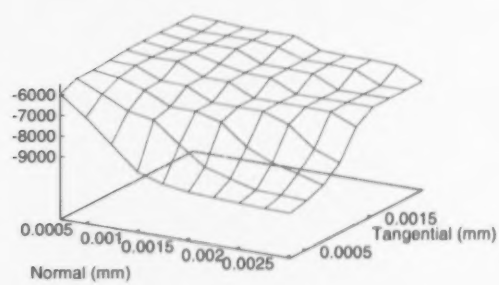

Figure 5.4: $\frac{\partial M_1}{\partial u_{x0}}$ *(N/mm) for line contact, as a function of* u_{z0} *and* u_{x0}.

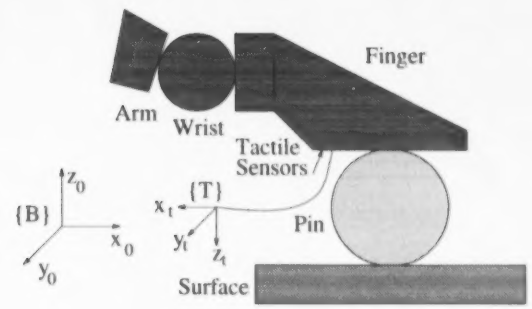

Figure 5.5: *Planar view of a robot arm equipped with a sensorized finger rolling a pin.*

5.3 Example task : Rolling a pin

To illustrate the approach outlined above in greater detail, consider the task of rolling a pin, as shown in Figure 5.5. In this task, the tactile sensors can be used to characterize the progress as long as contact is maintained between the finger and the pin. To use tactile servo for this task, we need to identify (a) the task state vector $\vec{X}$, (b) the corresponding feature vector $\vec{F}$ to be computed from the tactile image, and (c) the Jacobian matrix $\mathbf{J}_s$ that relates the differential change in the task state vector to differential change in the feature vector.

The various states of the manipulator/task correspond to the position and orientation of the finger, as defined by a homogeneous transformation from the base of the arm. As the task progresses, the differential change in the task state vector can be characterized by the change in the position and the orientation of the arm and this change is represented by the six-dimensional vector $d\vec{X} = [dx\ dy\ dz\ \delta x\ \delta y\ \delta z]^T$ where the first three components correspond to differential translations and the last three components correspond to differential rotations.

The tactile features to be used in the tactile servo depend on the forces acting on the rolling pin and the tactile sensor. These forces result in relative displacement between the sensor surface and the rolling pin. This displacement leads to a distribution of forces within the area of contact and these forces in turn result in the normal stress distribution measured by the sensor. To determine the features to be used in controlling the task of rolling a pin, we need to characterize the relationship between the forces applied to the pin, the displacement of the pin and the sensor, and the stresses measured by the tactile sensor.

5.3.1 Tactile images under varying loading conditions

Translation along z

Figure 5.6 shows the output of the tactile sensor for different forces applied on the pin along z in Figure 5.5. The darker areas in the image correspond to larger forces as detected by the sensor. The image on the right corresponds to a larger applied normal force. The force applied along z presses the pin into the elastic layer and the

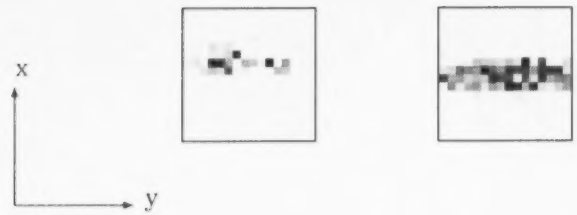

Figure 5.6: *The two-dimensional stress distributions obtained experimentally from the tactile sensor in which the darkness represents the pressure intensity. The image on the right corresponds to a larger force applied along z compared to the image on the left. The z-axis is normal to the page.*

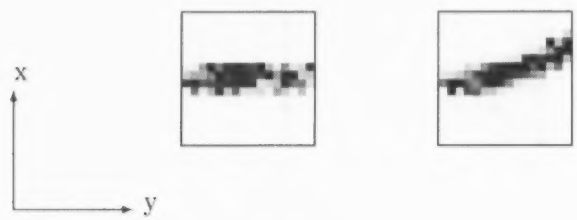

Figure 5.7: *The effect of a rotation about z, which is normal to the plane of this page.*

elastic layer deforms within the area of contact to conform to the shape of the rolling pin. Since no force is applied along x, the stress distributions are symmetrical about the line of action of the applied force. Increasing the magnitude of the applied force presses the pin further into the elastic layer, thus increasing both the maximum stress and the area of contact, as shown in the tactile images in Figure 5.6.

Rotation about z

Figure 5.7 shows the effect of a rotation about z, and that simply causes the stress distribution to rotate about z by the same angle.

Translation along y

This motion cannot be detected by the sensor because of the geometry of the cylinder and the sensor. Although this motion causes the relative position of the sensor to change with respect to the cylinder, the tactile image does not change with this motion.

Rotation about y

As mentioned above, the force along z presses the pin and the sensor together while the force along x causes a shearing effect in the area of contact. It also causes a turning moment in the area of contact and this has the effect of rotating the pin

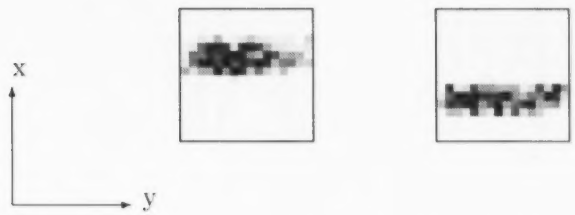

Figure 5.8: *The effect of a translation along x, which is along the vertical direction on this page.*

about y into the surface of the sensor. All this causes the resulting stress distribution to be skewed so that the stress in the top half of the sensor is large while the stress in the bottom half of the sensor is small. However, because of the sensitivity of the sensor and the noise, changes in the tactile image caused by this motion are extremely difficult to identify.

Translation along x

This motion simply causes the tactile image to translate by an equivalent amount. This is similar to a rotation about z in that, here, the stress distribution is simply translated along x and does not change in any other way. This motion is illustrated in Figure 5.8.

Rotation about x

Figure 5.9 shows the stress distributions obtained from the tactile sensor when a normal force acts along z and a tangential force is applied along y. The image on the left corresponds to a small applied tangential force while the image on the right corresponds to a larger applied tangential force. As before, the darker areas in the images correspond to larger values of force as detected by the tactile sensor. Here, the force along z presses the pin against the sensor while the force along y causes the pin to rotate about x into the sensor surface. This skews the stress distribution so that the stress in the left half of the sensor is large while the stress in the right half of the sensor is small. Here, because of the geometry of the pin and the sensor, the effect is a lot more dramatic than for the case of a force applied along x.

5.3.2 Identifying tactile features

To perform a task using tactile servo, we need to identify features in these stress distributions that relate in a unique and unambiguous way to the position and orientation of the finger. The discussion presented in the previous chapters and in [56] characterizes the stress distributions that are obtained for different applied forces and indenter geometries. It was found that the various moments associated with the stress distribution vary monotonically with the applied forces and displacements.

Based on the results presented earlier and on the discussion presented in the

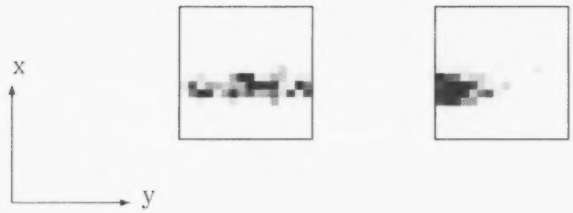

Figure 5.9: *The effect of a rotation about x. The image on the right results from an anti-clockwise rotation of the cylinder about x, which lies along the vertical direction in the plane of this page.*

previous subsection, the features used in this study are obtained from the zeroth-, first- and second-order moments, shown below:

$$\begin{aligned} M_0 &= \int\int \sigma_{zz}(x,y)dxdy \\ M_x &= \int\int y\sigma_{zz}(x,y)dxdy \\ M_y &= \int\int x\sigma_{zz}(x,y)dxdy \\ M_{xx} &= \int\int y^2\sigma_{zz}(x,y)dx\ dy \\ M_{yy} &= \int\int x^2\sigma_{zz}(x,y)dx\ dy \\ M_{xy} &= \int\int xy\sigma_{zz}(x,y)dx\ dy \end{aligned}$$

Here, M_0 is the zeroth-order moment of the stress distribution, M_x and M_y are the first-order moments of the stress distribution with respect to the axes x and y of the sensor. M_{xx}, M_{yy}, and M_{xy} are the second order moments associated with the stress distribution.

The zeroth-order moment, M_0, corresponds to the normal force acting on the sensor surface and is therefore equal to the normal contact force. The location of contact is characterized by the centroid of the stress distribution obtained from the tactile sensor. The x and y coordinates of the centroid, denoted by (x_c, y_c), are obtained from the zeroth- and first-order moments as shown below.

$$\begin{aligned} x_c &= \frac{M_y}{M_0} \\ y_c &= \frac{M_x}{M_0} \end{aligned}$$

Let $x'y'z'$ be the frame that is obtained by translating the xyz frame, fixed to the sensor, by (x_c, y_c). The second order moments with respect to this frame, denoted by $M_{x'x'}$, $M_{y'y'}$, and $M_{x'y'}$, are used to obtain an axis rotated about z' so that the moment of the stress distribution about that axis is a minimum. The angle made by the axis with x' is denoted by θ_p and is given by:

$$\tan(2\theta_p) = \frac{-2M_{x'y'}}{M_{x'x'} - M_{y'y'}}$$

The features discussed above are all related to the motion of the fingertip relative to the object being manipulated. M_0 is related to the relative movement of the finger, and hence the sensor, along z. Similarly, x_c and y_c are related to the motion of the sensor along x and y. However, as mentioned before, because of the geometry of the task, movement along y does not change the value of y_c. Hence, this motion cannot be controlled using tactile servo. $M_{x'}$ is related to rotations about x while $M_{y'}$ is related to rotation about y. It was found experimentally that the effect of a rotation about y on the sensor output was minimal and was effectively drowned out by noise. Hence, this is another movement that could not be controlled by tactile servo. Finally, θ_p is related directly to rotation about z.

Thus, four features can be identified and related to four of the six possible motions of a robot in a Cartesian frame. The feature vector is given by :

$$\vec{F} = \begin{bmatrix} x_c \\ M_0 \\ M_x \\ \theta_p \end{bmatrix}$$

and the differential task state vector is given by :

$$\begin{bmatrix} dx \\ dz \\ \delta x \\ \delta z \end{bmatrix}.$$

5.3.3 Obtaining the components of $\mathbf{J}_s$

As mentioned before, a differential change in $\vec{X}$ leads to a differential change in the associated feature vector $\vec{F}$. These changes are related by the feature sensitivity matrix, $\mathbf{J}_s$, also called the feature Jacobian, as shown below:

$$\mathbf{J}_s = \begin{bmatrix} \frac{\partial x_c}{\partial x} & \frac{\partial x_c}{\partial z} & \frac{\partial x_c}{\partial \Delta_x} & \frac{\partial x_c}{\partial \Delta_z} \\ \frac{\partial M_0}{\partial x} & \frac{\partial M_0}{\partial z} & \frac{\partial M_0}{\partial \Delta_x} & \frac{\partial M_0}{\partial \Delta_z} \\ \frac{\partial M_x}{\partial x} & \frac{\partial M_x}{\partial z} & \frac{\partial M_x}{\partial \Delta_x} & \frac{\partial M_x}{\partial \Delta_z} \\ \frac{\partial \theta_p}{\partial x} & \frac{\partial \theta_p}{\partial z} & \frac{\partial \theta_p}{\partial \Delta_x} & \frac{\partial \theta_p}{\partial \Delta_z} \end{bmatrix}. \tag{5.5}$$

Here, Δ_x refers to a rotation about x and Δ_z refers to a rotation about z.

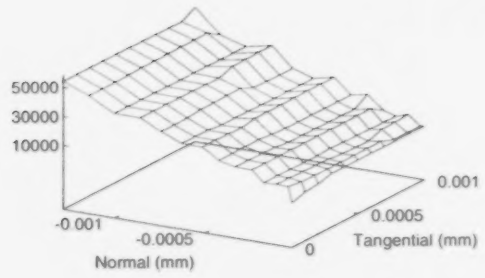

Figure 5.10: $\frac{\partial M_0}{\partial z}$ *(N/mm^2) for contact with a cylinder, as a function of displacements along z and x.*

To control this task using tactile servo, each component of $\mathbf{J}_s$ needs to be identified. The complete specification using theoretical considerations is an extremely difficult task. One approach to doing this, and the associated difficulties, are discussed below.

It has already been pointed out that a theoretical analysis of stress for contact with thin layers is an extremely difficult problem and in most cases closed-form expressions for the stress distribution cannot be obtained. The finite element method was identified as a general alternative method for analyzing contact and some simple cases of contact were characterized in Chapter 4 using this method. If the movement of the robot and the pin is restricted to the $x - z$ plane, then the plane strain assumption becomes applicable and the characterization in Chapter 4 can be used to formulate the Jacobian $\mathbf{J}_s$. Here, the differential task state vector is reduced to 3 components dx, dz, and δy. Correspondingly, the feature vector is also reduced to three components x_c, M_0, and M_y. The Jacobian has nine components obtained by deleting the last row and the last column in Equation 5.5. The Jacobian can be formulated using the procedure described in Chapter 4, and the formulation for x_c and M_0 is given here.

The variation of M_0 and M_y with dx and dz was considered in Chapter 4. Using numerical differentiation, four components of the Jacobian, $\frac{\partial x_c}{\partial x}$, $\frac{\partial x_c}{\partial z}$, $\frac{\partial M_0}{\partial x}$, and $\frac{\partial M_0}{\partial z}$, can be formulated. These are illustrated in Figures 5.10, 5.11, 5.12, and 5.13, respectively. The functions plotted in these figures are not smooth. For example, the functions shown in Figure 5.10 and Figure 5.12 have ridges, while the function illustrated in Figure 5.11 has isolated peaks. These are artifacts introduced by the numerical nature of the analysis. Although these features vary continuously with the displacements, there are discontinuities in these features because of the size of the elements in the finite element model. For example, a small, finite normal displacement is required before additional nodes in the model come in contact with the indenter, and this causes the above mentioned discontinuities.

To analyze the other three components of the differential task state vector, dy, δx, and δz, a three dimensional model of contact needs to be developed. The same

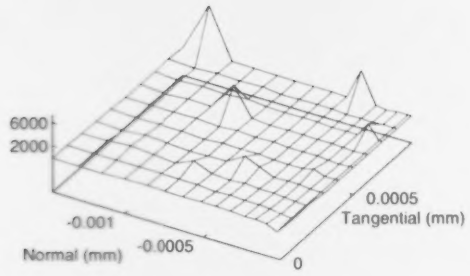

Figure 5.11: $\frac{\partial M_0}{\partial x}$ *(N/mm^2) for contact with a cylinder, as a function of displacements along z and x.*

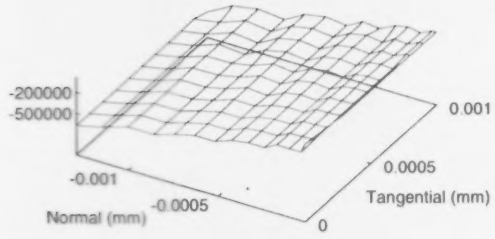

Figure 5.12: $\frac{\partial M_1}{\partial z}$ *(N/mm) for contact with a cylinder, as a function of displacements along z and x.*

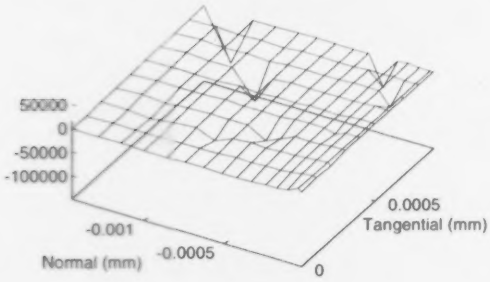

Figure 5.13: $\frac{\partial M_1}{\partial x}$ *(N/mm) for contact with a cylinder, as a function of displacements along z and x.*

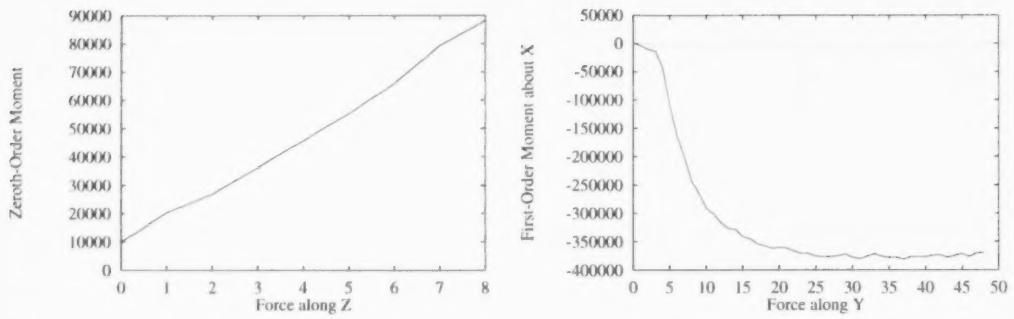

Figure 5.14: *The variation of M_0 and M_x with applied force, obtained experimentally. (a) The relationship between M_0 and increasing normal force. (b) The variation of M_x with increasing tangential force.*

procedure outlined in Chapter 4 can be used. However, the study of three dimensional models is computationally expensive and it was found that current computational resources are barely enough. Such an analysis is planned for the future.

Some experimental data is presented in Figure 5.14 to show the variation of some of these chosen features with the applied forces and displacements. The relationship between M_0 and dx and dz was presented in Chapter 4. It was found that the variation in M_0 is monotonic and non-linear with respect to dz and there is little variation with respect to dx. Figure 5.14(a) shows the variation of M_0 with increasing normal force as obtained experimentally from the tactile sensor. This relationship is monotonic as well and is similar to the one obtained from the model.

Similarly, Figure 5.14(b) shows the variation of M_x with applied tangential force as obtained experimentally from the tactile sensor. Here, the relationship is monotonic but non-linear. It also exhibits a saturation effect because the sensor has a maximum force that it can measure. However, it can be observed that the relationship is nearly linear until the applied force is large enough to cause the sensor to saturate.

The relationships obtained experimentally are shown on scales that differ greatly from those used in presenting the theoretical results. This is because the data from the sensors is used directly and the sensors are not calibrated for force or stress. As mentioned in Chapter 4, the finite element model is approximate and does not model the physical sensor exactly. The purpose of the model was to obtain a qualitative understanding of sensor behavior. To calibrate the tactile sensors and to obtain a quantitative agreement between the model and the sensor requires more accurate models and the exercise is planned for the future.

5.4 Summary

Tactile servo was introduced for controlling tasks involving contact, by analogy with visual servo where vision plays an important role in controlling the motion of an object. The task of rolling a cylindrical pin was used to illustrate tactile servo in detail. The finite-element method was used to model the contact between a cylindrical indenter and a tactile sensor. Using the results obtained from the finite-element analysis as well as experiments with a tactile sensor, a set of features to be used in the tactile servo was identified. These features were then used to develop the tactile servo algorithm. Experimental results are presented in the next chapter.

Chapter 6

Tactile servo : An experiment

The concepts presented in the preceding chapters were verified experimentally. This verification shows the correctness and the applicability of tactile servo. Tactile servo was used to control a robot arm to roll a cylindrical pin on a flat surface. Section 1 describes the experimental setup that was used to perform the given task. The experiment is described in some detail in Section 2, and the experimental results are presented in Sections 3 and 4. Finally, the chapter concludes with a summary and discussion.

6.1 Experimental setup

The hardware organization is shown in Figure 6.1. The backbone of the experimental setup consists of a VME-bus chassis connected to a SUN-3 computer. This machine provides the development environment for the robot system. The control programs are developed in C and then compiled using the standard C compiler available on the SUN-3. These programs are then linked with libraries developed in the laboratory to produce control programs that can be downloaded onto the processor boards for execution [1].

6.1.1 The hardware

The computing power for controlling the robot system is provided by two processor boards connected to the VME bus. Both of these boards support dual ported memory that can be accessed through the VME bus by the other processor boards and the SUN-3, thus leading to a shared-memory system. The Heurikon V2F board is based on the Motorola 68020 processor and the Motorola 68881 floating point co-processor. The Synergy SV400 board is based on the Motorola 68040 processor that has built-in floating point processing capabilities. These two processor boards are also connected

[1] This system was put together by Mr. Steve Sutphen.

to the Sun-3 through serial ports, allowing the Sun-3 to act as a virtual terminal that provides interaction with the ROM monitor programs on the processor boards.

The robot itself is a PUMA 260 and is connected to the VME bus through a set of interface cards. The Datel DVME-628 D/A board provides eight digital-to-analog conversion channels accessible through the VME bus and the analog outputs of six of these channels are connected to the six motors of the PUMA 260. A digital value output to one of these channels specifies the motor current that in turn defines the motor torque. The LYNX LXVME/801 board is wired to the joint encoders on the PUMA 260 and provides information about the joint positions using quadrature decoders for each joint. Thus, the arm is controlled by obtaining the joint positions through the second interface card by reading the given locations on the VME bus, and then computing the torque that is then applied to the motors by writing to the given VME bus locations. The Mizar VME-8605 A/D board provides eight analog-to-digital conversion channels.

The sensory system of the robot consists of two tactile sensors and a six-axis force/torque sensor. These sensors are interfaced to the EMSys IOM-1 processor board based on the Motorola 68000 processor. This board also contains dual-ported memory and is connected to the VME bus. A terminal connected to the processor board through a serial link provides access to the ROM monitor program on the board. The sensors are accessed through this board and are not directly connected to the VME bus. The tactile sensors are of the piezo-resistive type, i.e., the resistance of the sensor varies with the applied force. These sensors were purchased from Interlink Electronics. Each sensor consists of 16x16 elements spread over an area of 1 square inch. The sensor and a sample image obtained from it are shown in Figure 2.1. The sensors are interfaced to the processor board through an electronic interface card and a 10-bit A/D converter. The entire sensor can be scanned in about 5 ms, thus giving a scan rate of 200 Hz. The six-axis force/torque sensor is also connected to the processor board through an electronic interface card and a 10-bit A/D converter. The force is computed in software by using a calibration matrix supplied by the manufacturer. This sensor can be read in about 1 ms, thus giving a scan rate of 1000 Hz. However, this rate is reduced because of the computation required to obtain the force/torque vector.

6.1.2 The software

The robot control program [2] implements the finite-state machine shown in Figure 6.2. The program begins executing in the state labeled START. In this state, the program initializes the state of the robot by setting the joint encoder counts and the joint output torques to zero. The configuration of the robot is completely specified by the joint angles, which are directly related to the encoder counts obtained from the incremental encoders attached to the robot joints. The desired configuration of the

[2]The robot kinematics are taken from Paul and Zhang [51] and the software described here is based on the software developed by Dr. Zhang at the University of Pennsylvania.

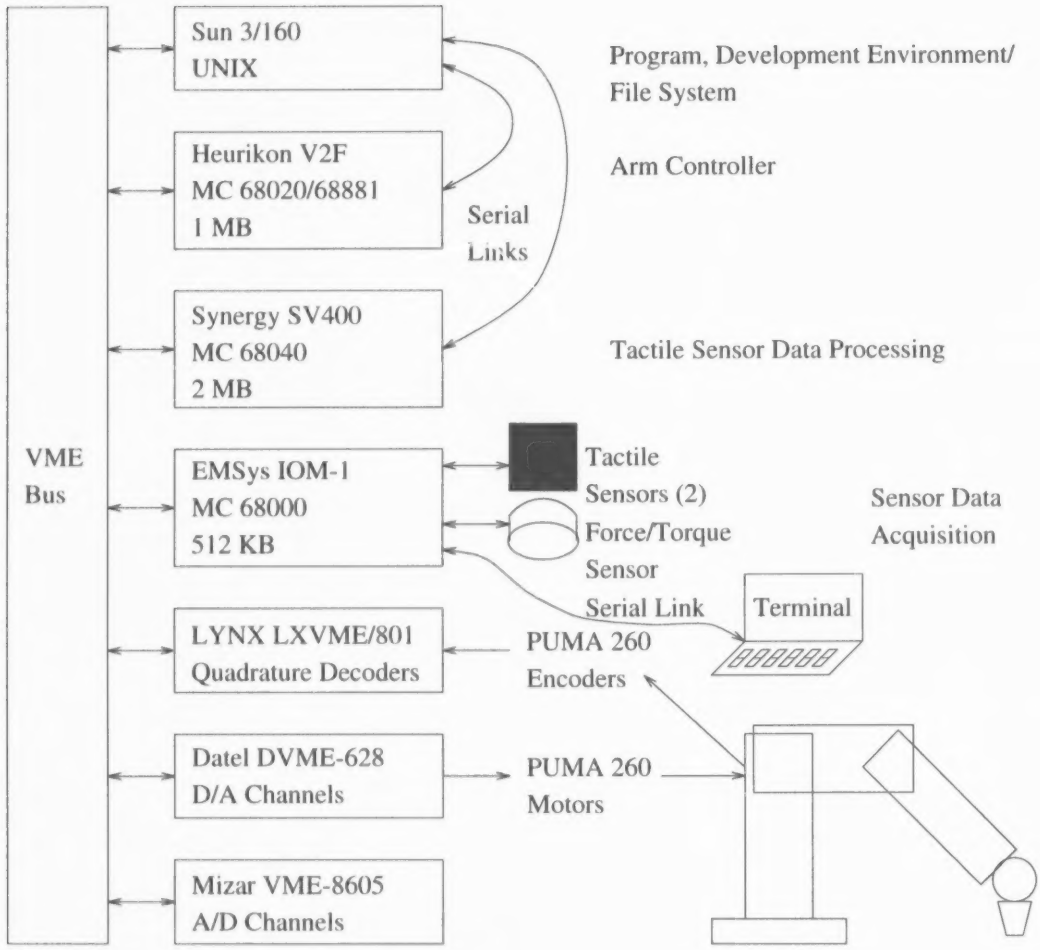

Figure 6.1: *The Experimental Setup.*

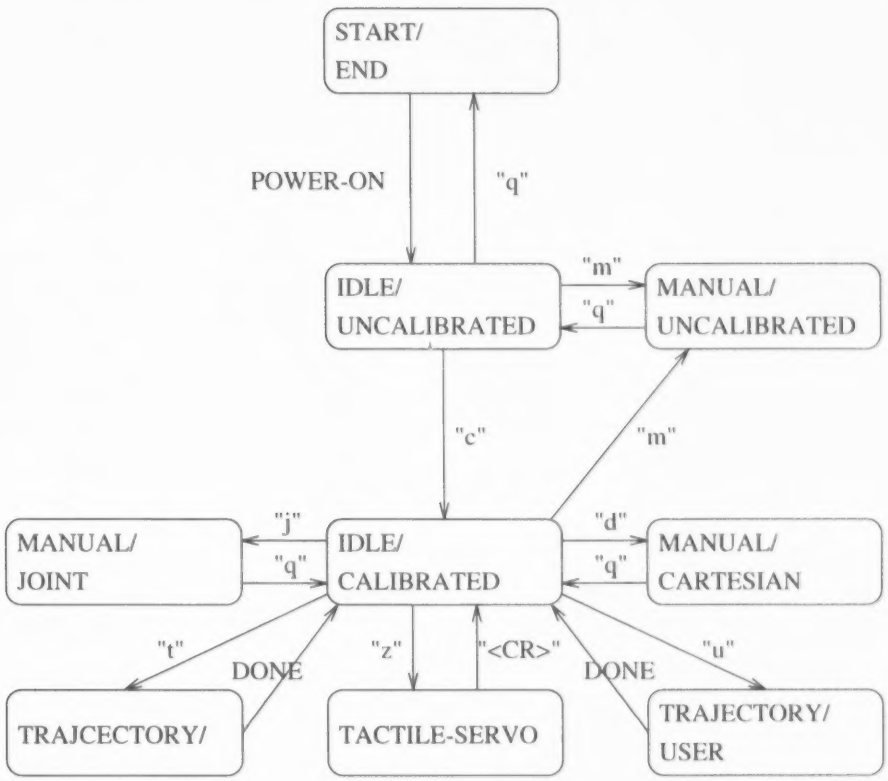

Figure 6.2: *The finite-state machine corresponding to the robot control program.*

robot, in terms of the desired encoder values, is initialized to zero. The program also sets up the timer interrupt.

When power to the robot is turned on, the program state changes from START to IDLE/UNCALIBRATED. In this state, the robot position is maintained in its current configuration by a low-level position control algorithm running in the background at a rate of 400 Hz, or once every 2.5 ms. In each time-step, this algorithm computes the error between the current values obtained from the joint encoders and the desired values of the joint encoders, and then uses proportional-derivative control to compute the required output torques needed to drive the joint motors. Since the incremental encoders were initialized to zero, and the desired encoder values were also initialized to zero, the control algorithm maintains the current configuration of the robot. Since the robot could be in some arbitrary position on startup, this state is called uncalibrated. To be able to specify trajectories in terms of joint angles or Cartesian coordinates, the robot must first be moved to the home position and then the incremental encoder counts must be reinitialized to zero. This is called calibration of the robot. To move the robot in the uncalibrated state, the user can change the robot state to MANUAL/UNCALIBRATED and then change the robot configuration joint-by-joint to the home configuration, using the keyboard as a joystick. The user

can then change the state of the robot back to IDLE/UNCALIBRATED and then to IDLE/CALIBRATED.

Once the robot is in the IDLE/CALIBRATED state, the user can specify any one of a number of different states to move the robot. The MANUAL/JOINT state allows the user to use the keyboard as a joystick to move the robot in the joint space. Similarly, the MANUAL/CARTESIAN state allows the control of the robot in the Cartesian space using the keyboard. The user can specify the direction of translation or rotation as well as the desired velocities. The TRAJECTORY state allows the robot to carry out pre-programmed moves. Each move specifies a goal configuration in Cartesian space and can be carried out in joint space or in Cartesian space. The TRAJECTORY/USER state is similar to the TRAJECTORY state except that in this state the user types in the moves on-line, using the keyboard. The TACTILE-SERVO state is used to perform the task of rolling a pin using *tactile servo* described in Chapter 5.

As mentioned above, the robot is controlled by a background process running every 2.5 ms, or at a frequency of 400 Hz. This background process is coded as an Interrupt Service Routine (ISR) for the timer interrupt and the desired rate is achieved by setting the time. The ISR computes the next desired set-point in terms of desired values for the incremental joint encoders. It then obtains the current values of the joint encoders and computes the error and the derivative of the error, which are then used to compute the required output torques for the joint motors using proportional-derivative (PD) control. The computation of the next desired set-point depends on the current state of the robot. In the IDLE/CALIBRATED state, the set-point remains the same. In the MANUAL/JOINT state, the set-point is obtained from the desired values of the joint angles. The computation in the MANUAL/CARTESIAN state is complicated. The desired change in Cartesian coordinates is obtained from the keyboard joystick and is converted to a change in the joint angles. This is then added to the current values of the joint angles to obtain the desired joint angles. The desired values of the encoder counts are obtained directly from the joint angles.

In the TRAJECTORY state, the desired moves are stored in a queue. The motion between two moves is interpolated using the method presented by Paul [50]. For moves in joint space, the interpolation is done for the joint angles. For moves in Cartesian space, the interpolation is done on the position of the robot in Cartesian space, after which inverse kinematic equations of the robot are used to obtain the corresponding joint angles. This interpolation is done on-line during each time-step by the ISR, depending upon the parameters of the current move. The desired values of the joint encoders are obtained directly from the joint angles.

The program implementing the robot control system and the ISR runs on the Heurikon V2F processor board. Tactile servo, because of the sensor data processing requirements, requires additional programs running on the other two processor boards, the Synergy SV400 and the EMSys IOM-1. In the TACTILE-SERVO state, the control of the robot is dependent on the tactile sensor. In each time-step, the ISR queries the tactile sensor through the program running on the Synergy processor

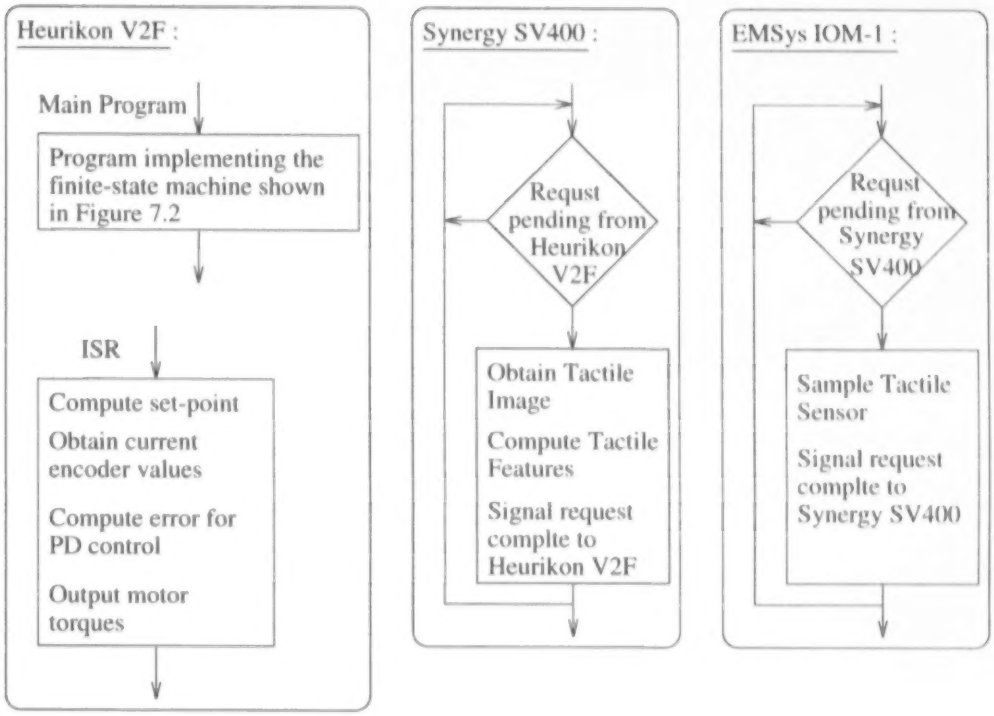

Figure 6.3: *The organization of the robot control software.*

board. This program obtains an image from the tactile sensor using the program running on the IOM-1 processor board and then computes several features from this image. The ISR uses these values to compute errors in the feature space, i.e., the difference between the desired feature values specified by the user and the feature values obtained from the sensor. These errors are then transformed into errors in the joint space using the feature sensitivity matrix and the manipulator Jacobian matrix, as described in Chapter 5. These errors in joint space are added to the current values of the joint angles to obtain the desired joint angles, which directly yield the desired values of the joint encoders. The system organization is shown in Figure 6.3. The tactile servo algorithm is shown in Figure 6.4.

6.2 Tactile servo : Rolling a pin

The algorithm outlined in the previous chapter was implemented for the simple operation of pushing a cylindrical peg on a planar surface, using a planar end-effector mounted on a PUMA 260 industrial robot.

To obtain $\mathbf{J}_s$, a relation between the selected features and the six components of the manipulator tip position must be obtained. However, as mentioned in Chapter 5, because of the geometry of the task, and because of noise in the sensor, information

let

$\vec{\theta}$: current joint angles

$\vec{F}$: measured feature vector

$= [M_0, x_c, M_x, \theta_p]^T$

$\vec{F}^d$: desired feature vector

$= [M_0^d, x_c^d, M_x^d, \theta_p^d]^T$

if (new data from the tactile sensor is available) **then**

compute M_0, M_x, M_y

compute $x_c = \frac{M_y}{M_0}$

compute $y_c = \frac{M_x}{M_0}$

compute $M_{x'x'}$, $M_{x'y'}$, $M_{y'y'}$

compute $\theta_p = \frac{1}{2}\tan^{-1}\frac{-2M_{x'y'}}{M_{x'x'}-M_{y'y'}}$

compute the feature error vector $d\vec{F} =$

$[M_0^d - M_0, x_c^d - x_c, M_x^d - M_x, \theta_p^d - \theta_p]^T$

compute $d\vec{X} = J_s^{-1} d\vec{F}$

compute $d\vec{\theta} = J_\theta^{-1} d\vec{X}$

Figure 6.4: *The tactile servo algorithm.*

about two of the components of the manipulator tip position, dy and δy, cannot be obtained from the tactile sensors. Therefore, four features are used to control four degrees of freedom of the arm in a Cartesian frame.

It was also mentioned in Chapter 5 that it is difficult to formulate the Jacobian completely using the available resources. It was found that sometimes the coupling between different features is minimal. Intuitively, it can be argued that the off-diagonal elements of the feature sensitivity matrix are small compared to its diagonal elements. For example, consider the first row of the feature sensitivity matrix. Compared to a movement along x_s, the effects on x_c of a translation along z_s or rotations about x_s and z_s are minimal. Similarly, considering the second row of the feature sensitivity matrix, it can be observed that compared to a translation along z_s, the effects of a translation along x_s and rotations about x_s and z_s are small. Similar arguments can be made for the third and the fourth rows of the feature sensitivity matrix. Therefore, the Jacobian matrix is dominated by the elements on the diagonal. It is easy to show that for matrices of order less than or equal to four, if the matrix is dominated by the elements on the diagonal, then the inverse of the matrix is also dominated by the diagonal elements. Here, as a crude approximation, $\mathbf{J}_s$ is assumed to be diagonal.

$$\mathbf{J}_s = \begin{bmatrix} k1 & 0 & 0 & 0 \\ 0 & k2 & 0 & 0 \\ 0 & 0 & k3 & 0 \\ 0 & 0 & 0 & k4 \end{bmatrix}. \tag{6.1}$$

This Jacobian was used in equation 5.3 in the previous chapter to provide the control algorithm for tactile servo for the given task of rolling a pin. A data collection rate of 200 Hz from the tactile array was achieved, while the position servo loop was running at 400 Hz. The robot was programmed to roll a cylindrical pin of radius 23 mm on a planar surface using tactile servo. For the robot to do the task without considering the contact stability problem, this surface was also covered with a layer of soft rubber. The rubber layers on the table top and tactile sensor also improve contact. The experimental setup is shown in Figure 6.5 along with the base frame and the sensor frame. The robot is shown in the home position.

The planar surface was mounted on a motorized pan-tilt table which itself was mounted on a pair of sliders. This provides two rotational degrees of freedom, pan about z_0 and tilt about x_0, and one translational degree of freedom, movement along x_0. By turning the pan-tilt table 90 degrees, panning about y_0 and translation along y_0 can be provided. This arrangement was used to examine the performance of tactile servo for different orientations of the planar surface as well as for dynamically changing orientations and translations of the planar surface. Figure 6.6 shows the robot rolling the pin on the pan-tilt table. Again, the frames are marked on the photograph. This is the normal configuration of the robot when rolling the pin and the picture shows that x_s is oriented at an angle of 180 degrees with respect to x_0 while z_s is oriented at an angle of 180 degrees with respect to z_0.

In the experiment, the orientation of the table top is not known to the tactile servo algorithm and it is able to control the robot to orient its end-effector appropriately

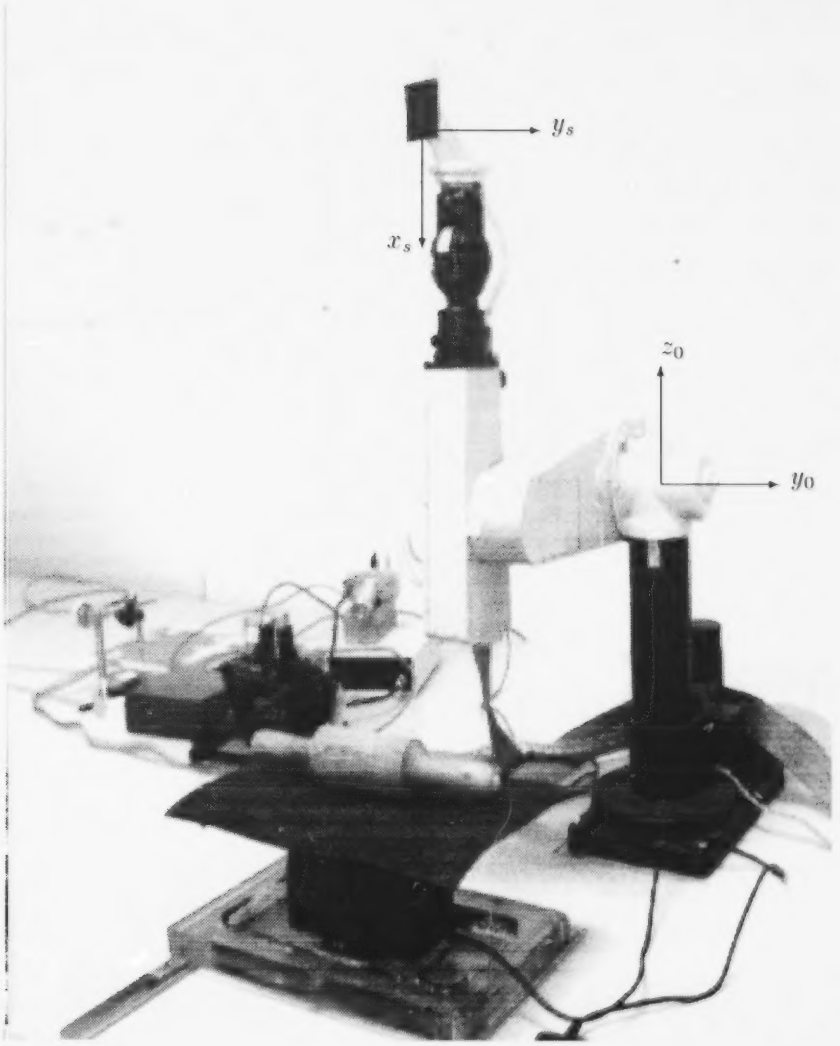

Figure 6.5: *A photograph of the robot, the pan-tilt table, and the rolling pin. The robot base frame, (y_0, z_0), and the sensor frame, (x_s, y_s), are both shown.*

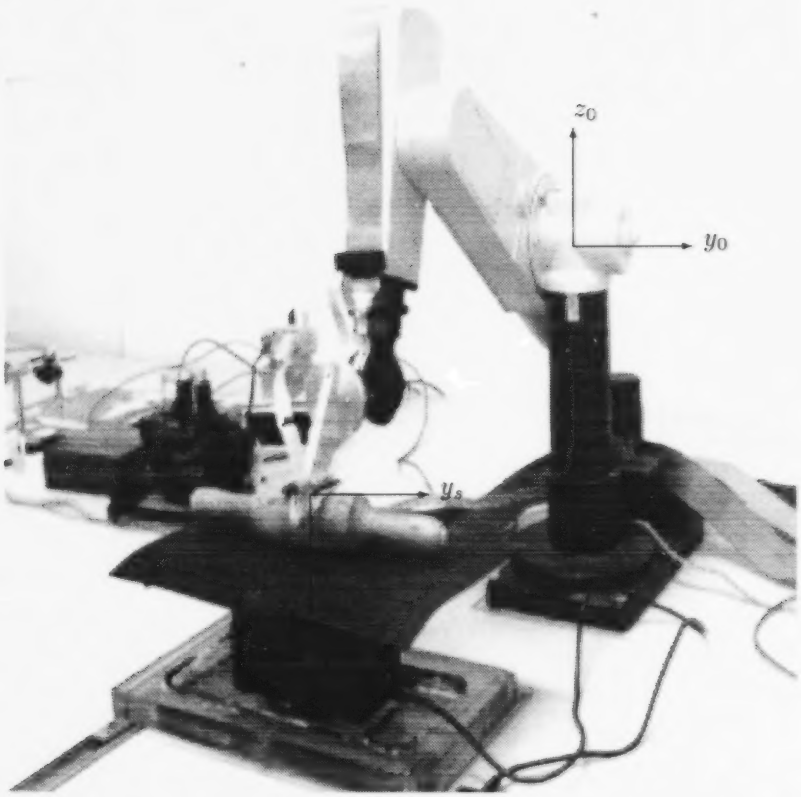

Figure 6.6: *A photograph of the robot rolling the pin on the pan-tilt table.*

to accommodate the changes in the orientation of the table top over time.

The robot was controlled to move back and forth along x_s. This was achieved by alternately setting the desired value of x_c to be close to the two ends of the tactile sensor. Figure 6.7 shows an enlarged view of the tactile sensor along with the sensor frame. The sensing sites are formed by superimposing two halves such that one half consists of rows of piezo-resistive material while the other half consists of columns of piezo-resistive material. The superimposition forms a matrix of sensitive sites. The rows and columns are numbered from 1 to 16 and the features are computed based on these numbers. Therefore, x_c must vary between 1 and 16. Initially, the desired value of x_c is set to be 2. Once this value is achieved to within a given tolerance, here set at 0.5, the desired value is changed to 15. The linear speed of this rolling motion along x_s is about 10 mm/s.

The desired value for M_0 was set to 15000. As mentioned before, M_0 is related to the normal force being exerted on the tactile sensor. Each sensing site on the tactile sensor is sampled using a 12-bit A/D converter and can hence correspond to a maximum value of 4095 for a given force, which in this case is obtained for a relatively small force of a few Newtons. Thus, a value of 15000 corresponds to a relatively small normal force.

The desired value for M_y was set to 0. This corresponds to a symmetrical stress distribution corresponding to zero tangential force and moment. Thus, these two set-points cause the robot to maintain an orientation normal to the cylinder.

The desired value for θ_p was also set to 0. This causes the robot to push the pin in a direction that is normal to both the axis of the cylinder and the surface normal of the sensor.

The numerical values for $k1$, $k2$, $k3$, and $k4$ were determined experimentally using trial and error and were set at 20, 20000, 200000, and 1000, respectively.

In summary, the controlled variables or the controlled tactile features, their desired values, and the elements of the feature sensitivity matrix are shown below:

$$
\begin{aligned}
x_c &= 2, 15 \\
M_0 &= 15000 \\
M_y &= 0 \\
\theta_p &= 0 \\
\mathbf{J}_s &= \begin{bmatrix} 20 & 0 & 0 & 0 \\ 0 & 20000 & 0 & 0 \\ 0 & 0 & 200000 & 0 \\ 0 & 0 & 0 & 1000 \end{bmatrix}.
\end{aligned}
$$

The motorized pan-tilt table was used to examine the performance of tactile servo for several orientations of the planar surface on which the cylinder was rolled by the robot. The setup was also used to study the dynamic performance of tactile servo by changing the orientation of the pan-tilt table while the cylindrical pin was being rolled. The results of these experiments are presented in the following sections.

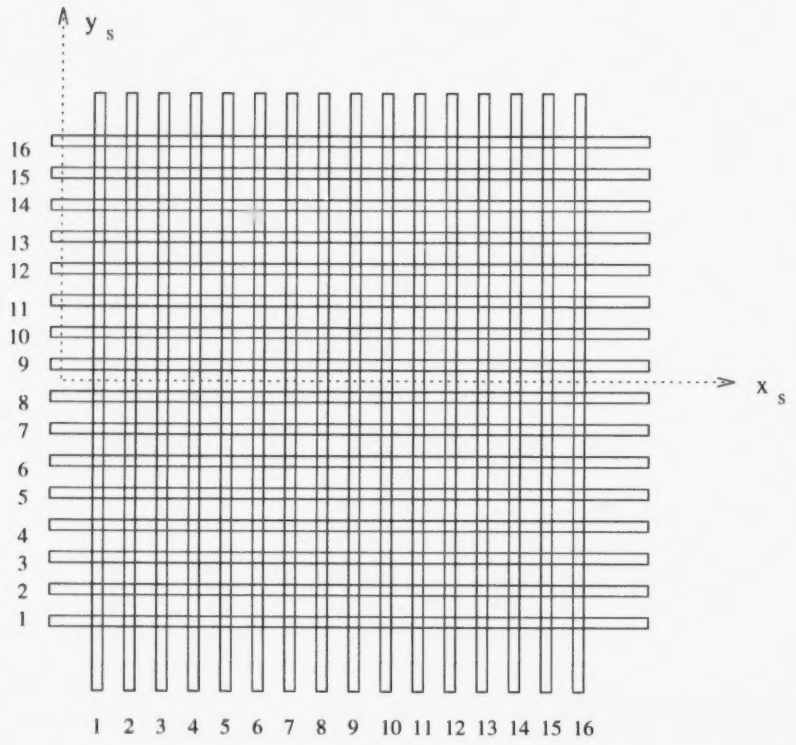

Figure 6.7: *Setting up the desired value of* x_c.

6.3 Rolling a pin on a flat surface

In this section, results from rolling a pin on a fixed plane are presented. A number of experiments were conducted by changing the orientation of the plane. The data was collected after the robot had adjusted to the change in orientation. Therefore, these results show the performance of tactile servo in a static environment. Figures 6.9 through 6.12 show the change in several different variables over a 10 second time interval as the robot rolled a pin along x_0, on a flat surface oriented approximately normal to z_0.

The orientations and attachments of the different frames are shown in Figures 5.5, 6.5, and 6.6. It can be observed from Figure 6.6 that x_s and z_s of the sensor frame attached to the robot fingertip are oriented 180 degrees from x_0 and z_0 of the robot base frame, respectively. This is the normal rolling configuration of the robot and as long as there are no changes in the orientation of the table, the orientation of the sensor frame does not change with respect to the base frame. However, tactile servo tracks changes in the orientation of the pin, and the commanded desired values cause the robot to always roll the pin in the plane of the pan-tilt table such that the face of the robot fingertip is parallel to the plane of the table and the direction of motion is normal to the axis of the rolling pin. Since no rotations are made about y_0, the response of the tactile servo to changing orientations of the pan-tilt table can be studied by examining the two angles illustrated in Figure 6.8. The first angle, θ_{z_s}, is the angle formed by z_s of the sensor frame attached to the fingertip and the plane formed by $x_0 - z_0$ of the base frame, and is shown in Figure 6.8(a). Figure 6.8(b) shows the other angle, θ_{x_s}, formed by x_s of the sensor frame and the $x_0 - z_0$ plane. In the following discussion, p_x, p_y, and p_z, refer to the position of the origin of the sensor frame with respect to the base frame.

6.3.1 Rolling a pin on a plane aligned with the base frame

Figure 6.9(a) shows the variation in x_c as computed from the tactile sensor while the robot was rolling the pin. During this 10 second interval, the robot reversed direction three times and this can be easily seen from the figure. Figure 6.9(b) shows the change in p_x as computed from the joint encoders while the pin was being rolled. As x_c changes from about 3 to 14, the fingertip position changes from about 308 mm to about 342 mm, respectively. The robot fingertip position closely follows the feature x_c.

The variation in the feature M_0 is shown in Figure 6.10(a), while Figure 6.10(b) shows the change in p_z. It changes by 1.4 mm between -148.2 mm and -149.6 mm. This is a large change for this variable and suggests that the pan-tilt table was slightly tilted about the y_0-axis. p_z changes from -149.4 mm to -148.8 mm as the arm rolls along x_0 from 342 mm to 308 mm. Then, as the arm rolls back to 340 mm along x_0, this position changes again to -149.6 mm. The change during the third stage from about 7 seconds to about 10 seconds closely follows the change during the first stage from 0 seconds to 3 seconds, suggesting that the arm is able to detect and track small

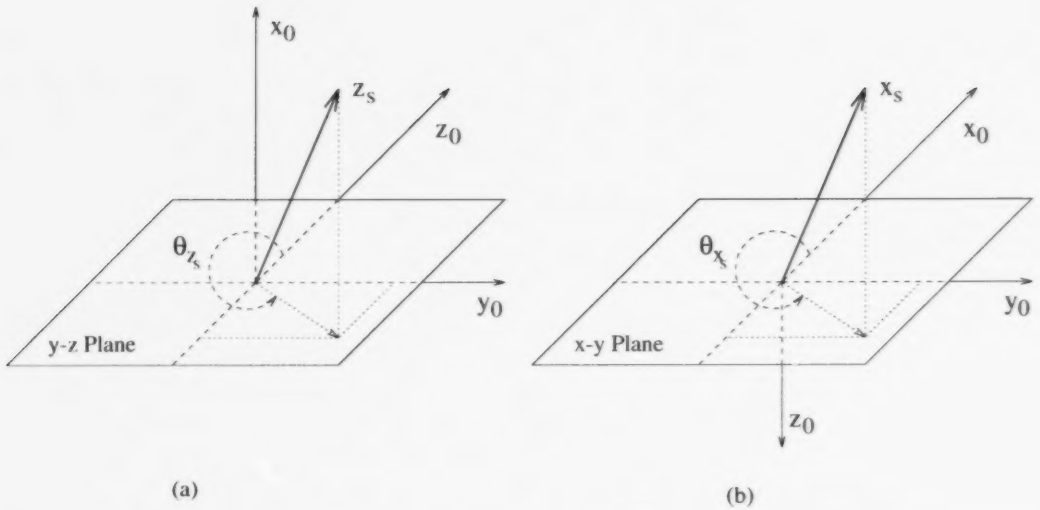

Figure 6.8: *The angles (a) θ_{z_s} and (b) θ_{x_s} used to demonstrate the effect of changing orientation of the pin on tactile servo.*

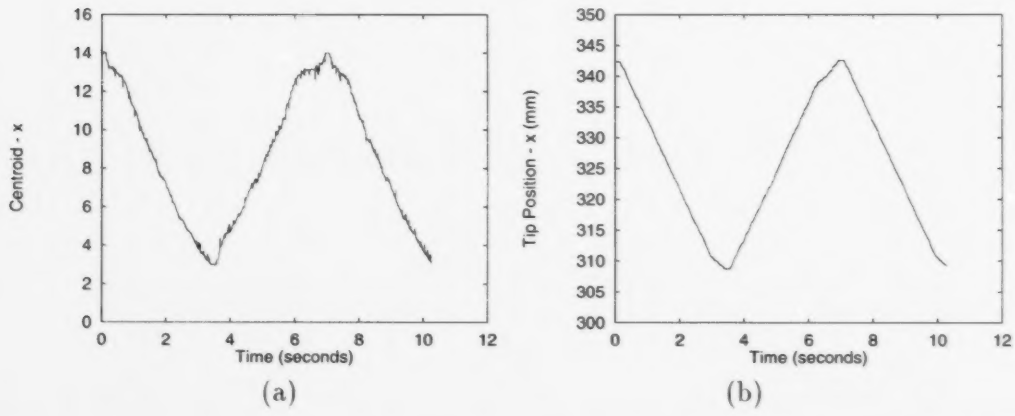

Figure 6.9: *The variation in (a) x_c and in (b) p_x while rolling the pin on a flat table aligned with the axes of the robot base frame.*

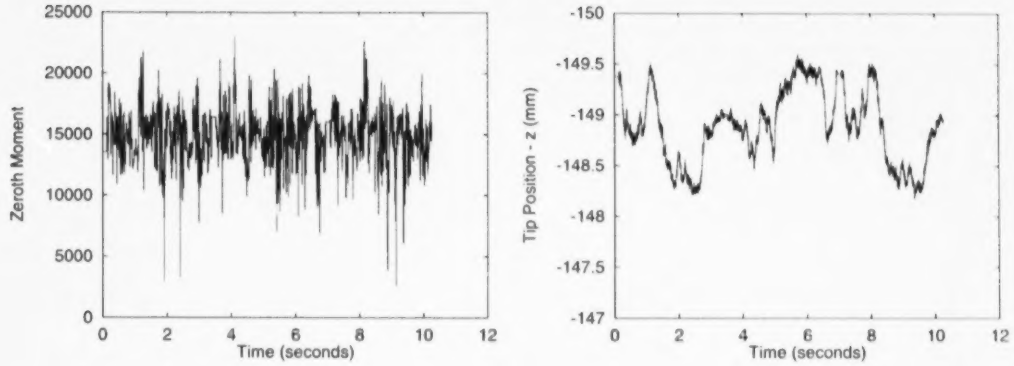

(a) (b)

Figure 6.10: *The variation in (a) M_0 and in (b) p_z while rolling the pin on a flat table aligned with the axes of the robot base frame.*

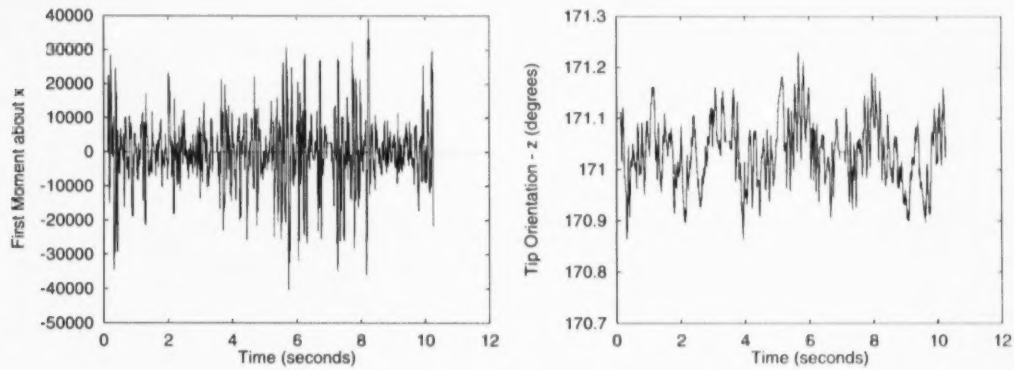

(a) (b)

Figure 6.11: *The variation in (a) M_x and in (b) θ_{z_s} while rolling the pin on a flat table aligned with the axes of the robot base frame.*

irregularities in the surface or the cylindrical pin. M_0 stays close to 15000, except for some large variations, and it is seen that the sensor data is noisy.

The change in the feature M_x as a function of time is plotted in Figure 6.11(a). Although centered around zero, this feature is also noisy, reflecting the noise in the sensor data. Figure 6.11(b) shows the variation in θ_{z_p}. The total change is 0.4 degrees varying between 170.85 degrees and about 171.25 degrees. Ideally, if there were no errors in the robot calibration and if the table was exactly aligned with z_0, this angle would be 180 degrees. The angle indicates that z_s-axis attached to the fingertip points downwards. However, it is off from 180 degrees by about 10 degrees. This error arises from calibration errors and errors in aligning the table with z_0. In particular, the fourth and sixth joints in the robot wrist are difficult to calibrate and are the major contributors to this error.

Finally, Figure 6.12(a) shows the change in the feature θ_p as a function of time.

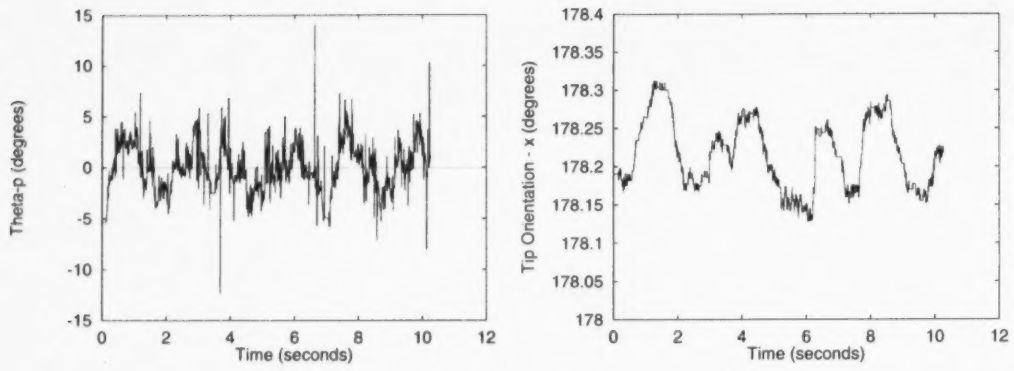

(a) (b)

Figure 6.12: *The variation in (a) θ_p and in (b) θ_{z_s} while rolling the pin on a flat table aligned with the axes of the robot base frame.*

Like all the other features, this feature too is noisy, and the noise here is more than for the other features. With the exception of a few peaks, the feature varies from about -5 degrees to about 5 degrees, a large change given that the task is performed without any disturbance. Figure 6.12(b) shows the corresponding variation in θ_{z_s}. Here, the change is about 0.2 degrees, from about 178.1 degrees to about 178.3 degrees.

6.3.2 Rolling a pin on an inclined plane

The next step is to study the performance of tactile servo for other orientations of the plane on which the pin is to be rolled. Figure 6.14 shows the pan-tilt table in the initial horizontal position with the rolling pin lying on it. The axes attached to the table are labeled x_t, y_t, and z_t, and in this initial position the axes are aligned with the robot base frame. The panning motion consists of a rotation about z_0, while the tilting motion consists of a rotation about x_0.

Figure 6.13 shows the variation in x_c, M_0, p_z, and p_x, as the pin is rolled on the pan-tilt table tilted about y_0 by a fixed angle. In this position, the elevation of the pin changes at a fixed rate as it is rolled on the table along x_0, depending on the angle of inclination. Figure 6.13(a) shows that x_c changes as before, between 3 and 14. Figure 6.13(b) shows the variation in p_x. It changes by 33 mm, from 285 mm to 318 mm, which is similar to the distance rolled on a platform that was horizontal. Figure 6.13(d) shows the change in p_z as the arm rolls the cylinder. This variable changes smoothly from -156.5 mm to about -152 mm, an increase of 4.5 mm. The change reflects the slope of the platform. This is in contrast to the small variation of about 1 mm for a horizontal plane, and corresponds to a slope of about 8 degrees from the horizontal. Figure 6.13(c) shows the corresponding variation in M_0. As the cylinder rolls along x_0 during the first forward movement form 285 mm to 318 mm, it gains height and this causes an increase in M_0, which is corrected by an upward motion of the fingertip. When the cylinder is rolled back, during the period from

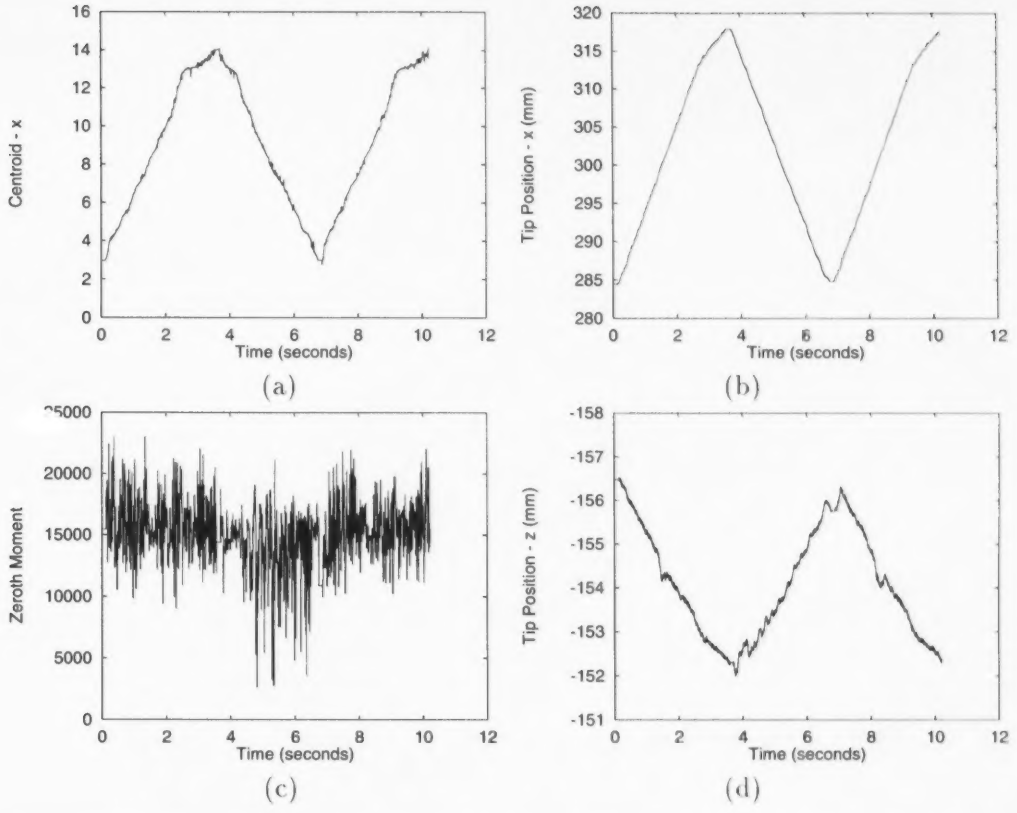

Figure 6.13: *The variation in (a) x_c, (b) p_x, (c) M_0, and (d) p_z, while rolling the pin on a flat table inclined about y_0.*

about 4s to 7s, the opposite takes place. The cylinder loses height, thus reducing M_0, which is then corrected by a downward motion.

Figure 6.15 shows the results obtained by rolling the pin on the table tilted about x_0. Figure 6.15(a) shows the variation in M_x, while Figure 6.15(b) shows the variation in θ_{z_s}. This angle lies between -174.5 degrees and -175 degrees, indicating a rotation of about 14 degrees from the first case.

The pan-tilt table is next panned by a fixed angle. This corresponds to a rotation about z_0 and the axis of the rolling pin is no longer aligned with y_0 and the robot rolls the pin in a direction at an angle to x_0. The results of rotating the table about z_0 are shown in Figure 6.16. The variation in θ_p is plotted in Figure 6.16(a) and is similar to that for the first case. Figure 6.16(b) shows the change in θ_{x_s}. Here, the angle changes from about -160 degrees to about -161.5 degrees, a change of 1.5 degrees. Comparing with the first case, the rotation is about 22 degrees. The change in θ_{x_s}, as the pin is rolled, is 1.5 degrees, which is larger than the change of 0.2 degrees in the first case. Since the variation in θ_p is similar to that for the first case, this large change could be a result of the inaccuracies in the manipulator Jacobian.

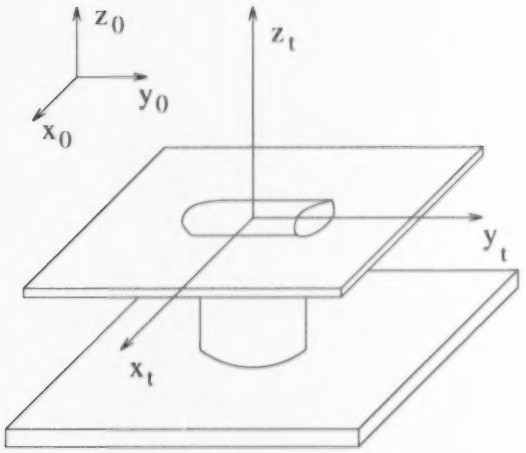

Figure 6.14: *The pan-tilt table shown with its axes aligned with the robot base frame.*

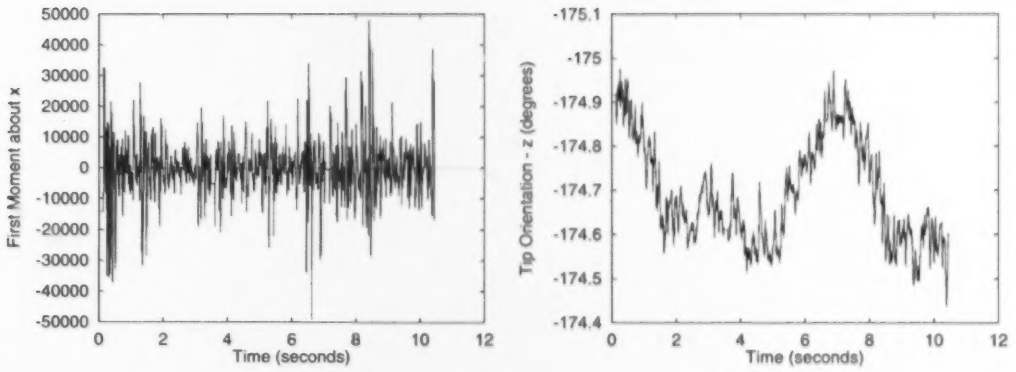

(a) (b)

Figure 6.15: *The variation in (a) M_x and (b) θ_{z_s}, while rolling the pin on a flat table inclined about x_0.*

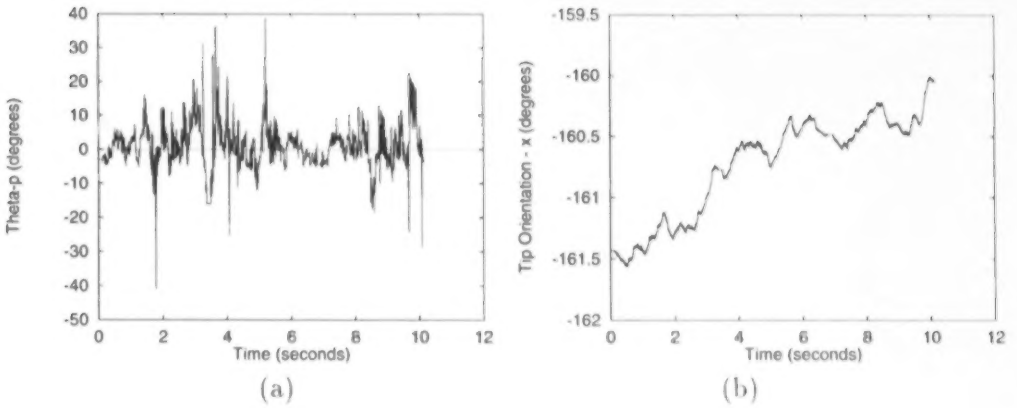

(a) (b)

Figure 6.16: *The variation in (a) θ_p and (b) θ_{x_s}, while rolling the pin on a flat table rotated about z_0.*

Finally, the orientation of the table was changed about the three axes simultaneously. The results of rolling the pin on this table are shown in Figures 6.17 through 6.20. Figures 6.17(a) shows x_c, while Figures 6.17(b) plots the variation in p_x. The change here is 32 mm, from 286 mm to 318 mm, similar to the change when the table was rotated about y_0 alone. The changes in M_0 and p_z are plotted in Figure 6.18, (a) and (b), respectively. The fingertip position changes from -146.5 to -141.5, a change of 5 mm. This, too, is similar to the change of 4.5 mm when the table was rotated about y_0 alone. Since the motorized tilt axis was aligned with y_0, a small tilt was provided about x_0 by placing an approximately 40 mm wide bar under one end of the pan-tilt table. The variations in M_y and θ_{z_s} are shown in Figure 6.19, (a) and (b), respectively. The angle varies between 171.6 degrees and 172 degrees, which is similar to the other cases for this variable. It indicates a small rotation of about 2 degrees. Figure 6.20 (a) and (b) shows the variation in θ_p and θ_{x_s}. The angle changes from -162.2 degrees to -162.7 degrees, which is similar to the orientation of about -161 degrees when the table was rotated about z_0 alone. However, the change of 0.5 degrees is less than that for the other case and is similar to the case when the table was aligned with the axes of the base frame.

These results show that tactile servo performs well under static conditions where the environment is not changing. It is difficult to quantify performance since a test case to compare with is not available. There is a variation in performance in terms of speed and jitter depending on the values assigned to the constants in the feature sensitivity matrix. These values were tuned experimentally to obtain the fastest possible speeds with acceptable jitter. The performance of tactile servo is generally not affected by the orientation of the table. The only problem that can be seen from these results is the behavior of the feature θ_p. The noise in this feature is large, and hence the noise in θ_{x_s} is also large.

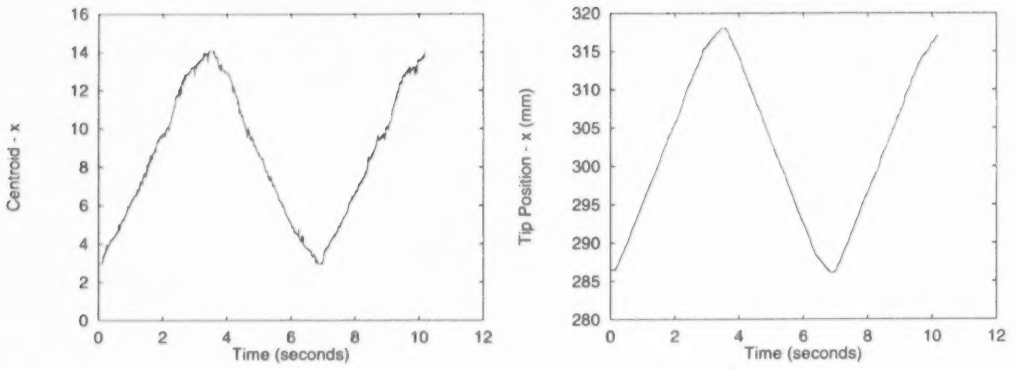

(a) (b)

Figure 6.17: *The variation in (a) x_c and (b) p_x while rolling the pin on a flat table inclined with respect to all three axes of the robot base frame.*

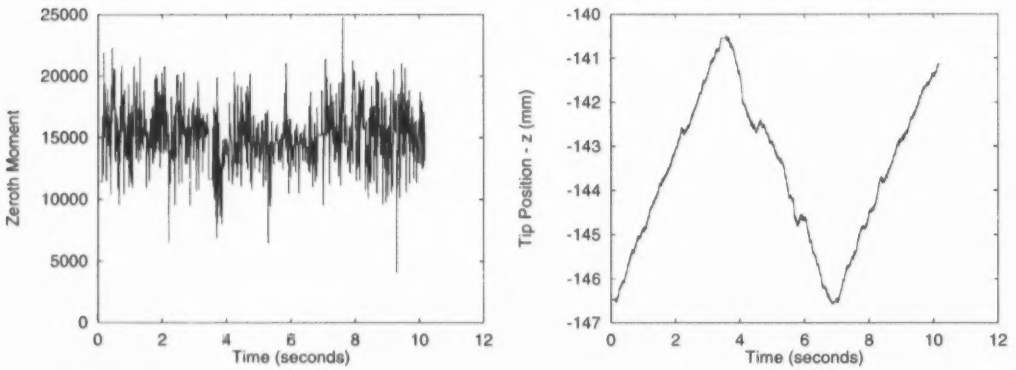

(a) (b)

Figure 6.18: *The variation in (a) M_0 and (b) p_z while rolling the pin on a flat table inclined with respect to all three axes of the robot base frame.*

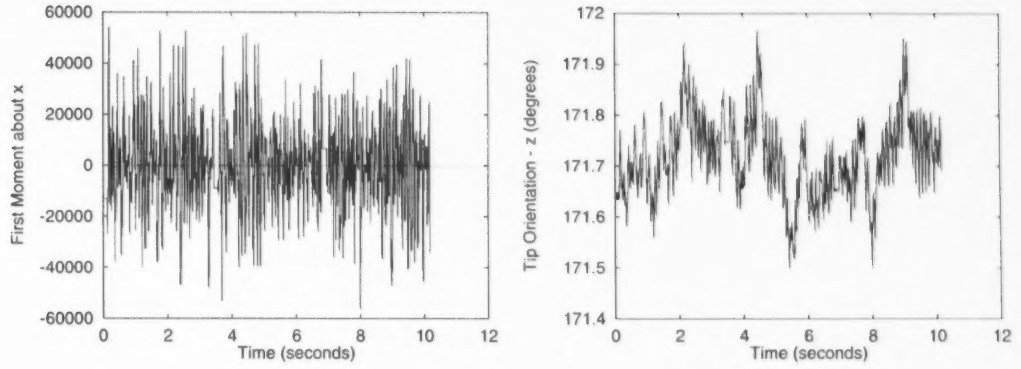

Figure 6.19: *The variation in (a) M_x and (b) θ_{z_s} while rolling the pin on a flat table inclined with respect to all three axes of the robot base frame.*

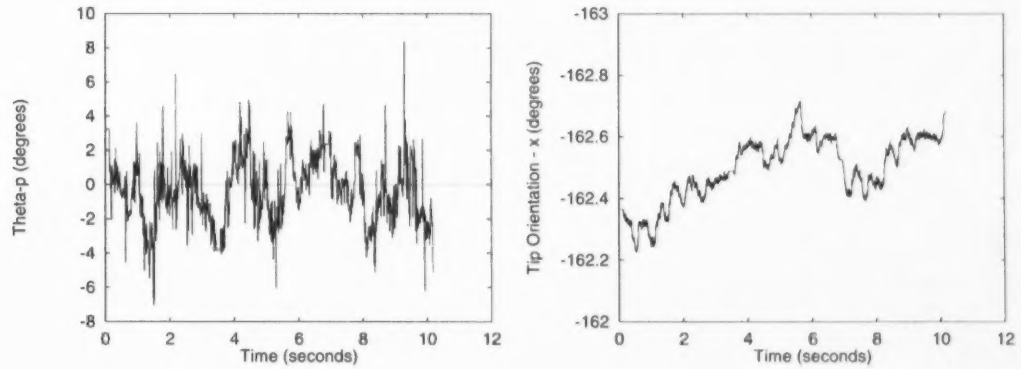

Figure 6.20: *The variation in (a) θ_p and (b) θ_{x_s} while rolling the pin on a flat table inclined with respect to all three axes of the robot base frame.*

6.4 Rolling the pin on a moving table

The performance of tactile servo is considered in the presense of disturbances as the task is performed. Disturbance is provided by changing the orientation of the motorized pan-tilt table while the robot is rolling the pin on it. The motors turn at a fixed speed and this allows the disturbance to vary in an even manner. This additionally allows an examination of the tracking performance of tactile servo.

6.4.1 Translation along z_0

Although the pan-tilt table cannot be moved up and down, a controlled disturbance along z_0 can be provided by aligning the tilt-axis of the table with y_0 and then tilting the table at a controlled rate about this axis, with reference to Figure 6.14. Due to this rotation, as the pin rolls along x_0, it moves up or down at a steady rate due to the steady rotation of the table. Figure 6.21 shows the change in p_x, the x-coordinate of the fingertip position in the base frame. The plot labeled (1) corresponds to the pin rolling on the flat surface aligned with the axes of the robot. The position changes from 291 mm to 325 mm. The plot labeled (2) shows the change in p_x as the pin rolls on the surface and the pan-tilt table is rotated about y_0 at a constant speed. The rotation of the table causes an additional movement of the pin along x and this is reflected in a longer distance traveled along x_0 in the first forward motion, and in the backward movement terminating before the original value of p_x is reached. The trajectory labeled (3) shows the movement of the pin on the tilted surface. Here, p_x changes from 297 mm to 332 mm. These limits are shifted along x_0 and do not change with time, reflecting the tilt of the surface. Figure 6.22(a) shows the variation in p_z, the z-coordinate of the fingertip position in the base frame. The trajectory labeled (1) corresponds to the pin rolling on a flat surface aligned with the axes of the robot, and here the position remains steady at about -149.5 mm. The curve labeled (2) shows the change in p_z as the pin rolls and the surface is tilted about y_0 at a constant rate. The position changes steadily to about -134.5 mm after about 6.75 s. The rotation of the table stops after about 6 s, and the change after this point corresponds to the constant tilt of the surface. The plot labeled (3) shows p_z changing steadily, reflecting the constant tilt of the surface. Figure 6.22 (b), (c), and (d), show the change in M_0 for the flat surface aligned with the robot axes, the surface being tilted about y_0 as the pin rolls, and the tilted surface, respectively.

6.4.2 Rotation about x_0

The tilt axis of the pan-tilt table is aligned with x_0. Rotating the table about this axis causes a change in the orientation of the surface that is used to study the response of tactile servo to rotational disturbance about x_0. Figure 6.23(a) shows the variation in θ_{z_s}. The plot labeled (1) corresponds to the pin being rolled on the table aligned with the axes of the robot. The angle stays constant around 170 degrees. The curve labeled (2) corresponds to the change in this angle as the table is rotated about x_0 at

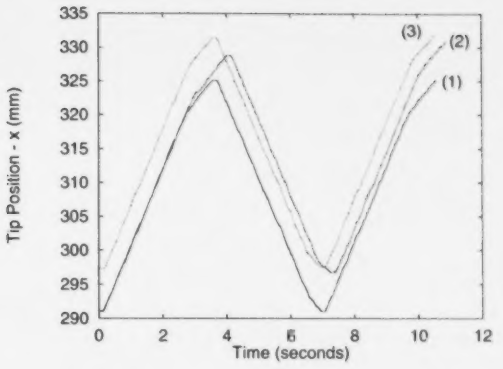

Figure 6.21: *The variation in p_x, while rolling the pin on a flat table that is (1) stationary, (2) rotating about y_0, and (3) inclined about y_0.*

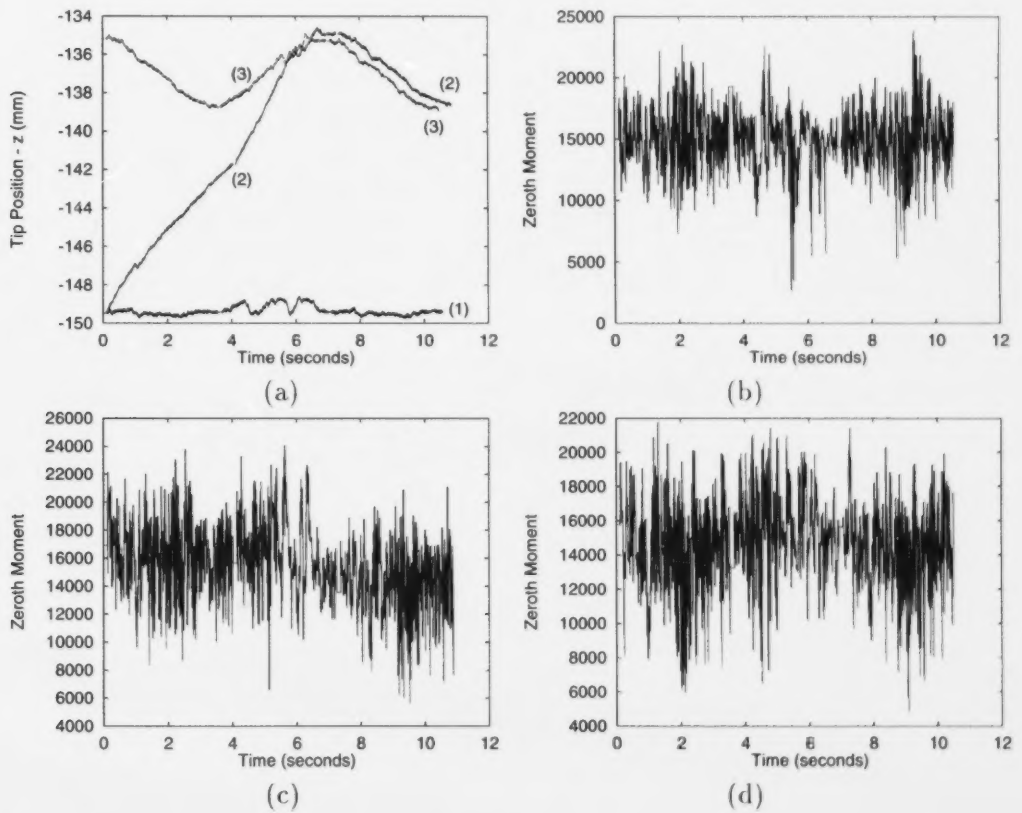

Figure 6.22: *The variation in (a) p_z as the pin is rolled on (1) a flat table aligned with the robot axes, (2) a flat table rotating about y_0, and (3) a flat table inclined about y_0-axis, and the variation in M_0 for (b) a flat table aligned with the robot axes, (c) a flat table rotating about y_0, and (d) a flat table inclined about the y_0.*

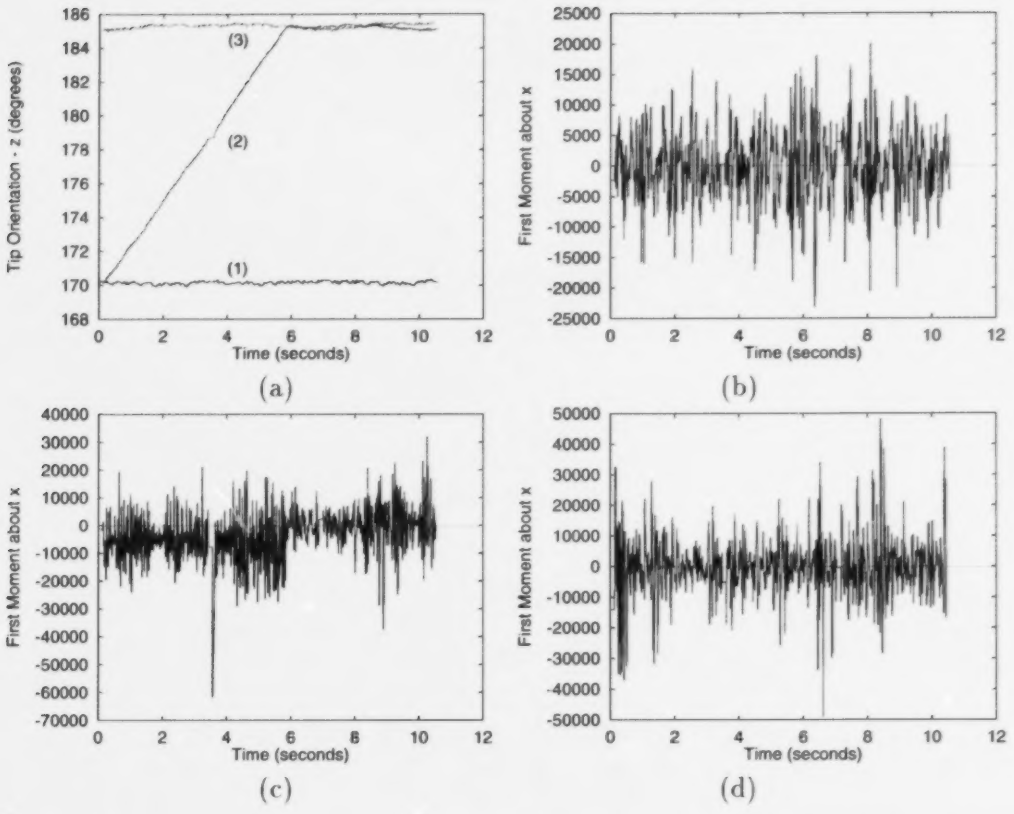

Figure 6.23: *The variation in (a) θ_{z_e} for the pin rolling on (1) a flat table aligned with the robot axes, (2) a flat table rotating about x_0, and (3) a flat table inclined about x_0, and the variation in M_y for (b) a flat table aligned with the robot axes, (c) a flat table rotating about x_0, and (d) a flat table inclined about x_0.*

a constant rate while the pin rolls. The angle changes steadily to about 185 degrees and then stays around that value. The point at which this happens indicates that the table has stopped rotating about x_0. Finally, the curve labeled (3) shows the change in this angle as the pin is rolled on the tilted table. Figure 6.23 (b), (c), and (d) show the change in M_y as the pin rolls on a flat stationary table, a rotating table, and an inclined stationary table.

6.4.3 Rotation about z_0

Panning the table provides a rotation about z_0, and this can be used to examine the effect of these rotations on the performance of tactile servo. Figure 6.24 shows the change in p_x. The curve labeled (1) corresponds to the pin being rolled along x_0. The curve labeled (2) shows the change in this position as the table is rotated about z_0 while the pin is being rolled. This rotation about z causes a shift in p_x as the pin

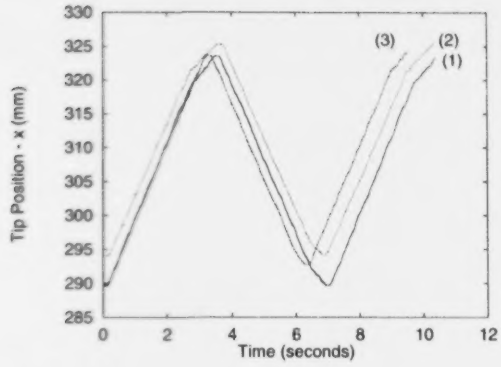

Figure 6.24: *The variation in p_x while rolling the pin on a flat table that is (1) stationary, (2) rotating about z_0, and (3) inclined about z_0.*

rolls. Curve (3) shows the pin being rolled at an angle to x_0. Figure 6.25(a) shows the change in θ_{x_s}. The curve labeled (1) shows the angle steady around 177 degrees. The curve labeled (2) shows the slow rate of change of 1.2 degrees/s as the table is rotated about z_0. The rotation of the table about z_0, and hence that of the pin, was faster at a value of about 5 degrees/s. Finally, curve (3) shows the angle steady at about 197 degrees after the robot has been given sufficient time to adapt to the rotation about z_0. Figure 6.25 (a), (b), and (c) show the change in θ_p for the corresponding cases (1), (2), and (3). Finally, Figure 6.26 shows the change in θ_{z_s}. While the table is rotated about z_0, there is a small change in this angle from about 181 degrees to about 184 degrees. This change is possibly due to the table surface being slightly tilted, an effect that gets accentuated by the panning motion. It could also be a result of some coupling between the features, although it is difficult to discern such a relationship because of the noise.

6.4.4 Translation along x_0

The pan-tilt table was mounted on sliders. When the sliders are aligned with x_0, the table can be moved along these sliders to provide a translational disturbance along this axis. Since this motion is not motorized, it is difficult to provide a steady disturbance. Figure 6.27(a) shows the change in p_x. The robot rolls the pin from about 356 mm to 320 mm in the first 4s, a distance of 36 mm. During this period, no disturbance is provided. Then, when the robot reverses direction, the table is moved along x_0 as the pin rolls on it. This causes the robot to roll the pin from 320 mm to about 400 mm, an additional distance of 44 mm. Figure 6.27(b) shows the change in the feature x_c. The sliding motion can be seen in the segment from about 4s to 8.5 s, where the value of x_c changes by a small value.

The above discussion shows that, in general, tactile servo performs well in static as well as changing environments. The data from the tactile sensor is noisy but the servo components corresponding to the features x_c, M_0, and M_y are able to respond

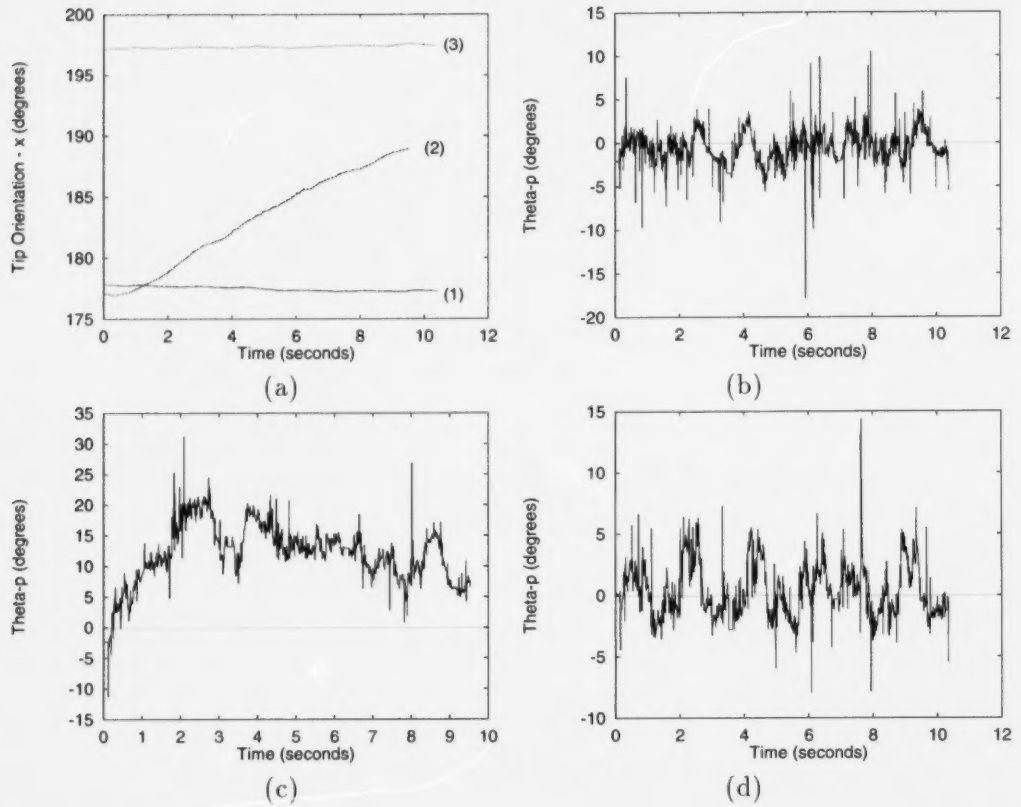

Figure 6.25: *The variation in (a) θ_{x_s} for the pin rolling on (1) a flat table aligned with the robot axes, (2) a flat table rotating about z_0, and (3) a flat table inclined about z_0, and the variation in θ_p for (b) a flat table aligned with the robot axes, (c) a flat table rotating about z_0, and (d) a flat table inclined about z_0.*

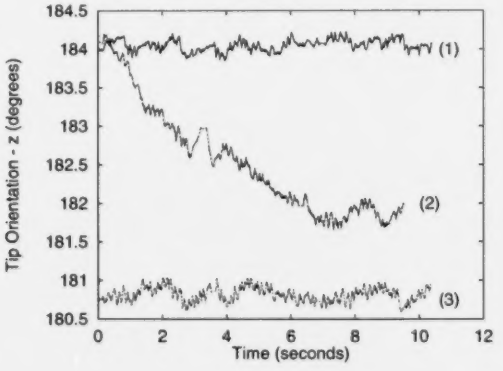

Figure 6.26: *The variation in θ_{z_s} while rolling the pin on a flat table that is (1) stationary, (2) rotating about z_0, and (3) inclined about z_0.*

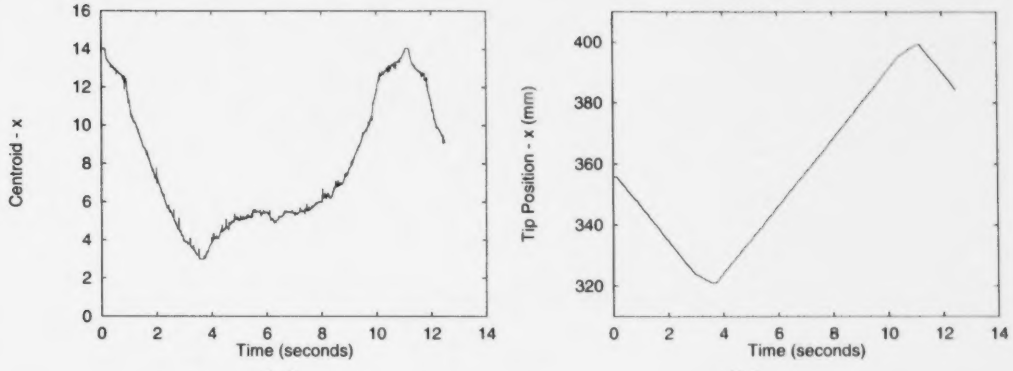

(a) (b)

Figure 6.27: *The variation in (a) x_c and (b) p_x rolling the pin on a flat table, aligned with the axes of the robot base frame, and moved along x_0.*

well without any filtering. However, the feature θ_p is more sensitive to noise and that makes the dynamic response of the servo, corresponding to this feature, comparatively slow. There may also be some coupling between M_0 and θ_p that could not be resolved.

6.5 Summary and discussion

Tactile servo was implemented experimentally for the task of rolling a cylindrical pin. Tactile servo presents a simple and effective method to control contact tasks that can be characterized by a sequence of states that are identifiable using the tactile sensors. Tactile sensors provide rich information about the contact and tactile servo uses this information directly in controlling the task. The experiments showed that the performance was satisfactory even though the contact model was approximate and the output of the tactile sensor was noisy.

The developments reported here represent a first step in developing effective methods to control contact tasks using touch. The control algorithm is simple and contact model is also simplistic and approximate. It is important to develop a more complicated model of contact that is able to bring out the interdependence amongst the different features. Such a model can then be used to develop more sophisticated control algorithms.

Chapter 7

Conclusion

The sense of touch is an important part of human perceptual capabilities. It is central to both exploration and manipulation tasks. This thesis has explored the application of tactile array sensors in manipulation tasks to be performed by a robot manipulator. The first section presents a summary of the results presented in the thesis. Section 2 highlights the contributions of the thesis and the last section presents several suggestions for further research.

7.1 Summary

An extensive survey of the literature on manipulation and on tactile sensing was conducted. The findings of this survey were used to identify areas where further research is required. It was found, as a result of this survey, that there were two main problems that needed research. The first problem was to build and analyze models of contact between a tactile array sensor and a given object. This task is important since such models help in the design of better tactile array sensors and also point the way towards how such tactile sensors can be used in exploration and manipulation tasks for the purposes of gathering information and for control. The second problem that was identified in this survey was to determine methods and techniques for using such tactile sensors in manipulation tasks.

A survey of the literature on elasticity theory and of the study of contact within this framework showed that the problem of determining the stresses within an elastic medium because of contact is difficult in general and often numerical methods offer the best alternative to solving a given contact problem. The finite element method was identified as a general method for analyzing contact problems. This method was used to show how closed-form solutions, obtained by making simplifying assumptions, are not appropriate for some cases. This is especially true when a tactile sensor is modeled as a thin layer. Specifically, limitations of the half-space assumption were highlighted in this context.

Several models and methods were then devised to study the contact between a tactile sensor and given objects of different shapes, namely, a knife edge, a long

cylinder, and a rectangular bar. The effect of different loading conditions, such as the force applied to the object or the displacement of the object relative to the sensor, on sub-surface stress was analyzed and several features were derived from the stress distributions and studied. It was found that a number of these features are related monotonically and smoothly to the variation in the loading conditions.

To apply tactile sensors in manipulation tasks, a new approach for the direct control of robot motion based on tactile sensory input was proposed. This approach is based on *visual servo*, where image features are derived from visual image data to control the motion of a robot manipulator directly. This control is based on the variation in image features as a result of small movements of the manipulator and this relation is called the feature sensitivity matrix or the feature Jacobian matrix. Similarly, our approach to touch-based manipulation is called *tactile servo* and is based on features that can be derived from tactile sensory data such that variations in the feature values can be directly related to small movements of the sensor with respect to the object in contact. From the analysis of contact performed earlier, it was found that moments associated with the stress distribution vary smoothly and monotonically with the applied force or the relative displacements between the sensor and the object. The variation of the different moments with the relative displacements were analyzed for three different types of contact — edge, cylindrical, and rectangular.

These relationships were experimentally verified qualitatively and the approach of tactile servo was then specified for the task of rolling a cylindrical pin. This task was implemented on a PUMA 260 arm equipped with tactile array sensors and tactile servo was experimentally verified.

7.2 Contributions

The major contributions of the thesis consist of the following:

1. The use of finite element analysis as a tool for studying contact problems from the perspective of tactile sensing.

   A survey of the literature on contact problems in elasticity showed the many limitations, as simplifying assumptions, of the analytical techniques for obtaining the solution of such problems. The finite element method provides a general and convenient tool for studying contact problems for which analytical methods prove to be inadequate. Often, this method presents the best available alternative for such studies.

2. A comprehensive study of several different types of contact.

   The finite element method was used to analyze the contact between several different objects and an elastic layer. The displacements and stresses within the elastic layer were obtained for contact with an

edge, a cylindrical object, and a flat-based rigid indenter, for a range of different loading conditions. Several interesting features of the stress distributions were identified and their relation to different loading conditions was studied. It was found that many of these features vary smoothly and monotonically with the applied load and hence can be used to identify the loading conditions in a given task.

3. A new approach to robot control using touch — *tactile servo.*

   A new approach for controlling robot motion in real-time during a manipulation task using tactile sensors was proposed. This approach, called *tactile servo*, is motivated by the notion of *visual servo*, a method to control the movement of a robot based on visual information. The control is based on tracking several features, obtained from tactile sensory data, that characterize contact between the robot and an object or the environment. Tactile Servo was implemented for the task of rolling a cylindrical pin on a given surface whose orientation is not known *a priori* and changes over time. The implementation was tested experimentally using a PUMA 260 manipulator equipped with a tactile array sensor. The following steps made possible the realization of tactile servo.

   (a) Identification of *tactile features* that can be used in tactile servo control of different manipulation tasks. Moments have been used extensively in image processing, both visual and tactile, for recognition purposes. However, here the moments are used as features in tactile servo control of manipulation tasks.

   (b) Derivation of the feature sensitivity matrices for different types of contact. The analysis using the finite element method was used to study the variation of tactile features for small movements of the object with respect to the sensor.

7.3 Future work

The research presented in this thesis points the way to further research. A general research problem consists of building on the notion of tactile servo to obtain a general framework for the specification and control of exploration and manipulation tasks based on tactile as well as other forms of sensing. Two other areas of further research are the extensions of the techniques for the modeling of contact and for the use of tactile servo in the control of manipulation tasks.

7.3.1 Modeling contact

There are several problems that need to be solved for modeling contact between a tactile sensor and an object. All the contact problems analyzed here were two-

dimensional, having been obtained from the three-dimensional case using the plane strain assumption. This restricted the analysis to the plane. To characterize contact more generally, the finite element method must be used to build three-dimensional models of contact with different objects. These three-dimensional models can then be used to study the effect of force or relative displacement in the three dimensions on the two-dimensional stress distribution.

Another problem to be considered is the development of more accurate models of a tactile sensor. In this study, a tactile sensor was modeled as a thin elastic layer that is fully constrained on one surface. In reality, a tactile sensor consists of several elastic layers that are bonded together with an adhesive. Furthermore, the relationship between the sensor output and the stress at the sensing sites is non-linear. Again, the finite element method can be used to build and analyze more realistic models of a tactile sensor so that the models can be used quantitatively rather than qualitatively. A related problem is to build better models of the contact between an object and the sensor by explicitly taking friction into account. Kikuchi and Oden [38] describe some work along these lines that could be used as a starting point for such studies.

Finally, other related methods for solving elasticity problems should be explored. For example, the boundary element method has been used for some time in solving problems in mechanics and could provide a better alternative than the finite element method.

7.3.2 Tactile servo

An important direction for future research is to identify a general framework for autonomous object exploration and manipulation by a robot. In early work [42], the geometry of the task was assumed to be known and then this information was used to plan motion trajectories to achieve the given task. In this approach, planning was emphasized over sensing. Some recent work [23] has argued that this emphasis is misplaced and that the ability to do a task depends more on what can be sensed by a robot. A mathematical framework was developed using this basic premise. An interesting problem is to study tactile servo in the context of this framework and to extend or change this framework to include tactile servo.

An alternative approach to exploration and manipulation by robots can be derived from the corresponding human capabilities. Lederman and Klatzky [41] have identified several of exploratory procedures — stereotypical hand movements — that humans tend to use when exploring an object. They have also attempted to identify similar procedures for manipulation [39]. An interesting problem is to attempt to build a manipulation system based on this approach of primitives by identifying tactile servo algorithms for individual exploratory and manipulation procedures.

The task of rolling a cylindrical pin was implemented using tactile servo to show the feasibility and effectiveness of this method for manipulation tasks. To show the generality of tactile servo, other tasks need to be identified and implemented. An important problem is implementing tactile servo on a multi-fingered robot hand to do manipulation tasks such as rolling an object between the fingers, holding an object

in the presense of external forces, and assembly tasks. In a multi-fingered hand, there are usually many more degrees of freedom to be controlled. For a multi-fingered hand with three fingers, each with three degrees of freedom, mounted on a manipulator with six degrees of freedom, the overall system has 15 degrees of freedom. In addition to a Jacobian that relates differential changes in the wrist frame to the changes in the six joints of the manipulator, such a system would have three additional Jacobians, one for each finger. Since each finger has only three degrees of freedom, the problem of choosing an appropriate set of tactile features and then using these to control the motion of the 15 joints in the system is a more complex problem than has been considered here.

Another interesting problem is to compare and contrast tactile servo with some of the existing schemes for force control, both experimentally and theoretically. A first comparison would categorize tasks that can be performed using tactile servo alone, using force control alone, using either tactile servo or force control, and using both tactile servo and force control. Such a comparison would clearly bring out the relative merits and demerits of the two schemes and also lead to a statement about the matching between tasks and these two control methods. This exercise would provide a good grounding for considering higher level frameworks of manipulation.

Bibliography

[1] Mongi A. Abidi and Rafael C. Gonzalez, editors. *Data Fusion in Robotics and Machine Intelligence*. Academic Press, 1992.

[2] J. B. Alblas and M. Kuipers. Contact problems of a rectangular block on an elastic layer of finite thickness : The thin layer. *Acta Mechanica*, 8:133–145, 1969.

[3] ALGOR Interactive Systems, Inc. *ViziCad Plus Volume 1 : Geometric Modeling and Visualization*, 1990.

[4] ALGOR Interactive Systems, Inc. *ViziCad Plus Volume 2 : Modeling for Finite Element Analysis*, 1990.

[5] P. Allen. Mapping haptic exploratory procedures to multiple shape representations. In *IEEE 1990 International Conference on Robotics and Automation*, pages 1679–1684, 1990.

[6] Peter K. Allen. *Robot Object Recognition Using Vision and Touch*. Kluwer, Boston, 1987.

[7] R. Bajcsy. What can we learn from one finger experiments ? In M. Brady and R. Paul, editors, *Robotics Research : The First International Symposium*. The MIT Press, 1984.

[8] Alan D. Berger and Pradeep K. Khosla. Using tactile data for real-time feedback. *International Journal of Robotics Research*, 10(2):88–102, 1991.

[9] A. Bicchi, M. Bergamasco, P. Dario, and A. Fiorillo. Integrated tactile sensing for gripper fingers. In *Proceedings of the 7th International Conference on Robot Vision and Sensory Controls*, pages 339–349, 1988.

[10] A. Bicchi and P. Dario. Intrinsic tactile sensing for artificial hands. In R. Bolles and B. Roth, editors, *Robotics Research*. MIT Press, 1987.

[11] A. Bicchi, J. K. Salisbury, and D. L. Brock. Contact sensing from force measurements. *International Journal of Robotics Research*, 12(3):249–262, June 1993.

[12] A. Bicchi, J. K. Salisbury, and P. Dario. Augmentation of grasp robustness using intrinsic tactile sensing. In *IEEE 1989 International Conference on Robotics and Automation*, pages 302–307, 1989.

[13] David S. Burnett. *Finite Element Analysis : From Concepts to Applications.* Addison-Wesley Publishing Company, 1987.

[14] H. D. Conway, S. M. Vogel, K. A. Farnham, and S. So. Normal and shearing contact stresses in indented strips and slabs. *International Journal of Engineering Science*, 4:343–359, 1966.

[15] P. Dario. Tactile sensing for robots : Present and future. In Oussama Khatib, John J. Craig, and Tomas Lozano-Perez, editors, *The Robotics Review 1.* The MIT Press, 1989.

[16] P. Dario. Tactile sensing : Technology and applications. *Sensors and Actuators A*, 1991.

[17] P. Dario and M. Bergamasco. An advanced robot system for automated diagnostic tasks through palpation. *IEEE Transactions on Biomedical Engineering*, 35(2):118–126, 1988.

[18] P. Dario and G. Butazzo. An anthropomorphic robot finger for investigating artificial tactile perception. *International Journal of Robotics Research*, 6(3):25–48, 1987.

[19] Danilo De Rossi. Artificial tactile sensing and haptic perception. *Measurement Science and Technology*, 2(11):1003–1016, 1991.

[20] Danilo De Rossi, A Caiti, R Bianchi, and G Canepa. Fine-form tactile discrimination through inversion of data from a skin-like sensor. In *IEEE 1991 International Conference on Robotics and Automation*, pages 398–403, 1991.

[21] R. S. Desai and R. A. Volz. Identification and verification of termination conditions in fine motion in presence of sensor errors and geometric uncertainties. In *IEEE 1989 International Conference on Robotics and Automation*, pages 800–807, 1989.

[22] B. R. Donald. *Eror Detection and Recovery in Robotics.* Springer–Verlag, New York, 1989.

[23] Bruce Donald and Jim Jennings. Sensor interpretation and task-directed planning using perceptual equivalence classes. In *IEEE 1991 International Conference on Robotics and Automation*, pages 190–197, 1991.

[24] N. R. Draper and H. Smith. *Applied Regression Analysis.* John Wiley and Sons, New York, 1966.

[25] R. E. Ellis. Planning tactile recognition paths in two and three dimensions. *International Journal of Robotics Research*, 11(2):87–111, 1992.

[26] R. S. Fearing. Tactile sensing mechanisms. *International Journal of Robotics Research*, 9(3):3–23, 1990.

[27] R. S. Fearing and J. M. Hollerbach. Basic solid mechanics for tactile sensing. *International Journal of Robotics Research*, 4(3):40–54, 1985.

[28] W. D. Hillis. A high resolution imaging touch sensor. In Wayne J. Book, editor, *Robotics Research and Advanced Applications*. The American Society of mechanical Engineers, 1982.

[29] N. Hogan. Impedance control: An approach to manipulation: Theory, implementation, and applications. *Journal of Dynamic Systems, Measurement, and Control*, pages 1–24, 1985.

[30] N. Houshangi and A. J. Koivo. Tactile sensor control for robotic manipulations. In *IEEE 1989 International Conference on Systems, Man, and Cybernetics*, pages 1258–1259, 1989.

[31] R. D. Howe and M. R. Cutkosky. Touch sensing for robotic manipulation and recognition. In O. Khatib, J. J. Craig, and T. Lozano-Perez, editors, *The Robotics Review 2*. The MIT Press, Cambridge, Ma, 1992.

[32] R. D. Howe and M. R. Cutkosky. Dynamic tactile sensing : Perception of fine surface features with stress rate sensing. *IEEE Transactions on Robotics and Automation*, 9(2):140–151, 1993.

[33] R. D. Howe, N. Popp, P. Akella, I. Kao, and M. R. Cutkosky. Grasping, manipulation, and control with tactile sensing. In *IEEE 1990 International Conference on Robotics and Automation*, pages 1258–1263, 1990.

[34] Interlink Electronics. *Product Design Guide*, 1989.

[35] K. L. Johnson. *Contact Mechanics*. Cambridge University Press, 1985.

[36] K. O. Johnson and S. S. Hsiao. Neural mechanisms of tactual form and texture perception. *Annual Review of Neuroscience*, 15:227–250, 1992.

[37] O. Khatib. A unified approach for motion and force control of robot manipulators: The operational space formulation. *IEEE Journal of Robotics and Automation*, RA-3(1):43–53, 1987.

[38] N. Kikuchi and J. T. Oden. *Contact Problems in Elasticity : A Study of Variational Inequalities and Finite Element Methods*. Society for Industrial and Applied Mathematics, Philadelphia, 1988.

[39] Roberta L. Klatzky, Susan J. Lederman, James W. Pellegrino, Sally Doherty, and Brian P. McCloskey. Procedures for haptic object exploration vs. manipulation. In Melvyn A. Goodale, editor, *Vision and action : The Control of Grasping*, chapter 8, pages 110 - 127. Ablex Publishing Corporation, 1990.

[40] Mitsuo Kobayashi, Tsuneki Shinokura, and Shinobu Sagisawa. Three-component detection type tactile sensor. *Journal of Robotics and Mechatronics*, 2(3):180–183, 1989.

[41] Susan J. Lederman and Roberta L. Klatzky. Hand movements : A window into haptic object recognition. *Cognitive Psychology*, 19:342–368, 1987.

[42] T. Lozano-Perez, M. T. Mason, and R. H. Taylor. Automatic synthesis of fine–motion strategies for robots. *International Journal of Robotics Research*, 3(1), 1984.

[43] H. Maekawa, K. Komoriya, and K. Tanie. Manipulation of an unknown object by multifingered hands with rolling contact using tactile feedback. In *IEEE/RSJ International Conference on Intelligent Robots and Systems*, pages 1877–1882, 1992.

[44] M. T. Mason. Compliance and force control for computer controlled manipulators. *IEEE Transactions on Systems, Man, and Cybernetics*, SMC-11(6):418–432, 1981.

[45] C. Muthukrishnan, D. Smith, D. Myers, J. Rebman, and A. Koivo. Edge detection in tactile images. In *IEEE 1987 International Conference on Robotics and Automation*, pages 1500–1505, 1987.

[46] H. Nicholls, editor. *Advanced Tactile Sensing for Robotics.* World Scientific Publishing, 1992.

[47] H. R. Nicholls and M. H. Lee. A survey of robot tactile sensing technology. *International Journal of Robotics Research*, 8(1):3–30, 1989.

[48] Y.C. Pati, P.S. Krishnaprasad, C.T.Yao, M.C. Peckerar R. Yang, and C.R.K. marrian. Neural network for tactile perception. In *Proceedings of the 1988 IEEE International Conference on Robotics and Automation*, pages 346–139, 1988.

[49] Y.C. Pati, P.S. Krishnaprasad, and M.C. Peckerar. An analog neural network solution to the inverse problem of "early taction". *IEEE Transactions on Robotics and Automation*, 8:196–212, 1992.

[50] Richard P. Paul. *Robot Manipulators : Mathematics, Programming, and Control.* MIT Press, 1981.

[51] Richard P. Paul and Hong Zhang. Computationally efficient kinematics for manipulators with spherical wrists based on the homogeneous transform representation. *International Journal of Robotics Research*, 5(2):32–44, 1986.

[52] M. H. Raibert and J. J. Craig. Hybrid position/force control of manipulators. *Journal of Energy Resources Technology*, 103(1):126–133, 1981.

[53] S. L. Ricker and R. E. Ellis. 2-d finite element models of tactile sensors. In *Proceedings of the 1993 IEEE International Conference on Robotics and Automation, Atlanta, Georgia*, pages 941–947, 1993.

[54] R. A. Russell. *Robot Tactile Sensing.* Prentice Hall, 1990.

[55] J. K. Salisbury, Jr. Active stiffness control of a manipulator in cartesian coordinates. In *IEEE Decision and Control Conference*, 1989.

[56] Pavan Sikka, Hong Zhang, and Roger W. Toogood. On modeling tactile sensors. Technical Report TR 93–08, Department of Computing Science, University of Alberta, 1993.

[57] R. E. Smith and M. Gini. Robot tracking and control issues in an intelligent error recovery system. In *IEEE 1986 International Conference on Robotics and Automation*, pages 1070–1075, 1986.

[58] I. N. Sneddon. *Fourier Transforms.* Mc-Graw Hill Book Company, New York, 1951.

[59] Thomas H. Speeter. A tactile sensing system for robotic manipulation. *International Journal of Robotics Research*, 9(6):25–36, 1990.

[60] Thomas H. Speeter. Three-dimensional finite element analysis of elastic continua for tactile sensing. *International Journal of Robotics Research*, 11(1):1–19, 1992.

[61] S. A. Stansfield. A robotic perceptual system utilizing passive vision and active touch. *International Journal of Robotics Research*, 7(6):138–161, 1988.

[62] S. T. Venkataraman and T. Iberall, editors. *Dextrous Robot Hands.* Springer-Verlag, 1990.

[63] P. C. Watson and S. H. Drake. Pedestal and wrist force sensors for automatic assembly. In *Proceedings of the 5th International Symposium on Industrial Robotics*, pages 501–511, 1975.

[64] John G. Webster. *Tactile Sensing for Robotics and Medicine.* John Wiley and Sons, Inc., 1988.

[65] L. Weiss, A. Sanderson, and C. Neuman. Dynamic sensor-based control of robots with visual feedback. *IEEE Journal of Robotics and Automation*, RA-3(5):404–417, October 1987.

[66] D. E. Whitney. Quasi-static assembly of compliantly supported rigid parts. *Journal of Dynamic Systems, Measurement, and Control*, 104:65–77, 1982.

[67] D. E. Whitney. Real robots don't need jigs. In *IEEE 1986 International Conference on Robotics and Automation*, pages 746–752, 1986.

Appendix A

Elasticity and the finite element method

Problems involving contact between deformable bodies have been extensively studied within the framework of the theory of elasticity This appendix provides a review of elasticity concepts followed by a consideration of some simple contact problems for which closed-form solutions exist. The material presented here can be found in texts on elasticity theory and has been adapted from the texts by Saada [8] [1] and Johnson [6]. It is included here to provide a review of the concepts and terms and to provide a basis for the contact problems considered in the thesis.

Section 1 starts with a review of some basic concepts in elasticity. It then presents a formulation of the boundary-value problem, followed by some closed form solutions, taken from the existing literature, to the problems of contact between a semi-infinite elastic medium and rigid objects, namely, a knife edge, a rectangular bar, and a cylinder, respectively. Some details of the finite element models used in the thesis are provided in Section 2 of the appendix.

A.1 Review of elasticity theory

When the forces applied to the surface of a body cause a deformation, reactive forces distributed within the volume of the body are set up to achieve equilibrium. These forces are studied using the notion of stress, which can be defined as the force acting per unit area on a given surface. There are two types of stress — normal stress that acts in a direction that is perpendicular to some specified plane, and shear stress that acts in a direction parallel to the specified plane. The deformation of the body can be described by the resulting displacements of points within and on the body. The deformation is also described by relative displacements of points similarly to the description of stress. The relative displacements are referred to as strains and, like stress, consist of normal strains and shear strains.

[1] The numbers in square brackets refer to the list of references at the end of this Appendix.

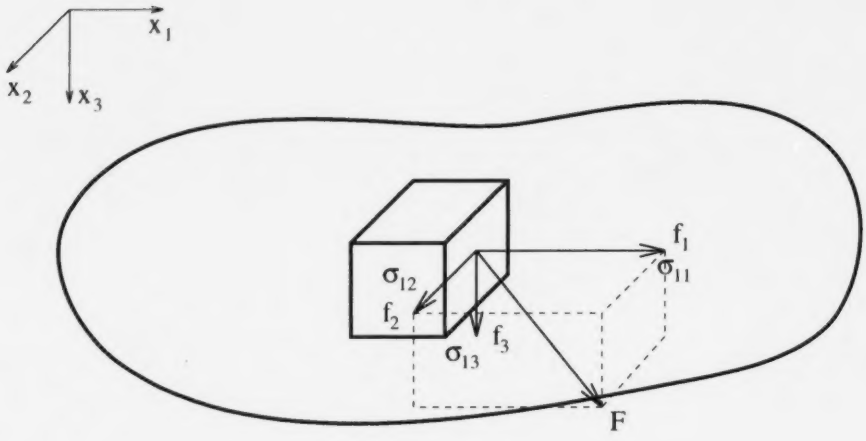

Figure A.1: *The different components of the stress tensor.*

Stress

Figure A.1 illustrates the notion of stress. It shows a small cubic element located within an elastic body that is under the effect of some deforming forces. The cubic element is aligned so that each face is normal to one of three axes. Let the area of a face be represented by δA. Let $\vec{F}$ be the force acting on the face whose outward normal is aligned with x_1. Then, the stress vector is defined as

$$\vec{\sigma} = \lim_{\delta A \to 0} \frac{\vec{F}}{\delta A}.$$

Thus, stress on a plane is characterized by the vector $\vec{\sigma}$ consisting of the three components resolved along the three axes — σ_{11}, σ_{12}, and σ_{13}. The first subscript denotes the direction of the normal to the plane under consideration, and the second subscript refers to the direction of the stress. The three axes are labeled x_1, x_2, and x_3, and the subscripts ij of the stress component σ_{ij} refer to the corresponding axes. These axes are also equivalently labeled x, y, and z, and, in the following discussion, the subscripts 1, 2, and 3 are used interchangeably with the subscripts x, y, and z. Considering the faces corresponding to the other two axes, the complete state of stress is described by the nine quantities expressed as a two-dimensional matrix shown below:

$$\begin{bmatrix} \sigma_{11} & \sigma_{12} & \sigma_{13} \\ \sigma_{21} & \sigma_{22} & \sigma_{23} \\ \sigma_{31} & \sigma_{32} & \sigma_{33} \end{bmatrix}$$

By considering the equilibrium of moments for the cubic element, it can be shown that the matrix shown above is symmetric, i.e.,

$$\sigma_{ij} = \sigma_{ji}.$$

Thus, the state of stress at a point within a body is characterized by six quantities instead of nine. By attempting to express the state of stress with respect to an oblique plane in terms of the matrix shown above, it can also be shown that the above matrix of the state of stress is a tensor of rank two. It is, therefore, called the stress tensor.

In addition to the stress acting within a body because of applied force, there exist other forces that are distributed within the volume of a body and are a function of the volume. These forces $\vec{f}$ are called body forces and are caused by factors like gravitation or magnetism. If the body is assumed to be in static equilibrium then the net force acting at any point within the body must be zero. By considering a balance of forces along each of the three axes for the cubic element shown in Figure A.1, the following equations of equilibrium can be derived:

$$\begin{aligned}
\frac{\partial \sigma_{11}}{\partial x_1} + \frac{\partial \sigma_{21}}{\partial x_2} + \frac{\partial \sigma_{31}}{\partial x_3} + f_1 &= 0 \\
\frac{\partial \sigma_{12}}{\partial x_1} + \frac{\partial \sigma_{22}}{\partial x_2} + \frac{\partial \sigma_{32}}{\partial x_3} + f_2 &= 0 \\
\frac{\partial \sigma_{13}}{\partial x_1} + \frac{\partial \sigma_{23}}{\partial x_2} + \frac{\partial \sigma_{33}}{\partial x_3} + f_3 &= 0
\end{aligned}$$

These equations can be represented succinctly in a simple notation called the index notation [8] as follows:

$$\frac{\partial \sigma_{ji}}{\partial x_j} + f_i = 0. \tag{A.1}$$

In this notation, whenever a subscript is repeated in a term, it is understood to represent a summation over the range 1, 2, and 3, unless an explicit range is also specified. The subscript j in the equation above represents such a subscript and is called the *summation index.* It generates the sum of three terms within each equation. The subscript i is called the *identifying index* and it generates an equation corresponding to each of the values 1, 2, and 3, unless otherwise specified.

Displacement and strain

The deformation of a body caused by an applied force is described in terms of displacements or relative displacements. Each point on the body moves to a new position as a result of the distortion. The movement to a new position is referred to as a displacement and in terms of the three axes, the displacement of a point is described by a vector function with each component of the displacement being a function of position along the three axes. The three components of displacement are represented as u_1, u_2, and u_3. When Cartesian coordinates are used, these displacements can also be expressed as u, v, and w.

In the theory of elasticity, the deformation of a body can also be expressed as a relative displacement. This relative displacement can be expressed in terms of a

matrix of components that are dependent on the displacements. The two dimensional matrix consists of nine elements shown below:

$$\begin{bmatrix} \epsilon_{11} & \epsilon_{12} & \epsilon_{13} \\ \epsilon_{21} & \epsilon_{22} & \epsilon_{23} \\ \epsilon_{31} & \epsilon_{32} & \epsilon_{33} \end{bmatrix}$$

where, in index notation [8],

$$\epsilon_{ij} = \frac{1}{2}\left(\frac{\partial u_i}{\partial x_j} + \frac{\partial u_j}{\partial x_i} + \frac{\partial u_m}{\partial x_i}\frac{\partial u_n}{\partial x_j}\delta_{mn}\right) \tag{A.2}$$

Here, δ_{mn} is called the Kronecker delta and is defined as follows:

$$\begin{aligned} \delta_{mn} &= 1, \ m = n, \\ &= 0, \ m \neq n \end{aligned}$$

From the above definition, it can be seen that the strain matrix is symmetric, i.e., $\epsilon_{ij} = \epsilon_{ji}$. Usually it is assumed that the displacements, strains and their partial derivatives are small. With this assumption, the non-linear terms in the above equations can be ignored and the resulting strain matrix is defined by:

$$\epsilon_{ij} = \frac{1}{2}\left(\frac{\partial u_i}{\partial x_j} + \frac{\partial u_j}{\partial x_i}\right) \tag{A.3}$$

It is clear from the above that if the displacements are specified then the strains are uniquely determined but if the strains are completely specified then the displacements are not uniquely determined. This is because displacements can involve both deformation and rigid body motion. To determine the displacements uniquely from strain, additional constraints on strain must be specified. These are called the Compatibility Conditions and are listed below [8]:

$$\frac{\partial^2 \epsilon_{11}}{\partial x_2 \partial x_3} = \frac{\partial}{\partial x_1}\left(-\frac{\partial \epsilon_{23}}{\partial x_1} + \frac{\partial \epsilon_{31}}{\partial x_2} + \frac{\partial \epsilon_{12}}{\partial x_3}\right) \tag{A.4}$$

$$\frac{\partial^2 \epsilon_{22}}{\partial x_3 \partial x_1} = \frac{\partial}{\partial x_2}\left(-\frac{\partial \epsilon_{31}}{\partial x_2} + \frac{\partial \epsilon_{12}}{\partial x_3} + \frac{\partial \epsilon_{23}}{\partial x_1}\right) \tag{A.5}$$

$$\frac{\partial^2 \epsilon_{33}}{\partial x_1 \partial x_2} = \frac{\partial}{\partial x_3}\left(-\frac{\partial \epsilon_{12}}{\partial x_3} + \frac{\partial \epsilon_{23}}{\partial x_1} + \frac{\partial \epsilon_{31}}{\partial x_2}\right) \tag{A.6}$$

$$2\frac{\partial^2 \epsilon_{12}}{\partial x_1 \partial x_2} = \frac{\partial^2 \epsilon_{11}}{\partial x_2^2} + \frac{\partial^2 \epsilon_{22}}{\partial x_1^2} \tag{A.7}$$

$$2\frac{\partial^2 \epsilon_{23}}{\partial x_2 \partial x_3} = \frac{\partial^2 \epsilon_{22}}{\partial x_3^2} + \frac{\partial^2 \epsilon_{33}}{\partial x_2^2} \tag{A.8}$$

$$2\frac{\partial^2 \epsilon_{31}}{\partial x_3 \partial x_1} = \frac{\partial^2 \epsilon_{33}}{\partial x_1^2} + \frac{\partial^2 \epsilon_{11}}{\partial x_3^2} \tag{A.9}$$

Stress and strain

The stress distribution within a body because of some deforming force is related to the distribution of the strain. In general, this relationship is non-linear and the relations are called the constitutive relations. However, if the strains are small, a linear relationship between the stress tensor and the stain matrix can be derived. Such a relationship is referred to as the Generalized Hooke's Law and involves 21 constants [8]. By making assumptions about the physical properties of the material under consideration, the number of constants can be reduced to two. This highly simplified relationship is based on the assumptions that the matrix relating stress and strain is symmetric and that the material is isotropic, i.e., the elastic properties of the material are independent of the orientation of the axes. The constitutive relations for this simplified case are shown below [8]:

$$\begin{bmatrix} \sigma_{11} \\ \sigma_{22} \\ \sigma_{33} \\ \sigma_{12} \\ \sigma_{13} \\ \sigma_{23} \end{bmatrix} = \frac{E}{1+\nu} \begin{bmatrix} \frac{1-\nu}{1-2\nu} & \frac{\nu}{1-2\nu} & \frac{\nu}{1-2\nu} & 0 & 0 & 0 \\ \frac{\nu}{1-2\nu} & \frac{1-\nu}{1-2\nu} & \frac{\nu}{1-2\nu} & 0 & 0 & 0 \\ \frac{\nu}{1-2\nu} & \frac{\nu}{1-2\nu} & \frac{1-\nu}{1-2\nu} & 0 & 0 & 0 \\ 0 & 0 & 0 & 1 & 0 & 0 \\ 0 & 0 & 0 & 0 & 1 & 0 \\ 0 & 0 & 0 & 0 & 0 & 1 \end{bmatrix} \begin{bmatrix} \epsilon_{11} \\ \epsilon_{22} \\ \epsilon_{33} \\ \epsilon_{12} \\ \epsilon_{13} \\ \epsilon_{23} \end{bmatrix} \tag{A.10}$$

or, alternatively,

$$\begin{bmatrix} \epsilon_{11} \\ \epsilon_{22} \\ \epsilon_{33} \\ \epsilon_{12} \\ \epsilon_{13} \\ \epsilon_{23} \end{bmatrix} = \frac{1}{E} \begin{bmatrix} 1 & -\nu & -\nu & 0 & 0 & 0 \\ -\nu & 1 & -\nu & 0 & 0 & 0 \\ -\nu & -\nu & 1 & 0 & 0 & 0 \\ 0 & 0 & 0 & 1+\nu & 0 & 0 \\ 0 & 0 & 0 & 0 & 1+\nu & 0 \\ 0 & 0 & 0 & 0 & 0 & 1+\nu \end{bmatrix} \begin{bmatrix} \sigma_{11} \\ \sigma_{22} \\ \sigma_{33} \\ \sigma_{12} \\ \sigma_{13} \\ \sigma_{23} \end{bmatrix}$$

Here, E is referred to as *Young's modulus*, while ν is referred to as *Poisson's ratio*. Young's modulus is the ratio between normal stress and normal strain along the axial direction, under conditions of uni-axial state of stress. Poisson's ratio is the ratio between the lateral contraction and the axial elongation, again under conditions of uni-axial state of stress. ν is indicative of the compressibility of the body. For a perfectly incompressible material, ν is 0.5 and the normal stress can no longer be derived from normal strain. These constants are generally used in engineering practice. The constitutive relations are also expressed in terms of other pairs of constants, for example, the *Lamé's constants* λ and μ, where,

$$\begin{aligned} \lambda &= \frac{\nu E}{(1+\nu)(1-2\nu)} \\ \mu &= \frac{E}{2(1+\nu)}. \end{aligned}$$

μ is also referred to as the modulus of rigidity G.

Formulation of elasticity problems

The internal state of an elastic body under the influence of deforming force is characterized by the six components of the stress tensor, the six components of the strain matrix, and the three components of the displacement vector. These fifteen variables are related by the three equations of equilibrium in terms of the six components of the stress tensor, the six constitutive equations relating the stress tensor to the strain matrix, and the six strain-displacement relations. Thus, we have a system of fifteen equations involving fifteen variables of interest. By eliminating the variables that are not of interest for a given problem, the internal state can be characterized by a set of six partial differential equations in terms of the stress tensor, or alternatively, by a set of three partial differential equations given in terms of the three components of the displacement vector. These equations are reproduced below.

In terms of stress, the equations are called the *Beltrami-Michell compatibility equations* and are shown below using the index notation [8]:

$$\nabla^2\sigma_{ij} + \frac{1}{1+\nu}\frac{\partial^2\theta}{\partial x_i \partial x_j} = -\frac{1}{1-\nu}\delta_{ij}\vec{\nabla}.\vec{F} - \left(\frac{\partial F_i}{\partial x_j} + \frac{\partial F_j}{\partial x_i}\right)$$

where,

$$\begin{aligned}
\theta &= \sigma_{11} + \sigma_{22} + \sigma_{33} \\
\vec{\nabla} &= \frac{\partial}{\partial x_1}\hat{x_1} + \frac{\partial}{\partial x_2}\hat{x_2} + \frac{\partial}{\partial x_3}\hat{x_3} \\
\nabla^2 &= \vec{\nabla}.\vec{\nabla} = \left(\frac{\partial^2}{\partial x_1^2} + \frac{\partial^2}{\partial x_2^2} + \frac{\partial^2}{\partial x_3^2}\right)
\end{aligned}$$

$\hat{x_1}$, $\hat{x_2}$, and $\hat{x_3}$ are the unit vectors along x_1, x_2, and x_3.

In terms of displacements, the equations are called *Navier's equations of elasticity* and are shown below in index notation [8]:

$$(\lambda + \mu)\frac{\partial \epsilon_\nu}{\partial x_i} + \mu\nabla^2 u_i + F_i = 0$$

where,

$$\epsilon_\nu = \epsilon_{11} + \epsilon_{22} + \epsilon_{33}$$

It must be pointed out here that the Navier's equations of elasticity cannot be used as shown here for incompressible materials, since for such materials $\epsilon_\nu = 0$, and $\lambda = \inf$.

A specification of the body forces, and either the displacements or the stresses on the surface of the body, leads to a boundary-value problem in terms of stress or displacement. It is also possible to specify the stress on some parts of the surface and displacements on other parts. This leads to a mixed boundary-value problem.

The solution of the boundary-value problem provides the desired stress tensor or displacement vector. Since problems in elasticity have been extensively studied for a long time, many different methods exist to obtain the solutions to the boundary-value problems arising from different contact conditions.

Broadly, there are two general methods to solve these boundary-value problems — analytical or numerical. Analytically, the solution of this problem is extremely difficult in general. Several techniques exist to solve some simplified problems. The simplest analytical technique is to guess the general form of the solution directly so that it satisfies all the elasticity equations, and then to use the specified boundary conditions to "fix" the solution or to determine the unknown parameters in the solution.

A similar method is to use potential functions related to stress or displacement. Again, the specified boundary conditions are used to determine the unknown parameters in the potential function. A big difference from the potential function method used in general is that here the potential function satisfies the bi-harmonic equation rather than the harmonic equation. Many of the techniques used in the solution of the harmonic equation do not generalize to the solution of the bi-harmonic equation.

The Integral Transform method [9] is another general method that has been used to solve problems in elasticity theory. Complex Analysis is also used but is limited to the solution of simplified two-dimensional problems. Finally, variational methods [7], i.e., methods based on the minimization of energy, provide another general approach to the solution of these problems.

Numerical methods provide an alternative way of solving elasticity problems and given the difficulty of solution in general, these methods often are the only means of obtaining the solution to a particular problem. Numerical methods based on variational principles, for example, the finite element method [4], provide a general framework for studying contact problems in elasticity.

A.1.1 Line contact

Figure A.2 shows the contact between a smooth surface on one elastic body and a sharp edge on the other rigid body. This example can be used to illustrate the different approaches to the solution of elasticity problems.

Several assumptions are made to simplify the analysis of this problem. First, it is assumed that the object with the sharp edge is rigid. With this assumption, the deformation of the rigid body can be ignored and the problem reduces to a consideration of the other body alone. The sharp edge serves to provide the boundary conditions for the problem. This is a common assumption and the hard, rigid body is called a rigid indenter.

A second assumption that is often made is based on the symmetry of the contact. Figure A.2(a) shows that the sharp edge in contact is aligned with x_2. Assume that the bodies are infinite along x_2 and that a uniform force P per unit length along x_2 is applied along x_3 at the origin. Figure A.2(b) shows a two-dimensional "slice" of the indenter and the object, taken normal to x_2. With this pair of assumptions, the

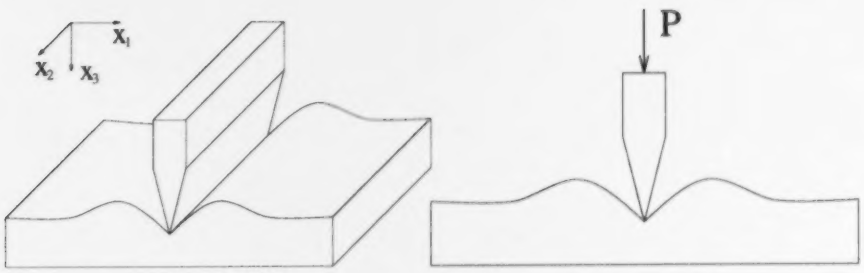

Figure A.2: *The contact between a smooth surface and a sharp edge.*

problem becomes two-dimensional and fewer variables need to be considered. Since no force is applied along x_2 and since the variation of the applied force is uniform along x_2, the stresses and strains within the body do not vary along x_2 and are a function of x_1 and x_3 only. Furthermore, here the displacement along x_2 is also zero. This problem is characterized below in terms of the different variables.

$$
\begin{aligned}
u_1 &= u_1(x_1, x_3), \\
u_3 &= u_3(x_1, x_3), \\
u_2 &= 0, \\
\epsilon_{11} &= \epsilon_{11}(x_1, x_3), \\
\epsilon_{33} &= \epsilon_{33}(x_1, x_3), \\
\epsilon_{13} &= \epsilon_{13}(x_1, x_3), \\
\epsilon_{22} &= \epsilon_{12} = \epsilon_{23} = 0, \\
\sigma_{11} &= \sigma_{11}(x_1, x_3), \\
\sigma_{33} &= \sigma_{33}(x_1, x_3), \\
\sigma_{13} &= \sigma_{13}(x_1, x_3), \\
\sigma_{22} &= -\sigma_{11} + \frac{\sigma_{33}}{\nu} \\
\sigma_{12} &= \sigma_{23} = 0.
\end{aligned}
$$

Thus, only eight variables consisting of two displacements, three strains, and three stresses need to be considered. The equations of equilibrium (equations 3.1, 3.2, and 3.3) reduce to two, the stress-strain relations (equations 3.22) reduce to three equations, and the strain-displacement relations (equations 3.10 to 3.15) also reduce to three equations. The set of assumptions together that made this simplification possible are referred to as the plane strain assumption. Using different symmetries for other type of contacts, a similar assumption called the plane stress assumption can also be used, which again reduces the number of variables to eight. Similarly, for contact involving objects that have symmetry about some axis, the axi-symmetric assumption is often used, again reducing the number of variables that need to be

considered.

Another common assumption that is often made with respect to contact problems is that the body forces are zero. Again, if the bodies are small or if the region of interest is small, then the body force because of gravity can be ignored. With all these assumptions, the simplified equations are reproduced below:

$$\begin{aligned}
\frac{\partial \sigma_{11}}{\partial x_1} + \frac{\partial \sigma_{31}}{\partial x_3} &= 0 \\
\frac{\partial \sigma_{13}}{\partial x_1} + \frac{\partial \sigma_{33}}{\partial x_3} &= 0 \\
\begin{bmatrix} \sigma_{11} \\ \sigma_{33} \\ \sigma_{13} \end{bmatrix} &= \frac{E}{1+\nu} \begin{bmatrix} \frac{1-\nu}{1-2\nu} & \frac{\nu}{1-2\nu} & 0 \\ \frac{\nu}{1-2\nu} & \frac{1-\nu}{1-2\nu} & 0 \\ 0 & 0 & 1 \end{bmatrix} \begin{bmatrix} \epsilon_{11} \\ \epsilon_{33} \\ \epsilon_{13} \end{bmatrix} \\
\epsilon_{11} &= \frac{\partial u_1}{\partial x_1} \\
\epsilon_{33} &= \frac{\partial u_3}{\partial x_3} \\
\epsilon_{31} &= \frac{1}{2}\left(\frac{\partial u_3}{\partial x_1} + \frac{\partial u_1}{\partial x_3}\right)
\end{aligned}$$

Also, the compatibility equations are all satisfied, except for the one shown below:

$$2\frac{\partial^2 \epsilon_{31}}{\partial x_3 \partial x_1} = \frac{\partial^2 \epsilon_{33}}{\partial x_1^2} + \frac{\partial^2 \epsilon_{11}}{\partial x_3^2}$$

Using the stress-strain relations and substituting for the strains in the above equation, the following equation is obtained:

$$\left(\frac{\partial^2}{\partial x_1^2} + \frac{\partial^2}{\partial x_2^2}\right)(\sigma_{11} + \sigma_{33}) = 0$$

Using a potential function for stress $\phi(x_1, x_3)$, also called an Airy stress function [8], such that:

$$\begin{aligned}
\sigma_{11} &= \frac{\partial^2 \phi}{\partial x_3^2} \\
\sigma_{33} &= \frac{\partial^2 \phi}{\partial x_1^2} \\
\sigma_{13} &= \frac{\partial^2 \phi}{\partial x_1 \partial x_3}
\end{aligned}$$

and substituting in the modified compatibility condition showed above, the following differential equation in terms of the stress function is obtained:

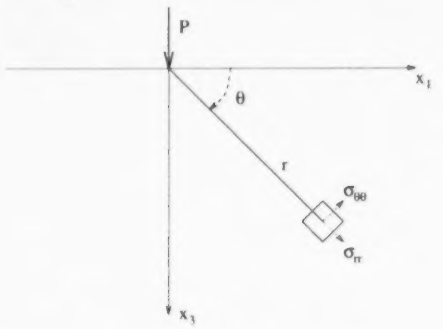

Figure A.3: *The line contact problem in cylindrical coordinates.*

$$\frac{\partial^4 \phi}{\partial x_1^4} + 2\frac{\partial^4 \phi}{\partial x_1^2 \partial x_3^2} + \frac{\partial^4 \phi}{\partial x_3^4} = 0$$

or

$$\nabla^4 \phi = 0$$

This equation is referred to as the bi-harmonic equation and all solutions of this equation are called bi-harmonic functions. The ease of obtaining solutions of this equation depends on the specified boundary-conditions. For example, if ϕ and its first derivative are specified on the surface, then the equation can be solved easily for a circle but no closed-form solution is known for the square [5]. The theory of the solution of the Laplace equation (the potential problem), also called the harmonic equation, does not generalize to the bi-harmonic equation because certain properties of the harmonic equation do not seem to exist for the bi-harmonic equation [9].

The solution of elasticity problems also depends on the geometry of the problem and the coordinate system used to express the problem. For example, for line contact being considered here, a simple solution exists if the problem is expressed in a cylindrical coordinate frame with its origin at the point of application of the load and the z-axis aligned with x_2. Figure A.3 shows the problem in cylindrical coordinates. The eight equations to be solved for this case are shown below:

$$\begin{aligned}
\epsilon_{rr} &= \frac{\partial u_r}{\partial r} \\
\epsilon_{\theta\theta} &= \frac{1}{r}\frac{\partial u_\theta}{\partial \theta} + \frac{u_r}{r} \\
\epsilon_{r\theta} &= \frac{1}{2}\left(\frac{1}{r}\frac{\partial u_r}{\partial \theta} + \frac{\partial u_\theta}{\partial r} - \frac{u_\theta}{r}\right) \\
\begin{bmatrix} \sigma_{rr} \\ \sigma_{\theta\theta} \\ \sigma_{r\theta} \end{bmatrix} &= \frac{E}{1+\nu}\begin{bmatrix} \frac{1-\nu}{1-2\nu} & \frac{\nu}{1-2\nu} & 0 \\ \frac{\nu}{1-2\nu} & \frac{1-\nu}{1-2\nu} & 0 \\ 0 & 0 & 1 \end{bmatrix}\begin{bmatrix} \epsilon_{rr} \\ \epsilon_{\theta\theta} \\ \epsilon_{r\theta} \end{bmatrix}
\end{aligned}$$

$$\frac{\partial \sigma_{rr}}{\partial r} + \frac{1}{r}\frac{\partial \sigma_{r\theta}}{\partial \theta} + \frac{1}{r}(\sigma_{rr} - \sigma_{\theta\theta}) = 0$$
$$\frac{\partial \sigma_{r\theta}}{\partial r} + \frac{1}{r}\frac{\partial \sigma_{\theta\theta}}{\partial \theta} + \frac{2}{r}\sigma_{r\theta} = 0$$

Here, the stress function $\phi(r, \theta)$ is defined as follows.

$$\sigma_{rr} = \frac{1}{r}\frac{\partial \phi}{\partial r} + \frac{1}{r^2}\frac{\partial^2 \phi}{\partial \theta^2}$$
$$\sigma_{\theta\theta} = \frac{\partial^2 \phi}{\partial r^2}$$
$$\sigma_{r\theta} = -\frac{\partial}{\partial r}\left(\frac{1}{r}\frac{\partial \phi}{\partial \theta}\right)$$

By following the steps similar to those for Cartesian coordinates, it can be shown that once again a bi-harmonic equation in ϕ results. For the problem of contact between a half space and a knife edge, illustrated in Figure A.2, the following simple stress function is used:

$$\phi = Ar \sin\theta$$

The constant A is determined from the applied force P, and the stress distribution in cylindrical coordinates is given by:

$$\sigma_{rr} = -\frac{2P}{\pi}\frac{\cos\theta}{r}$$
$$\sigma_{r\theta} = \sigma_{\theta\theta} = 0$$

At this point, it is important to point out another assumption that has not yet been made explicit. In the derivation of the expressions for stress distribution above, it was implicitly assumed that the body extends to infinity in the radial direction. The expression for σ_{rr} shows that the stress vanishes as r goes to infinity. This assumption, that the body is infinite in extent along the radial direction from the origin, is called the half-space assumption and is almost universally made in considering the solution of elasticity problems. This assumption leads to closed-form solutions for some simple contact problems. The importance of this assumption is that if it is not made, then even in extremely simple cases it becomes difficult to derive closed-form solutions. For example, if we assume that the elastic body has a small thickness and is rigidly supported, then cylindrical coordinates and the particular stress function cannot be used. Sneddon [9] has considered both a semi-infinite elastic medium and a thin layer, and, using transform methods, has shown that while closed-form solutions can be obtained for the semi-infinite elastic medium, the same cannot be said of the thin layer.

Once the stress distribution within the body is known, the stress-strain relations can be used to derive the expressions for strain and the strain-displacement equations

can then be used to determine the displacements. The details can be found in a standard text [8]. The expressions for displacement are given below:

$$
\begin{aligned}
u_r &= \frac{2(1-\nu^2)}{\pi E} P\cos\theta \ln\frac{d}{r} - \frac{P}{\pi E}(1-2\nu)(1+\nu)\theta\sin\theta + \\
&\quad \frac{P(1+\nu)}{\pi E}\cos\theta \\
u_\theta &= \frac{2\nu(1+\nu)}{\pi E} P\sin\theta - \frac{2(1-\nu^2)}{\pi E} P\ln\frac{d}{r}\sin\theta - \frac{P(1+\nu)}{\pi E}\sin\theta + \\
&\quad \frac{P}{\pi E}(1-2\nu)(1+\nu)(\sin\theta - \theta\cos\theta)
\end{aligned}
$$

These expressions were derived on the assumptions that the displacement is purely radial along x_3 and that u_θ is zero at a distance d along x_1.

Similar expressions can be derived for a tangential force Q applied along x_1. The expressions are identical in form to those for a normal force with the exception that, for a tangential force, θ is measured from x_1. The two sets of expressions can be transformed to Cartesian coordinates using the well-known mapping between cylindrical and Cartesian coordinates and combined using the superposition principle for a general applied force with both a normal and a tangential component. These expressions are reproduced below [8]:

$$\sigma_{11} = -\frac{2P}{\pi}\frac{x_1^2 x_3}{(x_1^2+x_3^2)^2} - \frac{2Q}{\pi}\frac{x_1^3}{(x_1^2+x_3^2)^2} \tag{A.11}$$

$$\sigma_{33} = -\frac{2P}{\pi}\frac{x_3^3}{(x_1^2+x_3^2)^2} - \frac{2Q}{\pi}\frac{x_1 x_3^2}{(x_1^2+x_3^2)^2} \tag{A.12}$$

$$\sigma_{13} = -\frac{2P}{\pi}\frac{x_1 x_3^2}{(x_1^2+x_3^2)^2} - \frac{2Q}{\pi}\frac{x_1^2 x_3}{(x_1^2+x_3^2)^2} \tag{A.13}$$

$$
\begin{aligned}
u_1 &= -\frac{P}{\pi E}(1-2\nu)(1+\nu)\sin^{-1}\frac{x_1}{(x_1^2+x_3^2)^{\frac{1}{2}}} + \frac{P}{\pi E}(1+\nu)\frac{x_1 x_3}{x_1^2+x_3^2} + \\
&\quad \frac{2(1-\nu^2)}{\pi E} Q\ln\frac{d}{(x_1^2+x_3^2)^{\frac{1}{2}}} + \frac{Q(1+\nu)}{\pi E}\frac{x_1^2}{(x_1^2+x_3^2)^{\frac{1}{2}}}
\end{aligned} \tag{A.14}
$$

$$
\begin{aligned}
u_3 &= \frac{2(1-\nu^2)}{\pi E} P\ln\frac{d}{(x_1^2+x_3^2)^{\frac{1}{2}}} + \frac{P(1+\nu)}{\pi E}\frac{x_3^2}{(x_1^2+x_3^2)^{\frac{1}{2}}} - \\
&\quad \frac{Q}{\pi E}(1-2\nu)(1+\nu)\cos^{-1}\frac{x_1}{(x_1^2+x_3^2)^{\frac{1}{2}}} + \frac{Q}{\pi E}(1+\nu)\frac{x_1 x_3}{x_1^2+x_3^2}
\end{aligned} \tag{A.15}
$$

A.1.2 Contact with a flat indenter

The problem of contact between a knife-edge and a semi-infinite elastic medium i.e., line contact, is perhaps the simplest contact problem that can be considered. The shape of the bodies in contact and, therefore, the shape of the area of contact, can

vary greatly and this is reflected in the difficulty of solving such contact problems in general.

The problem of contact between a rigid body and a semi-infinite elastic medium has been studied extensively in the theory of elasticity. The shape of the rigid body is constrained to confirm to some simple mathematical form and general solutions have been obtained [6] for bodies whose shape can be described by a polynomial of the form:

$$x_3 = Ax_1^n$$

In this section, contact between a rigid indenter with a flat base and an elastic layer is considered. Figure A.4 shows a rigid, flat rectangular bar in contact with an elastic layer. Closed-form expressions for stress obtained by using the half-space assumption are compared with the stress distributions obtained using the finite element method for a thick layer and for a thin layer.

The problem of contact between a rigid indenter and an elastic half-space can be classified as one of four types depending on how the boundary conditions are specified. Let $p(x_1)$ refer to the distribution of normal force applied to the surface and $q(x_1)$ to the tangential force. Then, the following classes of boundary conditions can be defined [6]:

1. Class I : $p(x_1)$ and $q(x_1)$ are specified on the surface.
2. Class II : (a) $u_3(x_1)$ and $q(x_1)$ are specified on the surface, or alternatively, (b) $u_1(x_1)$ and $p(x_1)$ are specified on the surface.
3. Class III : $u_3(x_1)$ and $u_1(x_1)$ are specified on the surface.
4. Class IV : $u_3(x_1)$ is specified on the surface, and the tractions are related by $q(x_1) = \pm\eta p(x_1)$

where η is the coefficient of friction.

The solution to problems in any of the above classes is based on the solution for the case of line contact and superposition. Thus, for example, given $p(x_1)$ and $q(x_1)$, the subsurface stress within the half space is given by [6]:

$$\begin{aligned}
\sigma_{11} &= -\frac{2x_3}{\pi}\int_{-\infty}^{+\infty}\frac{p(s)(x_1-s)^2ds}{[(x_1-s)^2+x_3^2]^2} - \frac{2}{\pi}\int_{-\infty}^{+\infty}\frac{q(s)(x_1-s)^3ds}{[(x_1-s)^2+x_3^2]^2} \\
\sigma_{33} &= -\frac{2x_3^3}{\pi}\int_{-\infty}^{+\infty}\frac{p(s)ds}{[(x_1-s)^2+x_3^2]^2} - \frac{2x_3^2}{\pi}\int_{-\infty}^{+\infty}\frac{q(s)(x_1-s)ds}{[(x_1-s)^2+x_3^2]^2} \\
\sigma_{13} &= -\frac{2x_3^2}{\pi}\int_{-\infty}^{+\infty}\frac{p(s)(x_1-s)ds}{[(x_1-s)^2+x_3^2]^2} - \frac{2x_3}{\pi}\int_{-\infty}^{+\infty}\frac{q(s)(x_1-s)^2ds}{[(x_1-s)^2+x_3^2]^2}
\end{aligned}$$

The solution of these integrals in closed-form is usually difficult. The solution of problems in the classes mentioned above is obtained by substituting for the stresses

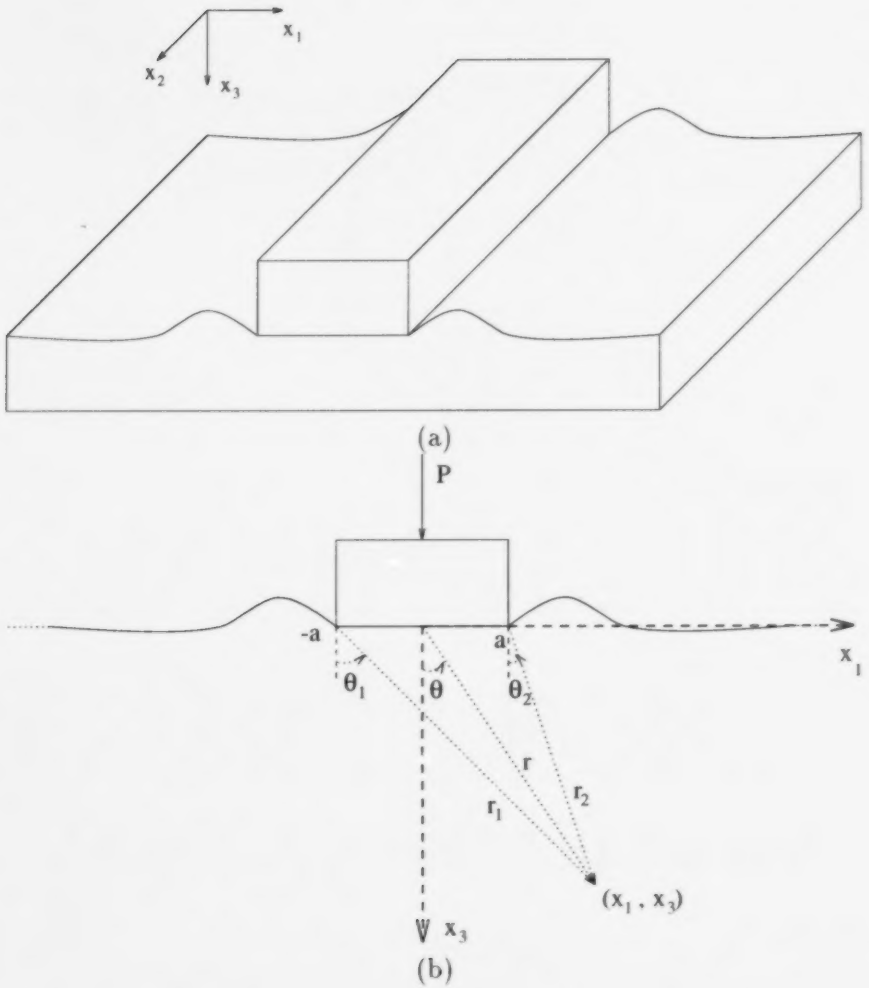

Figure A.4: *The contact between a flat rectangular object and a semi-infinite elastic medium.*

in the left hand side by the derivatives of the displacements and then rearranging depending on the particular class being considered. The details are presented in [6].

The case of frictionless contact with a rigid flat-based indenter corresponds to class II above and the normal surface traction $p(x_1)$ is given by [6]:

$$p(x_1) = -\frac{P}{\pi}\frac{1}{\sqrt{a^2 - x_1^2}} \tag{A.16}$$

The subsurface stresses can be derived by using the superposition integrals shown above. The closed-form expression here is obtained by using transform methods and complex analysis [9] and is given by:

$$\sigma_{33} = -\frac{P}{(r_1 r_2)^{\frac{1}{2}}}\left(\cos[\frac{1}{2}(\theta_1 + \theta_2)] + \frac{r^2}{r_1 r_2}\cos\theta\cos[\theta - \frac{3}{2}(\theta_1 + \theta_2)]\right) \tag{A.17}$$

A.1.3 Contact with a cylindrical indenter

The problem of contact between a semi-infinite elastic medium and a cylindrical pin is illustrated in Figure A.5. The problem can be simplified to two dimensions by making the plane strain assumption, as was done in the previous examples.

There are two methods to approach the solution of these problems. The first is to consider Hertz contact [6]. The contact is assumed to be between two bodies with different curvatures. The solution can be obtained from the solution for Hertz contact if one body is rigid compared to the other, and if the radius of the other body is infinite. The other method is to approximate the contour of the cylinder in the area of contact by a parabola and then use the general solution introduced in the previous section. This is shown below.

$$\begin{aligned}
(x_3 - (-R))^2 + x_1^2 &= R^2 \\
x_3 &= -R + R(1 - (x_1/R)^2)^{\frac{1}{2}} \\
&\approx -R + R(1 - \frac{1}{2}(x_1/R)^2) \\
x_3 &\approx -\frac{1}{2R}x_1^2
\end{aligned}$$

Using either of the two methods mentioned above, the stress distribution in the area of contact is given by:

$$p(x_1) = \frac{2P}{\pi a^2}(a^2 - x_1^2)^{\frac{1}{2}} \tag{A.18}$$

$$P = \frac{\pi a^2 E}{4R} \tag{A.19}$$

Following the method given in [9], the subsurface stress here is derived to be:

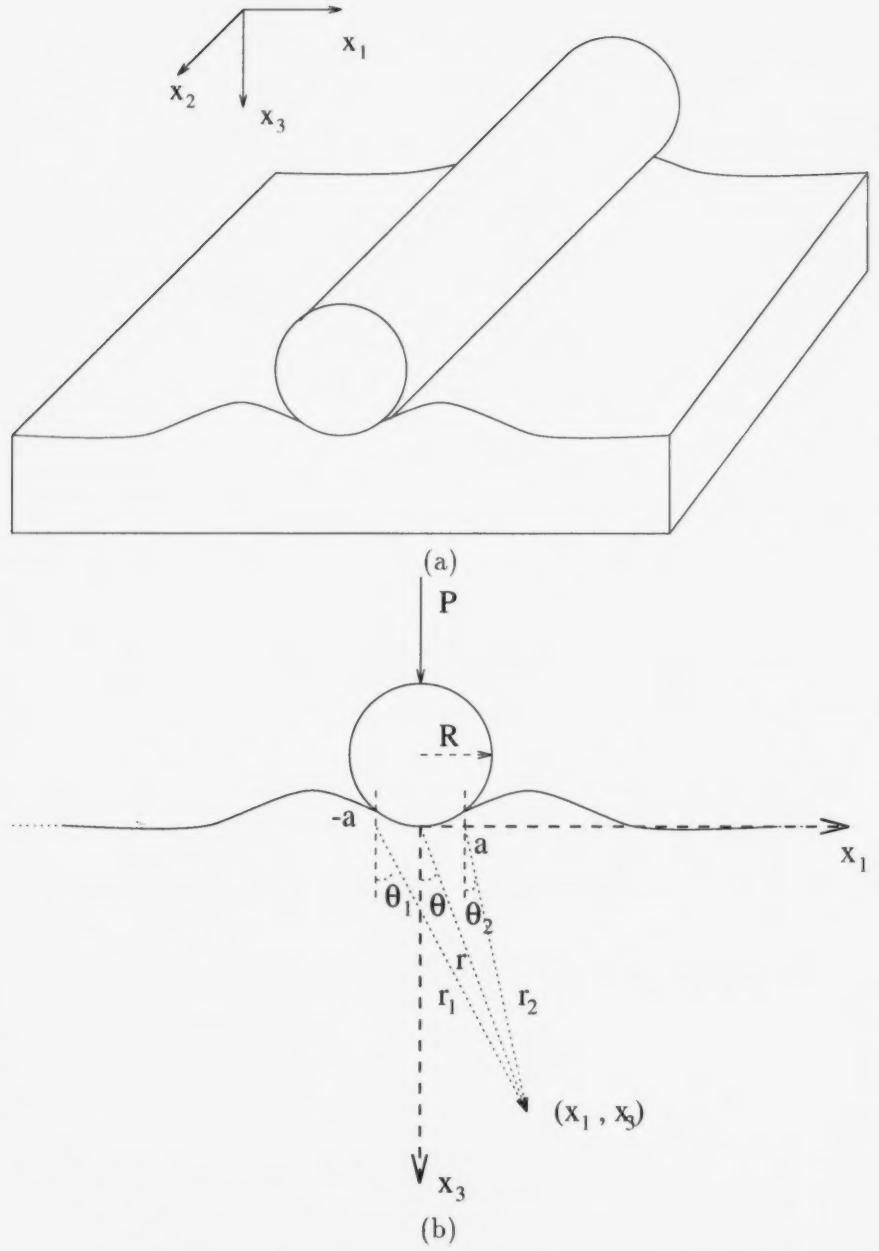

Figure A.5: *The contact between a cylinder and a semi-infinite elastic medium.*

$$\sigma_{33} = -\frac{P}{\pi a^2}[(r_1 r_2)^{\frac{1}{2}} \cos\frac{\theta_1 + \theta_2}{2} + \frac{2r^2}{(r_1 r_2)^{\frac{1}{2}}} \cos\theta \cos(\theta - \frac{\theta_1 + \theta_2}{2}) - 3r\cos\theta] \quad \text{(A.20)}$$

A.2 Contact and the finite element method

The finite element method provides another way of studying contact problems in elasticity. In this thesis, the finite element method was used to study the contact between a layer of elastic material and rigid indenters of three different shapes — edge, flat, and cylinder. The following sections present the details of the finite element models used in the analysis.

A.2.1 General considerations

Figure A.6 shows the two-dimensional model used for solving the problem of contact with a knife edge using the finite element method. The model consists of a layer that is divided up into a rectangular mesh. Each little rectangular area in the mesh is called an element and the four corners of each element are called nodes. The nodes at the bottom of the layer are completely constrained, i.e., the displacements at these nodes are specified to be zero. A line load is applied at the top of the layer.

These elements are referred to as two-dimensional stress elements and the accuracy of the solution is determined by the geometrical properties of these elements. The more the number of elements, the more the accuracy of the finite element solution. However, the more the number of elements, the more the computational and memory requirements of the finite element method. The accuracy of the solution is also affected by the ratio of the two sides of an element. This ratio is called the aspect ratio and it should be as close to 1 as possible. Large (10) or small (0.1) aspect ratios can lead to inaccurate results. The number of elements per unit area is referred to as the mesh density and several different values must be used to determine the best choice for use in the analysis. The mesh density can be variable and it is usually made higher in regions where the stresses change more rapidly. In the three-dimensional model used to study the effect of the plane strain assumption, the elements are three-dimensional and are called brick elements or three-dimensional stress elements.

The layer used in characterizing the different types of contact was 25.4 mm wide and 0.8 mm thick. The width was divided into 64 parts and the thickness was divided into 4 parts, giving a mesh of 64×4 elements, or 65×5 nodes. This mesh was selected after considering several different meshes. The size of elements in the mesh was decreased until the solution obtained using the finite element method became unstable, containing oscillations. The nodes at the bottom of the layer were completely constrained i.e., the displacements at these nodes were zero.

The elastic layer covering the sensor was assumed to be made of rubber. The material properties used for this elastic layer were taken from Ashby and Jones [3]. The indenter was assumed to be made of steel and its material properties were taken

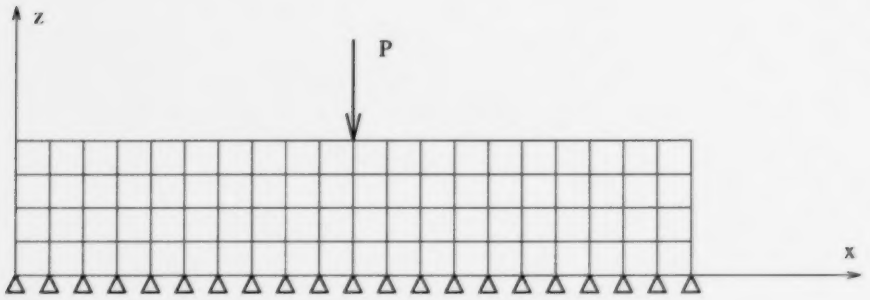

Figure A.6: *A finite element mesh for modeling an elastic layer. The mesh density used in the analysis was larger than that shown in this figure.*

	Young's Modulus E (MPa)	Poisson's Ratio ν
Rubber	27.58	0.49
Steel	2.069×10^5	0.30

Table A.1: *The material properties used in the thesis.*

from the library provided by the finite element method software used for the analysis [1,2]. These values are shown in Table A.1.

Since it is assumed that the materials are linear and isotropic, the modulus of rigidity μ is determined from the Young's modulus E and Poisson's ratio ν using the equation below.

$$\mu = \frac{E}{2(1+\nu)}$$

The above assumptions are not entirely correct since rubber is elastically non-linear. However, if the displacements and strains are constrained to be small, say 0.001, then these assumptions are applicable.

Also, notice that the value chosen for ν is 0.49. The finite element method makes use of the constitutive relations (equation A.10) and these do not apply to perfectly incompressible materials for which ν is 0.5. When ν is chosen to be 0.5, the stiffness matrix becomes singular and the system of linear equations cannot be solved. When the value of ν is near 0.5, the stiffness matrix can become ill-conditioned and lead to inaccurate solutions. A number of values for ν were considered to ascertain that the stiffness matrix is not ill-conditioned. Figure A.7 shows the sub-surface stress obtained for a ν of 0.49 and 0.499999. As can be seen, the stress distributions are similar, indicating that a value of 0.49 is within the realm of numerical stability.

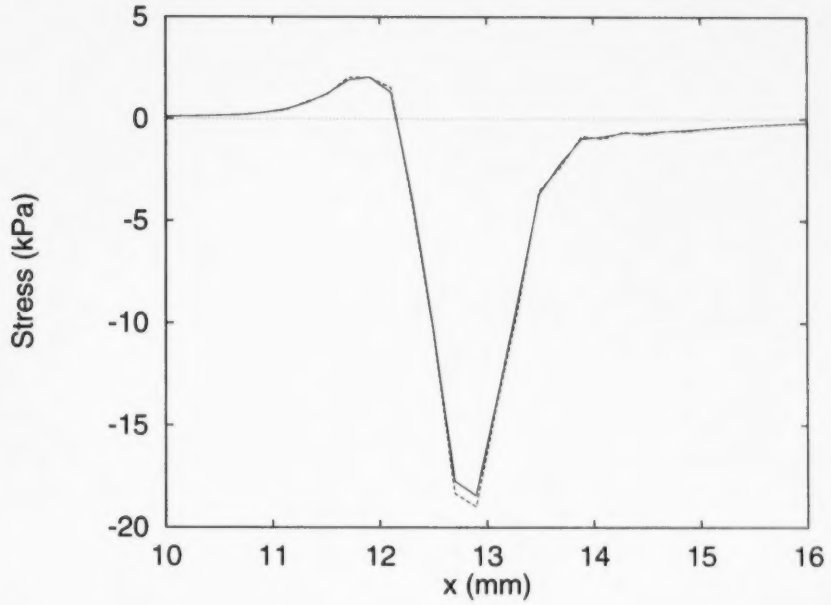

Figure A.7: *A comparison between the sub-surface stress distributions in the case of edge contact for two different values of ν. The solid line corresponds to $\nu = 0.49$, while the dashed line corresponds to $\nu = 0.499999$.*

A.2.2 Contact with a flat indenter

The layer is modeled as in the previous section by a rectangular mesh. The indenter is also explicitly modeled using the finite element method. The height of the indenter was chosen to be 6.35 mm after trying several different heights. This was the smallest height that did not deform appreciably compared to the rubber layer as a result of applied force.

The finite element software [1,2] requires that all objects in the analysis be rigidly constrained to prevent rigid body motion under the applied forces. As for line contact, the elastic layer was rigidly constrained at the bottom surface. The indenter was constrained by using two elastic boundary elements at one corner and one elastic boundary element at the opposite corner. The elastic boundary elements act as springs and so allow some movement when force is applied. The stiffness was chosen to be small with a value of 6.9 Pa.

The contact between the indenter and the elastic layer was modeled using gap elements. These elements are used to connect the two surfaces in contact. One gap element connects one node on the indenter and one node on the elastic layer. These elements are inactive as long as the distance between the connected nodes is greater than zero. When the distance becomes less than zero, these elements apply opposite forces at the two connected nodes so that the gap distance between the two nodes remains zero. The applied force depends on a user specified stiffness, and this was

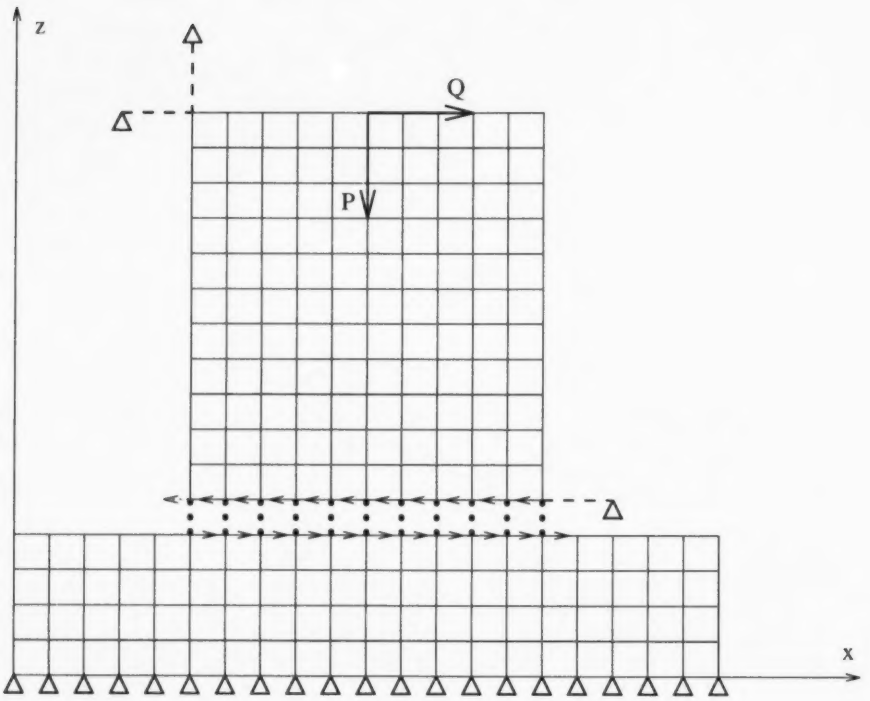

Figure A.8: *The finite element model used for examining the relationship between the stress distribution and the applied normal force, tangential force, and the indenter width. In the analysis, a larger mesh density was used than that shown in this figure.*

set to a value of 6.9×10^9 kPa. The complete model is shown in Figure A.8. This model corresponds to the case of frictionless contact.

A.3 References for appendix

1. ALGOR Interactive Systems, Inc. *ViziCad Plus Volume 1 : Geometric Modeling and Visualization*, 1990.

2. ALGOR Interactive Systems, Inc. *ViziCad Plus Volume 2 : Modeling for Finite Element Analysis*, 1990.

3. M. F. Ashby and D. R. H. Jones. *Engineering Materials: An Introduction to their Properties and Applications.* Pergamon Press, 1980.

4. David S. Burnett. *Finite Element Analysis : From Concepts to Applications.* Addison-Wesley Publishing Company, 1987.

5. Clive R. Chester. *Techniques in Partial Differential Equations.* McGraw Hill Book Company, New York, 1971.

6. K. L. Johnson. *Contact Mechanics*, Cambridge University Press, 1985.

7. N. Kikuchi and J. T. Oden. *Contact Problems in Elasticity : A Study of Variational Inequalities and Finite Element Methods.* Society for Industrial and Applied Mathematics, Philadelphia, 1988.

8. Adel S. Saada. *Elasticity Theory and Applications.* Pergamon Press Inc., New York, 1974.

9. I. N. Sneddon. *Fourier Transforms.* Mc-Graw Hill Book Company, New York, 1951.